THE USE OF PHOTOCATALYTIC DEGRADATION TO IMPROVE THE QUALITY OF CRUDE REFINERY EFFLUENT

Submitted in fulfilment of the requirements for the Degree of Master of Engineering in the Department of Chemical Engineering in the Faculty of Engineering and the Built Environment at the Durban University of Technology

DUSHEN BISETTY NAIDOO

January 2018

Supervisor: Sudesh Rathilal

DECLARATION

I hereby declare that the content put forward in this dissertation is a record of my original research work for the attainment of the Master of Engineering in Chemical Engineering at the Durban University of Technology (DUT). The content provided in this document has not been previously published or written by another person for the award of any other degree at DUT or any other educational institution. I would also like to declare that the content of this dissertation does not violate any copyright as all indication to the work of others has been indicated and acknowledged by means of citation and a comprehensive reference list.

Dushen Bisetty Naidoo

Signature: _____ Date: _____

Supervisor:

Prof. Sudesh Rathilal

Signature: _____ Date: _____

DEDICATION

This thesis is dedicated to my father, my mother and brother;

Ravy, Glad and Nikhil

Your continuous support, positivity and guidance are what made this possible.

ACKNOWLEDGEMENTS

I would like to express my gratitude to my academic supervisor, Professor Sudesh Rathilal for his guidance and support whilst carrying out my research. The insight he shared regarding the research and life was most valuable. I would also like to thank Professor Paul Musonge and Ms Ritha Pambi for their assistance during the conceptual stages of this research study. To the above mentioned, I am truly grateful for your assistance and for affording me the opportunity to conduct my Masters.

I would like to thank my colleagues at DUT as well as Huntsman Tioxide S.A for their support and experience shared on the uses of Titania. I am grateful to the Durban University of Technology and the Department of Chemical Engineering for their efficient handling of the project, the technical resources as well as continuous assistance they rendered when required.

ABSTRACT

Water plays a fundamental role in sustaining life on Earth. Water is largely used by industries to support their processes and utilities. Through growing industrialisation, each year more and more wastewater is generated and the demand for water rises rapidly. The incorrect and unsustainable use of water is placing a great strain on the South African water supply. Much emphasis is now being placed on industries re-using and treating their effluent and wastewater.

Of recent, government has placed stringent specifications for industrial effluent quality and industry find it difficult to continuously improve their effluent quality to be within acceptable limits. Crude refineries are major contributors to wastewater, producing effluent comprising largely of Oil, grease and hydrocarbon. Much focus is placed on finding alternate means of wastewater treatment to assist with the removal of oil and hydrocarbon contaminants. More effluent treatment processes need to be explored to ensure industries operate in a sustainable manner and do not place unnecessary strain on the South African water supply.

Photocatalytic degradation is a wastewater treatment technique that has drawn a lot of attention in the last decade. This is an Advanced Oxidation Process (AOP) which involves the production of a hydroxyl radical (OH^-) which is then used for the degradation of organic contaminants. The degradation converts the organic pollutants into CO_2 and H_2O.

A synthetic crude refinery effluent was developed and underwent the photocatalytic degradation process. The catalyst concentration was varied at 2 g/L, 5 g/L and 8 g/L. The oxidation reaction took place over time intervals of 30, 60 and 90 minutes and aeration to the reaction vessel was supplied at 0.768 L/min, 1.11 L/min and 1.48 L/min. This photodegradation took place under UV light conditions. The degradation process was conducted with the aim of evaluating the degradation of oil and phenol in crude refinery effluent. Sulphates were also monitored to observe if an effect was noticed.

Design of Experiment (DOE) involved the development of experimental run matrices for a multilevel factorial design, Central Composite Design (CCD) and Box-Behnken Design (BBD) model. Randomized runs were then conducted as per the design matrix for each model.

Model verification and evaluation was then conducted and the best suited degradation models were selected. It was observed that the best fitted model for the degradation of oil in water was the BBD. The best design model for phenol degradation was the CCD. Throughout the photocatalytic degradation process, it was noted that no change took place with the sulphates.

The models were then optimised to determine the optimum degradation conditions. This was carried out using Response Surface Methodology (RSM) techniques. The CCD model yielded a combined oil

and phenol degradation of 71.5%. This occurred at a catalyst concentration of 2.07g/L, a run time of 90 minutes and an air flow rate of 0.768L/min. The BBD model produced a combined oil and phenol degradation of 68%. This took place at a catalyst concentration of 2 g/L, a run time of 30 minutes and an air flow rate of 1.04 L/min. pH were monitored throughput the degradation process and both these models yielded output products within the stipulated pH band.

The testing of a local crude refinery effluent was conducted using the CCD and BBD optimum conditions. When using the CCD optimum conditions degradation of 76.98% and 84.21% was observed for both oil and phenol respectively. The BBD optimum conditions yielded a degradation of 83.33% for oil and 78.95% for phenol. This indicated that the photocatalytic process can be considered for degrading crude refinery effluent as its products met the specifications of municipal industrial waste water.

The above results clearly indicate a positive outcome for the treatment method of photocatalytic degradation on the synthetic crude refinery effluent. This technique can therefore be further explored when considering crude effluent treatment and the treatment advantages should be used by all industries to improve effluent quality and allow for more sustainable and environmentally friendly operations.

TABLE OF CONTENTS

LIST OF FIGURES

CHAPTER 2

LIST OF TABLES

LIST OF ABBREVIATIONS

ANOVA	- Analysis of variance
AOP	- Advanced Oxidation Process
AP	- Adequate Precision statistic
API	- American Petroleum Institute
BBD	- Box-Behnken Design
CCD	- Central Composite Design
CV	- Coefficient of variation
df	- Degrees of freedom
DOE	- Design of Experiment
DUT	- Durban University of Technology
EPA	- Environmental Protection Agency
LOF	- Lack of fit
MS	- Mean Square
RSM	- Response Surface Methodology
OFAT	- One factor at a time
TiO_2	- Titanium Dioxide

CHAPTER 1: INTRODUCTION

1.1. Background

South Africa is faced with the harsh reality of drought. Being semi-arid in nature, South Africa's average annual rainfall is 492 mm which is well below the global average of 985 mm (Rand Water, 2017, Pambi, 2015). Pollution of water sources is also a contributing factor as the flow of water from highly industrialised regions brings with it contaminants, thus preventing water from being used efficiently (Pambi, 2015). South Africa's major water sources are its rivers and pollution seems to be degrading water quality at a tremendous rate (Schwikkard, 2001). Water use in South Africa is critical in sustaining key industries such as agriculture, which uses 62% of South Africa's water (Rand Water, 2017). For these reasons, it is vital that measures be put in place to combat pollution and newer technologies be explored for the treatment of industrial effluent.

Industry is a large contributor to wastewater as it uses a large quantity of water and in turn generates a lot of wastewater through its water intensive processes. The industry of focus is the petrochemical industry. Crude refineries are a very important part of any country as they provide fuel which supports several public and private structures, which with it brings good job creation and economic contribution (Hasan et al., 2012). It is estimated that wastewater generated by crude refineries range between 0.4 to 1.6 times the quantities of crude processed. This is excessive and with the steady rise in population and the demand for energy, the wastewater generation is bound to increase even more. Crude refineries do place emphasis on wastewater treatment, however only up to a certain extent. Crude refinery effluent treatment plants treat effluent with the aim of reaching the specification put in place by government for industrial effluent. This treatment generally involves oil in water separation, coagulation and flocculation as well as dissolved air flotation. These techniques assist with the removal of oil from water; however the effluent still contains oil and a significant amount of other hydrocarbon contaminants.

1.2. Problem statement

Refinery effluent treatment is vital as the growing need for water places a larger strain on the supply. Traditional wastewater treatment options involve physical and chemical treatments. These methods are effective but cannot cope with reducing contaminants efficiently as legislative specifications become more stringent. It is key that emphasis be placed on cheap, efficient and environmentally friendly methods of treating wastewater. This will ensure industry reduces some of the strain on the water supply. The three major issues faced by refineries regarding industrial wastewater are quality, financial implications and water saving initiatives. Refineries are finding it difficult to meet the effluent specifications for industrial wastewater, which was introduced by government. The use of

traditional treatment methods poses a great financial implication as processes are energy intensive and sometimes inefficient. Water saving initiatives come in as industry uses large quantities of water for irrelevant operations and processes such as dilution of wastewater. Industry needs to put plans in place to reduce water usage and roll out more water saving strategies to encourage sustainable and eco-friendly industrial operations.

1.3. Objectives

The main aim of the research was to improve the quality of crude refinery effluent. The specific objectives were to:

- Evaluate the effectiveness of using photocatalytic degradation for the treatment of crude refinery effluent. This was conducted through an in-depth literature survey on the treatment methods and observation of the current research outputs. This was also evaluated by a comparison of the current best effluent outputs and what could be achieved by the use of photocatalytic degradation. Traditional methods are finding it difficult to meet effluent specifications of oil in water less than 50 ppm and phenol less than 10 ppm (Tetteh and Rathilal, 2018).
- Development of a predictive model for the degradation of contaminants using the multilevel factorial design, Central composite design and Box-Behnken design. This involved randomised runs to provide outputs to the degradation process. This section included model development, model verification and model selection based on best degradation performance.
- Optimisation of the photocatalytic degradation process using Response surface methodology being applied to the most significant model. This involved optimisation of the model in terms of catalyst concentration, run time and air flow rate. This eventually resulted in the optimum conditions for photocatalytic degradation.

1.4. Approach

A synthetic effluent was developed with guidelines taken from the local municipality as well as from the available literature. This synthetic effluent was the feed for the photocatalytic degradation process. Design of experiment (Design Expert Version 10) was conducted and randomised run matrices for the multilevel factorial design, central composite design and Box-Behnken designs were developed. The process involved a glass reaction vessel with UV light being the energy source for the photoreaction. The reaction vessel was charged with synthetic effluent and air was then sparged through the bottom of the reaction vessel. The air aided the advanced oxidation reaction as well as kept the catalyst particles in solution. Micro scaled titania catalyst was then introduced and the runs occurred for a specific reaction time. Oil in water, phenols, pH and sulphates of the feed to the reactor as well as outputs from the reactor were analysed. This allowed for evaluation of the contaminant degradation

performance. Models were then developed, evaluated and the best model selected and optimised for the optimum reaction conditions.

1.5. Structure of dissertation

Chapter 1: Introduction

This section presents the reader with a background and relays some direction as to where this study is headed. It assists with outlining some of the current problems faced by industry and provides the motivation as to how this research will assist. Some of the key issues include water scarcity in South Africa, how water is used in industry and more especially the petrochemical industry. Finally it presents the problem statement and establishes the objectives and approach.

Chapter 2: Literature Review

This section focuses on previous work very similar to what is being intended to be carried out. This makes use of reviewing and surveying of previous or existing knowledge and findings, with the aim of refining the approach and technique adapted in this study. The review also allows for observation of previous studies and at times can be a good guide as to what outcomes can be expected. The literature review focuses on the importance and use of water, traditional treatment methods as well as how photocatalytic degradation can be used to improve the quality of crude refinery effluent.

Chapter 3: Methodology

This section makes mention of the equipment and chemicals to be used for experimentation. It also indicates how the range selection for variables took place as well as development of the synthetic feed. Much detail is shown on the chemical analysis techniques used as well as design of experiment using the Design Expert software package.

Chapter 4: Results and Discussion

This section displays graphically all the outputs from the experimental runs conducted. The graphs are then discussed with the aim of determining at which point the degradation process was most effective. This analysis takes place by evaluating one factor at a time (OFAT).

Chapter 5: Optimisation using Response Surface Methodology (RSM)

This section dealt with optimisation of the photocatalytic degradation process using RSM. This involved the development of the multilevel factorial design, Central composite design and Box-Behnken design predictive models. Model evaluation and verification was then conducted. The best fitted models were then optimised to identify the optimum degradation conditions for organic contaminants in crude refinery effluent.

Chapter 6: Conclusion and Recommendations

This section draws on the outcomes of the results and concludes the dissertation based on the findings and outputs. A brief summary of how the degradation process performed and the optimum conditions for the process are identified. Recommendations are presented based on the experience from the research and findings.

CHAPTER 2: LITERATURE REVIEW

2.1. Understanding Water and how it is used

Water is a fundamental component to sustaining life on earth. The water molecule is a very versatile structure and tends to be a universal solvent. This molecule has the ability to absorb and release large amounts of energy as it changes phase (Rand Water, 2017). Most of the Earth's surface is covered with water, however 98% of this is salt water, leaving less that 1% of the water fit to be consumed by humans (The Water Information Program, 2004). Water is an abundant molecule even in the human body as it makes up over 75% of human mass (Rand Water, 2017).

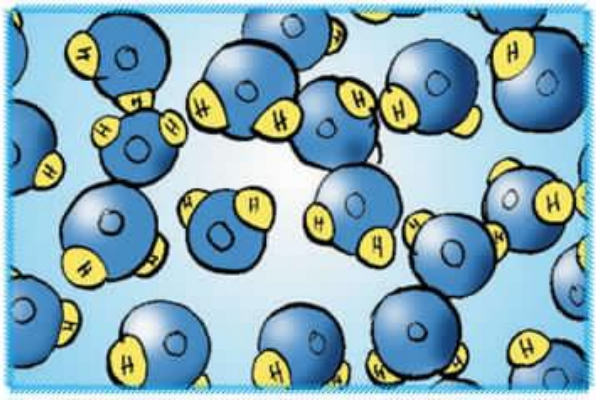

Figure 2.1: The water molecule (Rand Water, 2017)

2.1.1 Water Scarcity

Most forms of life on Earth are dependent on water, so this scarce resource needs to be used efficiently and in a more sustainable manner. A few of the key freshwater applications include drinking, cooking, agriculture, production processes and infrastructure development (Hoekstra and Hung, 2005). The rapidly increasing population as well as the agricultural and industrial boom that comes with it, puts a strain on the current limited water supply (Dlamini, 2016). Similar thoughts are shared by Postel (2000) and Adewumi et al. (2010) indicating that South Africa, being a semi-arid country, has high water stress due to the low rainfall volume and high evaporation rates. The variability and uneven distribution of rainfall contributes to this water stress significantly. Rand Water (2017) explains that South Africa receives an annual rainfall of approximately 492 millimetres; however the rest of the earth obtains rainfall in the region of 985 millimetres per annum. The rainfall distribution extracted from Rand Water (2017) can be observed in the picture below:

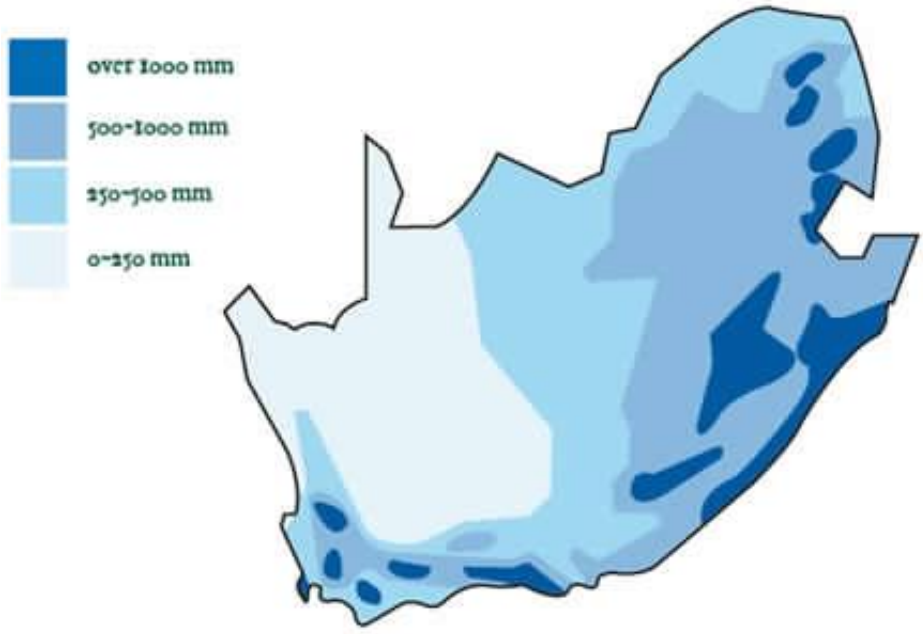

Figure 2.2: Annual rainfall distribution in South Africa (Rand Water, 2017)

The Lesotho Highlands Water Project and the Thukela-Vaal Water Transfer schemes are put in place to assist with the uneven distribution of water across South Africa (Rand Water, 2017). These transfer schemes feed into the Vaal dam catchment area. The Department of Water and Environmental affairs indicated that the demand for water will outweigh the water supply in the whole of South Africa, should sustainable water usage not be implemented (Department of Water and Environmental Affairs, 2017). Tables 2.1 and 2.2 indicate water usage in South Africa and water usage in households respectively.

Table 2.1: Water use in South Africa (Wessels et al., 2007)

Agricultural Use (including irrigation)	**60%**
Environmental Use	18%
Urban & Domestic Use	11.5%
Mining & Industrial Use	10.5%

Table 2.2: Water usage in households (Rand Water, 2017)

	Low-Income Household	**Mid to High-Income Household**
Toilets	73%	37%
Baths & Showers	19%	32%
Washing Machine	NA	17%
Other eg. cooking, washing dishes and clothes, drinking, etc.	8%	14%

2.1.2. Water and Wastewater Quality

Schwikkard (2001) explains that rivers are the most important water source in South Africa; hence it is important to implement waste minimisation and pollution prevention strategies as pollution compromises water quality drastically. The importance of river water and pollution prevention is also echoed by Kahinda et al. (2007) who claimed that 3.7 million people have no access to any form of water supply infrastructure. Hoekstra and Hung (2005) indicated that a means of preventing the deterioration of water quality was to treat water as an economic good, thus placing more economic value on the product. Wastewater quality is important as this can be reused and now poses less of a threat to aquatic life as well as the environment (Adewumi et al., 2010, Savenije, 2000). The ability to maintain good water and wastewater quality is vital in water resource management as this then allows for the reuse of wastewater, resulting in a reduced load on the limited water supply (Adewumi et al., 2010).

2.1.3. Crude Refinery Effluent

The petrochemical industry is identified as one of the largest wastewater contributors. Stepnowski et al. (2002) explained that these industries have a vested interest in enhancing wastewater management through optimisation of water use and improving recycling technologies. Refineries are highly beneficial, however produce large quantities of effluent (Hasan et al., 2012). The estimated water consumption in producing a barrel of crude oil is between 246 to 341 litres of water (Hasan et al., 2012). Similarly indicated by Coelho et al. (2006) and Hasan et al. (2012) that petroleum refineries are large water consumers and also generate wastewater in the range of 0.4 to 1.6 times the volume of oil they produce. The ratio of oil refined to wastewater produced is important and can range between 3.5 to 5 meter cubed of wastewater per ton of crude oil (Hayder et al., 2014). The fact that world oil demand is on the rise and by 2030 will account for 32% of the worlds energy supply, means crude refinery effluent will drastically increase (El-Naas et al., 2014).

Petroleum refinery wastewater is very complex as it contains various inorganic and organic constituents such as emulsified oil, ammonia, sulphides, sulphates, cyanides as well as phenol and phenolic derivatives (Pakravan et al., 2015). Petroleum refinery effluent varies from refinery to refinery due to variation in plant configuration as well as the type of crude oil being processed. Refinery wastewater contains aliphatic and aromatic organic compounds which contribute largely to environmental pollution (Khan et al., 2015). Oil and grease content is one of the most detrimental pollutants to marine and aquatic life (Ahmadun et al., 2009). The table below indicates some of the maximum permitted oil and grease contents that can be found in produced wastewater.

Table 2.3: Maximum permitted oil and grease limits

Industry Location / Organisation	**Oil and Grease limit (mg/L) daily average**
Australia	30 mg/L (Ahmadun et al., 2009)
United states of America	15 mg/L (Moslehyani et al., 2015)
China	10 mg/L (Ahmadun et al., 2009)
North East Atlantic	40 mg/L (Ahmadun et al., 2009)
Malaysia	10 mg/L (Moslehyani et al., 2015)
European Union	5 mg/L (Moslehyani et al., 2015)

Chen et al. (2014) shares information on the fact that not enough emphasis is placed on oil in crude refinery wastewater, yet this can cause serious water pollution and poses a health risk. This is validated by Grzechulska et al. (2000) who documents that several environmental and ecological issues have been linked to the presence of oil or oil derivatives in water. What makes oil in water dangerous is the fact that it has a very long degradation time (Grzechulska et al., 2000).

Phenol and phenolic derivatives are also of great importance as they pose a major environmental threat due to their high toxicity, relative stability and poor biodegradability (Shahrezaei et al., 2012). The aromatic ring structures of phenolic compounds make it difficult to remove from wastewater, posing a long term environmental hazard (Liwsirisaeng et al., 2011). Phenols are harmful to humans at low concentrations and are hazardous pollutants, which is why they are referred to as priority pollutants (Abdelwahab et al., 2009). It is therefore vital that phenol content in wastewater be lowered. The Environmental Protection Agency (EPA) aims at dropping phenol content to less that 1 mg/L. Das et al. (2013) explains that phenols tend to be carcinogenic in nature and the prolonged exposure to phenol could result in liver damage, hemolytic anemia, paralysis as well as damage to internal organs. The table below (Table 2.4) indicates the maximum limit of phenol content in industrial wastewater.

Table 2.4: Maximum permitted phenol content in wastewater

Industry Location / Organisation	**Phenol limit (mg/L) daily average**
Japan	5 mg/L (Nickheslat et al., 2013)
United states of America	0.3 mg/L (Nickheslat et al., 2013)
Canada	4 µg/L (Canadian Water Quality Guidelines for the Protection of Aquatic Life, 1999)
World Health Organisation (WHO)	2 µg/L (Nickheslat et al., 2013)

Choquette-Labbé et al. (2014) states that phenols pose a great threat to many ecosystems and human health, which is why the United States, Canada and the European Union regards this as a priority pollutant.

2.2. Refinery Effluent Treatment

One of the major forms of industrial wastewater is oil refinery effluent. Oil refinery wastewater treatment can be broken up into four treatments namely physical, chemical, biological and physicochemical. Physical and chemical treatments are commonly used in crude refinery effluent treatment plants (Yang et al., 2016). Figure 2.3 below presents a schematic view of crude refinery effluent treatment.

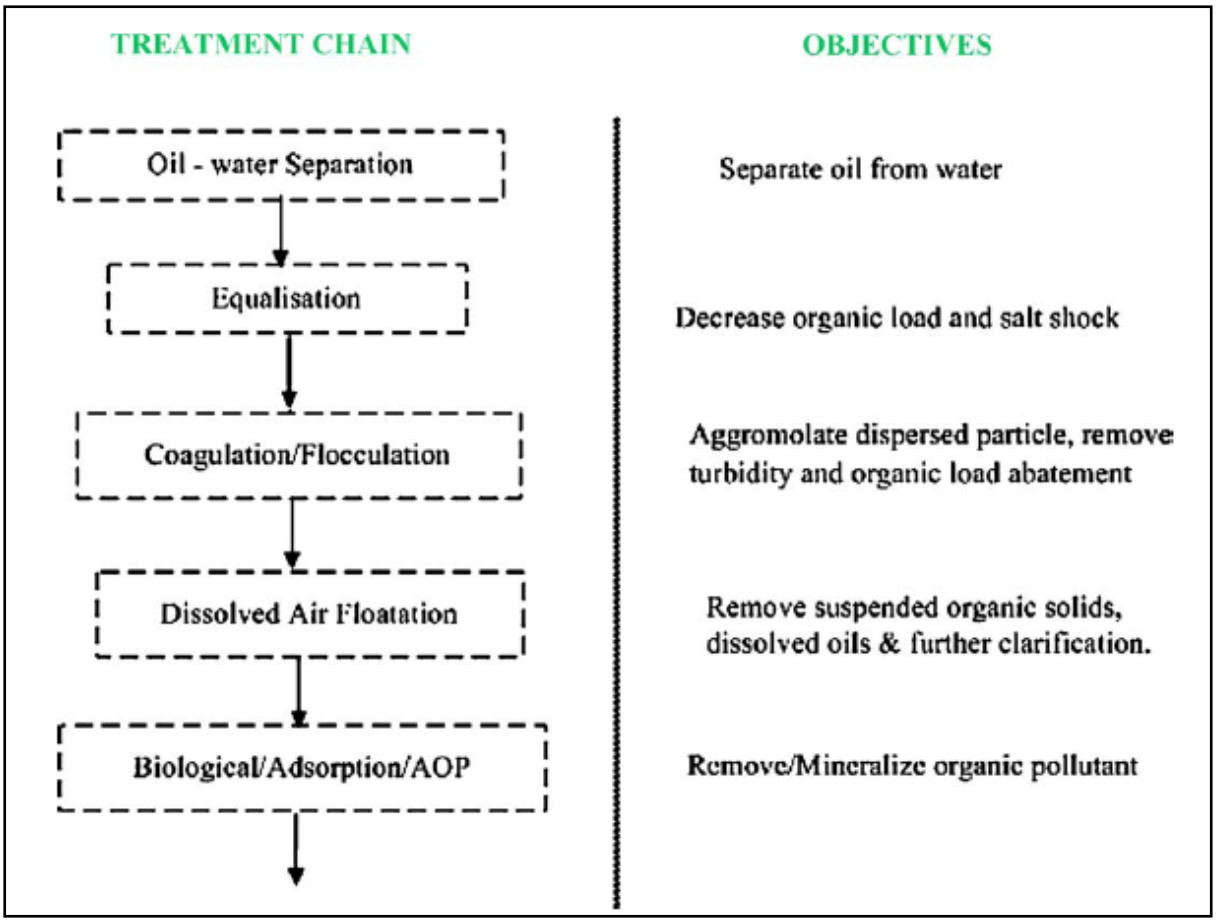

Figure 2.3: Sequence of petroleum refinery effluent treatment (Diya'uddeen et al., 2011)

2.2.1. Physical Treatment

A few common types of physical treatments are clarification, gravity settling, dissolved air flotation, filtration, cyclone separation and API(American Petroleum Institute) oil-water separators (parallel or corrugated plate interceptors) (Yang et al., 2016). A common treatment sequence for crude refinery effluent treatment involves the use of API oil-water separation followed by dissolved air flotation (DAF) (Soltanian and Havaee Behbahani, 2011).

API Oil-water separation involves a gravity separation device that is designed based on the Stokes' law principle (Siemens, 2017). The Stokes law equation gives a relationship between the terminal rise or settling velocity of a sphere in a fluid of known density and viscosity, to the diameter of the sphere when subjected to the force of gravity (Skimoil, 2017).

Stokes' law equation: $V = \frac{(2gr^2)(d1-d2)}{9\mu}$ (Skimoil, 2017) (1)

Where: V = Rise velocity $\left(\frac{cm}{s^2}\right)$

g = Gravitational acceleration $\left(\frac{cm}{s^2}\right)$

r = Equivalent radius of particle (cm)

d_1 = Density of particle $\left(\frac{g}{cm^3}\right)$

d_2 = Density of medium $\left(\frac{g}{cm^3}\right)$

μ = Viscosity of medium $\left(\frac{dyne\ .Sec}{cm^2}\right)$

Gravity separation makes use of the difference in specific gravity of the oil and water mixture with the rate of separation being indicated by stokes law. The suspended solids tend to settle at the bottom as a sediment layer, while the oil rises to the top and the wastewater is the middle layer formed (Skimoil, 2017). The oil layer is then skimmed off and sometimes reprocessed. Figure 2.4 below presents an API separator and its components.

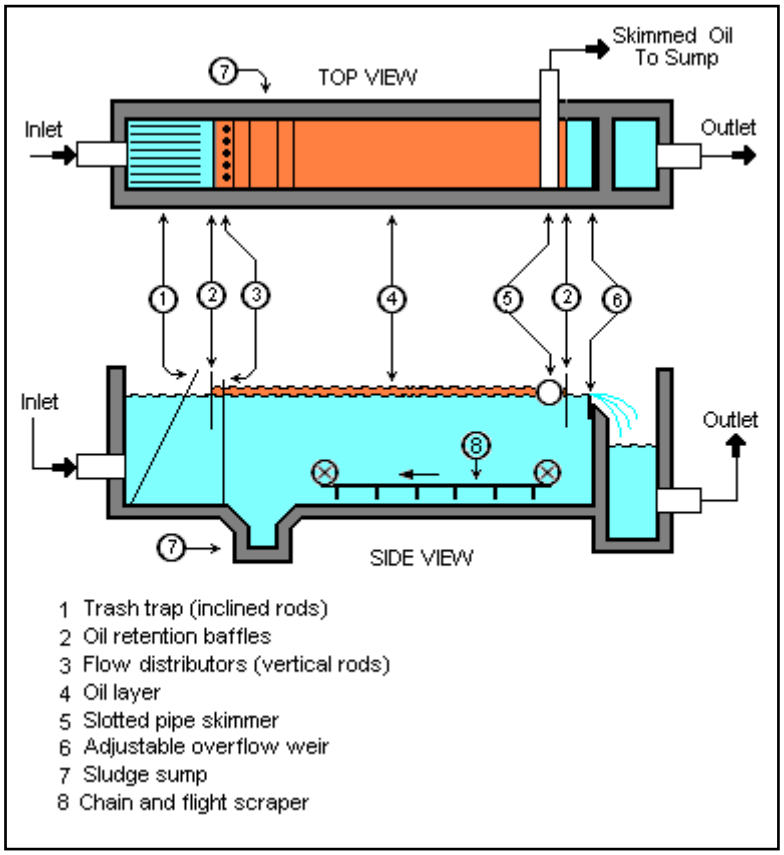

Figure 2.4: Gravimetric API separator (Siemens, 2017)

Dissolved air flotation (DAF) is a technique used to clarify wastewater by removing suspended matter like oil and solids. Air is dissolved in the water under pressure and is then expelled at atmospheric pressure into a flotation tank (Siemens, 2017). This release of air produces tiny bubbles which cling

to the suspended matter and then float to the surface. A skimming device is used to then remove this matter (The North Salt Spring Waterworks, 2017). Figure 2.5 below presents a DAF unit.

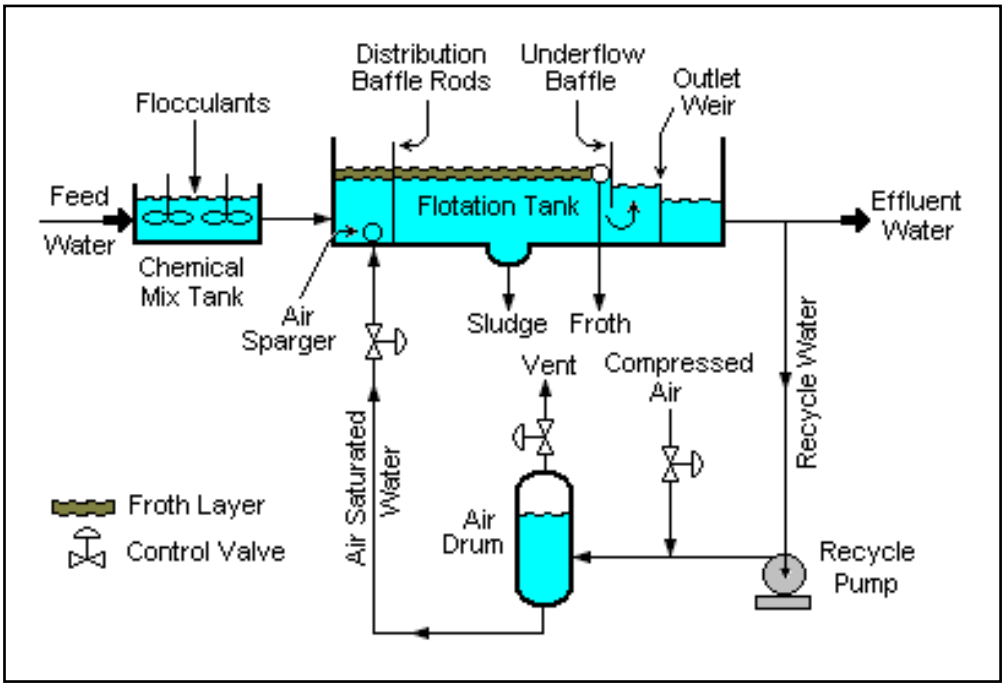

Figure 2.5: Dissolved air flotation unit (DAF) (Siemens, 2017)

The three key steps involved in the DAF unit are coagulation, flocculation and air flotation. The North Salt Spring Waterworks (2017) explains that a coagulant is added during a rapid mixing process. Flow is then decreased allowing materials to clump up resulting in floc formation. This then passes through the air flotation chamber where the floc is floated to the top of the tank for skimming to take place.

2.2.2. Chemical Treatment

API oil-water separation does not make use of chemical addition as this is a purely mechanical process (Skimoil, 2017). The initial stages of the dissolved air flotation process requires the use of chemicals to aid coagulation and flocculation (The North Salt Spring Waterworks, 2017). Coagulation is the chemical addition which produces positive charges which neutralise the negatively charged particles. The coagulation process involves chemical addition and rapid mixing for dissolving and distributing the chemicals (Michigan Environmental Education Curriculum, 2016). These neutrally charged particles are then able to stick together forming larger particles. Flocculation is the gathering of these destabilized particles which cause them to agglomerate and form larger particles or floc (ChemTreat, 2017). This floc is then floated to the surface for skimming during the air flotation stage of the DAF unit. Figure 2.6 below illustrates the typical coagulation treatment process employed by various wastewater treatment plants.

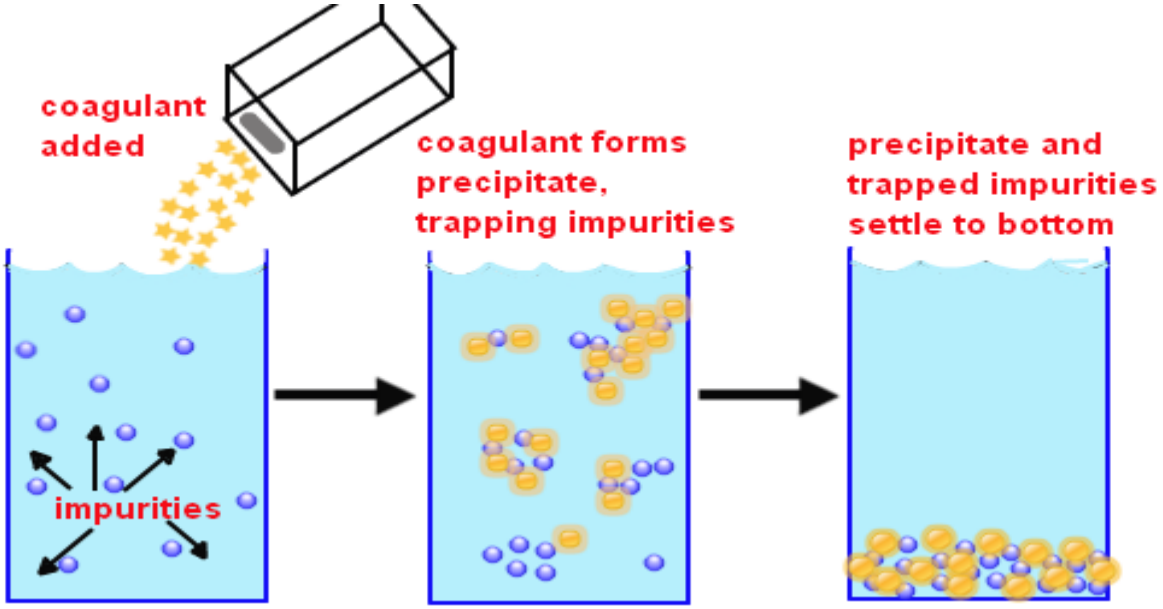

Figure 2.6: Process of coagulation, flocculation and sedimentation (Tutorvista.com, 2017)

2.2.3. Summary of refinery effluent treatment

Refinery effluent treatment is of great importance as crude oil refineries are highly beneficial industries, however are also large producers of wastewater (Saien and Nejati, 2007). Traditional refinery effluent treatment involves physical and chemical means. These processes are API oil-water separation followed by the dissolved air flotation which uses chemical addition for coagulation and flocculation (The North Salt Spring Waterworks, 2017). Traditional methods are effective, however are not the most efficient, which is why much emphasis is being placed on finding cheap and efficient means of improving the quality of crude refinery effluent (Oller et al., 2011). Traditional wastewater methods are partly effective, inefficient and generally tend to transfer pollutants from water into another phase as secondary pollutants (Prabha and Lathasree, 2014). Similar thoughts are shared by Chong et al. (2010) who explained that by transferring pollutants from one phase to another, they are not being completely eliminated or destroyed, thus not solving the problem.

2.3. Photocatalytic Degradation

In recent years, much emphasis has been placed on introducing photodegradation techniques into wastewater treatment and promising results have been observed (Stepnowski et al., 2002). The photocatalytic degradation technique is commonly referred to as "Advanced oxidation processes (AOP's)" as they involve the generation of a hydroxyl radical ($OH^{\cdot}$) which is used for the degradation of organics (Shahrezaei et al., 2012). The hydroxyl radical produced acts as the primary agent responsible for the oxidation of several aqueous organic contaminants (Laoufi et al., 2008). Advanced

oxidation processes can completely degrade organic pollutants into harmless substances such as CO_2 and H_2O (Saien and Shahrezaei, 2012).

Heterogeneous photocatalytic degradation are AOP's that occur in the presence of a semiconductor such as Titanium dioxide (TiO_2) and Zinc oxide (ZnO) (Pakravan et al., 2015). Much focus is placed on the use of AOP's for the treatment of petrochemical industry wastewater as well as other effluents produced during oil extraction processes (Oller et al., 2011). Grzechulska et al. (2000) indicates that photocatalytic degradation is required under light illumination with an energy that is higher than the band gap of the semiconductor, which then induces the degradation process. Titanium dioxide (TiO_2) is the best semiconductor for practical wastewater treatment (Ghasemi et al., 2016). TiO_2 is commonly studied due to its ability to break down organic pollutants effectively and at times even achieve total demineralisation of organic pollutants (Umar and Aziz, 2013). The table below mentions common semiconductors and their band gaps.

Table 2.5: Semiconductors and their band gaps at specific wavelengths

Semiconductor	Band gap energy (eV)	Wavelength
TiO_2 (rutile)	3	413
TiO_2 (anatase)	3.2	388
ZnO	3.2	388
ZnS	3.6	335
CdS	2.4	516
Fe_2O_3	2.3	539

2.3.1. Titanium Dioxide (TiO_2)

Umar and Aziz (2013) documents that TiO_2 can be regarded as the most effective photocatalyst and is extensively used in the water and wastewater treatment industries. TiO_2 is cost effective, stable, non-toxic and is capable of inducing an oxidation reaction to degrade organic compounds (Gaya and Abdullah, 2008, Naeem and Feng, 2009).

Titanium dioxide or Titania exists in three major crystal forms and these are anatase, rutile and brookite. Anatase is a white powder and rutile grades have an off-white colour (Dlamini, 2016). Anatase TiO_2 has a crystalline structure of tetragonal nature and is usually irradiated with UV light during photocatalysis. Rutile TiO_2 has a tetragonal structure and its common use is as a paint pigment, while brookite TiO_2 has an orthombic structure (Akpan and Hameed, 2009). Titanium dioxide of rutile or anatase forms are manufactured using either the sulphate or chloride processes with the main

feedstock for these processes being impure titanium dioxide feedstock (Dlamini, 2016). Figure 2.7 below displays the crystal structure of TiO_2 in its anatase, rutile and brookite formations.

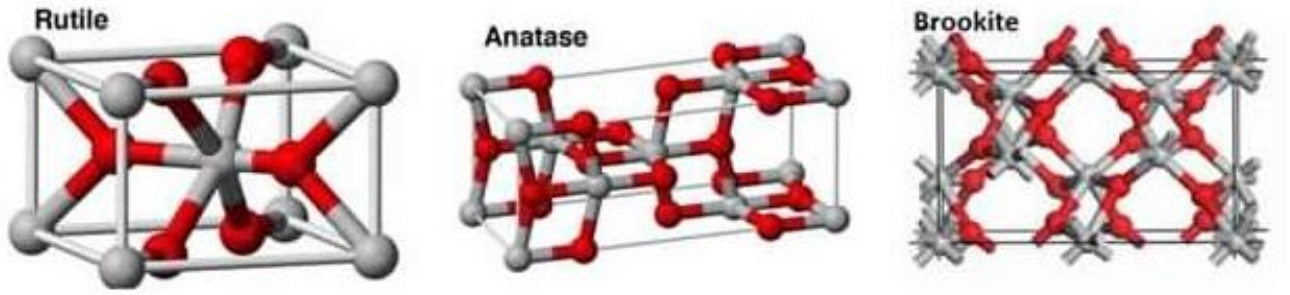

Figure 2.7: Crystal structures of TiO_2 (Pave Maintenance, 2017)

2.3.2. Mechanism of TiO_2 Photocatalytic Degradation

Advanced Oxidation Processes rely on the generation of highly reactive radical species (generally OH^-) by solar, chemical or other forms of energy. One of the best features of AOP's is that the strong oxidising radicals produced are able to eliminate a large array of organic chemical species and do so in a non-selective manner (Gaya and Abdullah, 2008). TiO_2 is classified as a photocatalyst due to its lone electron properties in the particles outer orbital (Dlamini, 2016). A photocatalyst is described by Umar and Aziz (2013) as a substance which is activated by the absorption of a photon and is then capable of speeding up a reaction without itself being consumed in the reaction. TiO_2 is activated by UV light with a wavelength less than 400 nm as it has a band gap of 3.2 eV (Laoufi et al., 2008). Figure 2.8 below presents the advanced oxidation process (AOP).

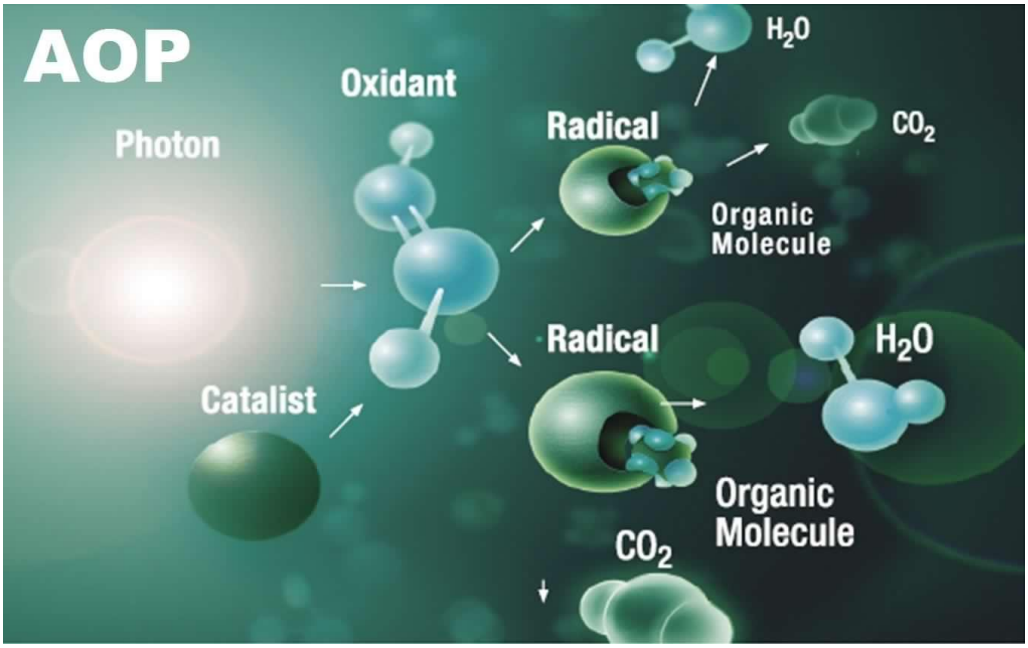

Figure 2.8: Advanced oxidation processes on a molecular level (Palayesh, 2015).

Photo-induced reactions are activated by absorption of a photon with energy equal to or higher than the band-gap energy of the catalyst (Akpan and Hameed, 2009). This absorption results in charge separation as the electron (e^-) moves from the valence band to the conduction band of the semiconductor catalyst, resulting in a hole (h^+) in the valence band (Chong et al., 2010). For the photocatalytic reaction to be favoured, the recombining of the electron and hole must be prevented. This allows for a reaction of electrons with an oxidant resulting in a reduced product, as well as a hole reacting with a reductant to produce an oxidised product (Gaya and Abdullah, 2008).

The hydroxyl radicals produced (OH^-) are very reactive species and are therefore able to oxidise a wide variety of organic pollutants in a quick, efficient and non-selective manner (Konstantinou and Albanis, 2004). Chong et al. (2010), Akpan and Hameed (2009) explain the series of chain oxidative-reductive reaction equations that take place at the photon activated surface. These reactions can be observed below.

Photoexcitation: $$TiO_2 + hv \rightarrow e^- + h^+ \quad (2)$$

Charge-carrier trapping of e^- : $$e^-_{CB} \rightarrow e^-_{TR} \quad (3)$$

Charge-carrier trapping of h^+ : $$h^+_{VB} \rightarrow h^+_{TR} \quad (4)$$

Electron-hole recombination: $$e^-_{TR} + h^+_{VB}\ (h^+_{TR}) \rightarrow e^-_{CB} + heat \quad (5)$$

Photoexcited e^- scavenging: $$(O_2)_{ads} + e^- \rightarrow O_2^{\cdot -} \quad (6)$$

Hydroxyl h^+ scavenging: $$OH^- + h^+ \rightarrow OH^{\cdot} \quad (7)$$

Photodegradation by $OH^{\cdot}$: $$R - H + OH^{\cdot} \rightarrow R^{'\cdot} + H_2O \quad (8)$$

The figure below explains the photo-induced mechanism of the electron-hole pair in a TiO_2 semiconductor particle.

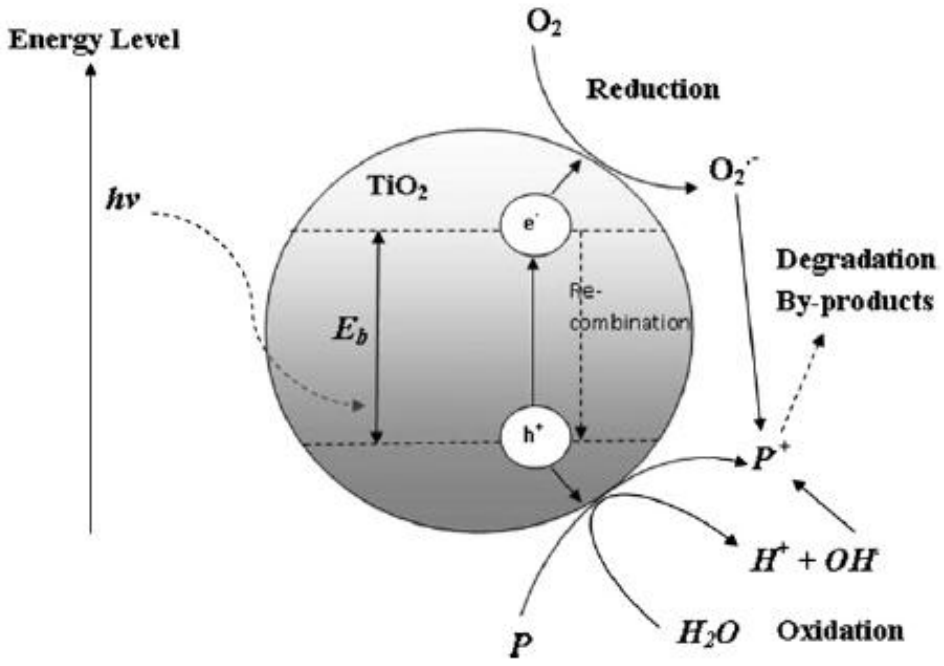

Figure 2.9: Photocatalytic mechanism in a TiO_2 semiconductor particle with a water pollutant (P) present (Chong et al., 2010).

The photocatalytic reaction mechanism indicates that the degradation method is a clean technology and can be applied to the treatment of several wastewater applications where unwanted organics may exist (Corrêa et al., 2010). Similar thoughts are shared by Ghasemi et al. (2016) who indicates that some of the key benefits of using TiO_2 for photocatalytic degradation include the fact that no sludge formation occurs, there is complete elimination of contaminants, TiO_2 particles can be reused as well as that it removes organic and in some cases inorganic pollutants. The TiO_2 photocatalyst has attracted the attention of many and is close to being an "ideal photocatalyst in several respects" (Fujishima and Zhang, 2006).

2.4. Factors Affecting Photocatalytic Degradation

Some of the main factors affecting the performance of photocatalytic degradation with TiO_2 include photocatalyst concentration, pH of the solution, reaction temperature, concentration of the pollutants, presence of inorganic ions, flow rate of sparged air, light intensity or wavelength and reaction time (Gaya and Abdullah, 2008, Umar and Aziz, 2013).

2.4.1. Catalyst concentration or catalyst loading

Gaya and Abdullah (2008) indicated that the photocatalyst concentration has a strong influence on the photocatalytic reaction and the reaction is shown to increase photodegradation proportionally with an increase in catalyst loading. TiO_2 loading is proportional to the photocatalytic reaction and the concentration of catalyst particles affects the reaction rate greatly especially in the heterogeneous regime (Umar and Aziz, 2013). During the photodegradation of phenols, Naeem and Feng (2009) ranged the TiO_2 concentration from 50 to 500 mg/L and observed that the degradation rate increases with an increase in concentration. The results produced can be observed in Figure 2.10 below.

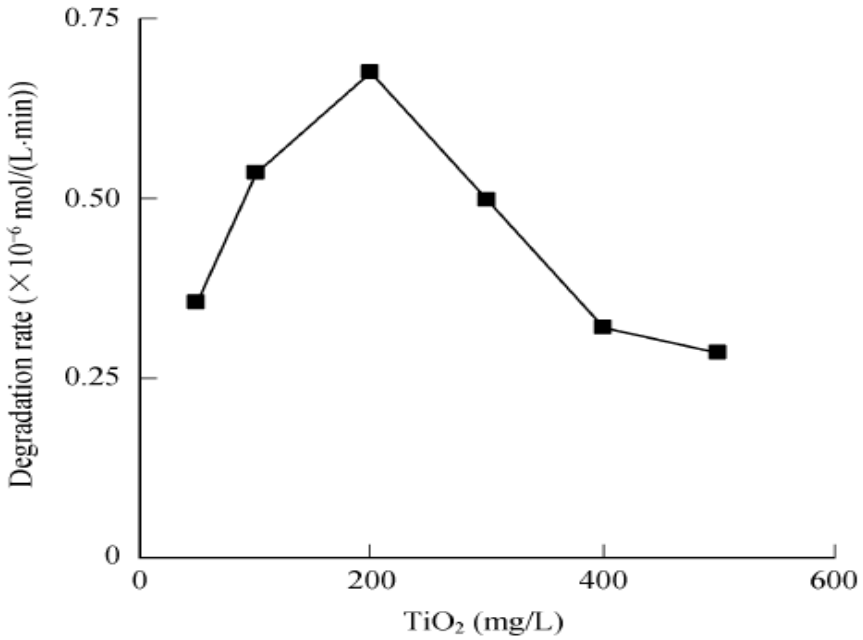

Figure 2.10: The effect of TiO_2 catalyst loading on the degradation rate of phenol (Naeem and Feng, 2009).

This proportional increase occurs only up to a certain limit of 200 mg/L as above this a decrease in degradation is observed. Several researchers indicate that when catalyst loading exceeds the optimum quantity, a significant decrease in efficiency is observed as excess particles tend to scatter light.

An increase in degradation of phenol with increasing catalyst loading was also observed by Laoufi et al. (2008). Degradation of phenol with the use of a composite nanocatalyst highlighted that the maximum degradation occurs at a catalyst concentration of 0.35 g/L (Das et al., 2013). The use of zinc as a catalyst was also successful for the complete degradation of phenol using solar energy, This took place at a catalyst concentration of 0.25 g/L and degraded a phenol solution of 75ppm to 0ppm (Pardeshi and Patil, 2008).

Work done on photodegradation of petroleum refinery wastewater also show an increase in reaction rate as catalyst concentration is increased. This was reported to occur up to concentrations of 100 mg/L of TiO_2, thereafter degradation was noted to decrease (Saien and Nejati, 2007). Chemical oxygen demand (COD) removal was the key output response of Shahrezaei et al. (2012) for work carried out on crude refinery effluent. It was found that the same trend occurred where efficiency increased up to 100 mg/L and thereafter decreased. At 100 mg/L the reduction in COD was found to be 83.1%.

Saien and Shahrezaei (2012) conducted work using nanotitania photocatalyst and the same optimum catalyst loading of 100 mg/L was achieved. Once the optimum quantity was exceeded, degradation of organics in refinery wastewater began to decline. Similar trends surfaced when the degradation of organic sulphides in refinery wastewater was targeted (Habibi and Vosooghian, 2005). When solar photocatalytic degradation was conducted on tartrazine in an immobilized system, it was observed that degradation increased linearly with higher catalyst loading. The optimum catalyst loading was found to be in the range of 0.5 to 5 g/L and this depended on the types of pollutants involved (Hashim et al., 2001). Micro-scale TiO_2 was used to degrade organics in treated drinking water and the optimum range for catalyst loading was found to be between 5 and 7.5 g/L. Dlamini (2016) explains that an increase in concentration from 0 to 5 g/L shows an increase in photocatalytic degradation efficiency from 0 to 90%.

A higher catalyst concentration means a greater number of active sites available for adsorption. As catalyst concentration climbs above a certain limit, the degradation efficiency is not as significant and at times can lead to a decrease in degradation (Diya'uddeen et al., 2011). During phenol degradation when catalyst loading exceeded 0.35 g/L, Das et al. (2013) explains that degradation reaction rate decreased significantly. This could be due to a light scattering effect where light penetration of effluent was retarded as there was a large number of solid particles present in solution (Neppolian et al., 2002). It was further indicated that the photoactivated volume of the suspension decreased. Particle-particle interaction or agglomeration generally takes place at high solids concentrations and this results in a lower surface area for light absorption, thus decreasing the degradation efficiency (Ahmed et al., 2010b).

2.4.2. pH of the solution

pH is an important parameter as it dictates the surface charge properties of the photocatalyst (Gaya and Abdullah, 2008). pH plays an important role in photocatalytic treatment as it affects the charge of the catalyst particles, the aggregate sizing as well as the position of the conduction and valence bands (Umar and Aziz, 2013). The point of zero charge (PZC) of TiO_2 is 6.8, so below this value the surface is positively charged and above this it is negatively charged. Naeem and Feng (2009) explain that low degradation occurs at high pH and this is because the concentration of OH^- is higher in the solution,

thus preventing penetration of UV light from contacting the catalyst surface. This occurs since TiO_2 is amphoteric in aqueous solutions.

Saien and Nejati (2007) indicated that when Chemical Oxygen Demand (COD) in refinery effluent was the target pollutant, efficiencies of 63% and 61% were obtained for pH values of 5 and 6 respectively. pH is a major factor influencing degradation rate, however, the effect depends greatly on the reaction time involved. At short reaction times pH was found to have a more significant effect on degradation as compared to larger reaction times (Shahrezaei et al., 2012).

The importance of pH is further emphasized by Saien and Shahrezaei (2012) who explain that pH influences the pollutant molecule, the catalyst charge as well as the degradation mechanism and generation rate of the hydroxyl radical. Their work carried out when degrading organic pollutants achieved the best efficiency at a pH of 3. The degradation of refinery waste water organics with both TiO_2 and ZnO catalysts obtained the best degradation results at a pH of 4. During the degradation of phenol, it was observed that percentage phenol removal is greater under acidic conditions and when pH climbed above 7, a drastic decrease in efficiency from 82.42% to 65.12% was noted (Das et al., 2013). Phenol degradation was tested using TiO_2 under both solar and UV light irradiation. The pH ranged from 3 to 8 and it was noted that optimum pH for degradation under solar light was between 5 to 7 and the ideal pH for UV irradiated catalysis was 5 (Ahmed et al., 2010b).

Khan et al. (2015) denotes that the adsorption of anions is favoured when the pH is less than the point of zero charge. At low pH, positive holes are considered major oxidation species however at high pH hydroxyl radicals are considered the predominant species and would aid degradation (Habibi and Vosooghian, 2005, Noorjahan et al., 2003). The pH is known to affect the surface of titania by either protonation or deprotonation (Diya'uddeen et al., 2011). The reactions below explain the protonation and deprotonation process (Gaya and Abdullah, 2008).

$$Protonation \quad TiOH + H^+ \rightarrow TiOH^{2+} \tag{9}$$

$$Deprotonation \quad TiOH + OH^- \rightarrow TiO^- + H_2O \tag{10}$$

2.4.3. The Reaction Temperature

When the temperature increases it promotes the recombining of charge carriers and the desorption process of adsorbed reactants. This results in an increase in photocatalytic activity (Gaya and Abdullah, 2008). This further conforms to that of the Arrhenius equation as shown in Figures 2.11 and 2.12.

The rate equation for the reaction of two substances A and B

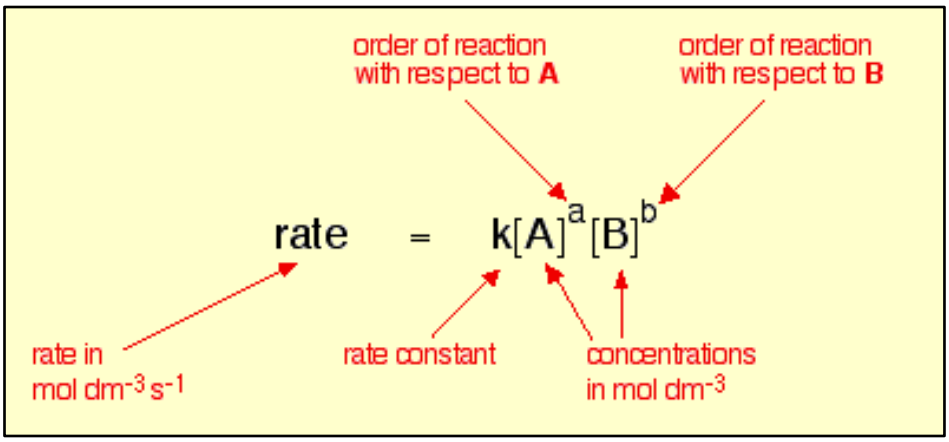

Figure 2.11: The rate equation (Clark, 2013)

The Arrhenius equation relating temperature and reaction rate

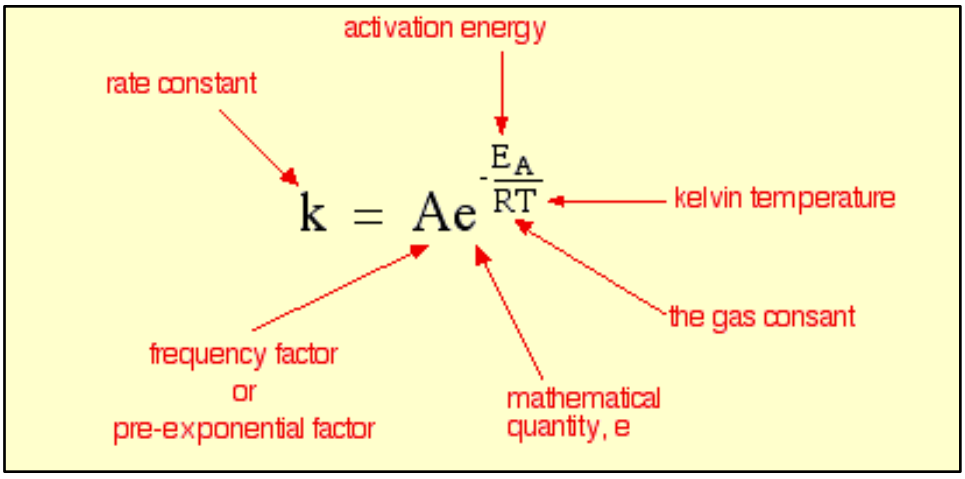

Figure 2.12: The Arrhenius equation (Clark, 2013)

The Arrhenius equation exhibits the above mentioned relationship indicating that the first order rate constant should increase linearly with $exp\left(\frac{-1}{T}\right)$ (Gaya and Abdullah, 2008).

Work conducted by Umar and Aziz (2013) on the degradation of organic pollutants indicates that an increased reaction temperature results in an increased reaction rate. This occurs provided the temperature is less than 80˚C with an ideal reaction temperature ranging between 20˚C and 80˚C. Degradation of refinery effluent also showed an increase in reaction rate when temperature was increased. Saien and Nejati (2007) indicated that an increase in temperature from 293K to 318K reduced the reaction time significantly as it was almost halved.

Similar trends were reported by Shahrezaei et al. (2012) on degradation of refinery wastewater using TiO_2 nanoparticles. Increasing the temperature resulted in the TiO_2 electron transfer in the valence

bond to that of a higher energy level thus facilitating electron hole production. Saien and Shahrezaei (2012) explained that by increasing the temperature of the solution from 20˚C to 45˚C it resulted in a decrease in run time from 100 minutes to 60 minutes. The above mentioned indicate that reaction temperature does play a key role in the photocatalytic degradation process.

2.4.4. Concentration of Pollutants

Several studies make mention of the concentration or nature of the pollutants and how this affects the TiO_2 reaction rate. Umar and Aziz (2013) explain that high pollutant concentration results in a decrease in photodegradation efficiency and causes deactivation of catalyst as the TiO_2 surface becomes saturated. Work carried out on phenol degradation indicates that a high initial concentration reduced the generation of hydroxyl radicals as there were fewer sites present for hydroxyl ion adsorption (Lazar et al., 2012). Phenol degradation with the use of ZnO catalyst also indicated similar trends on the effect of initial concentration on degradation. Figure 2.13 below illustrates the experimental findings for phenol degradation.

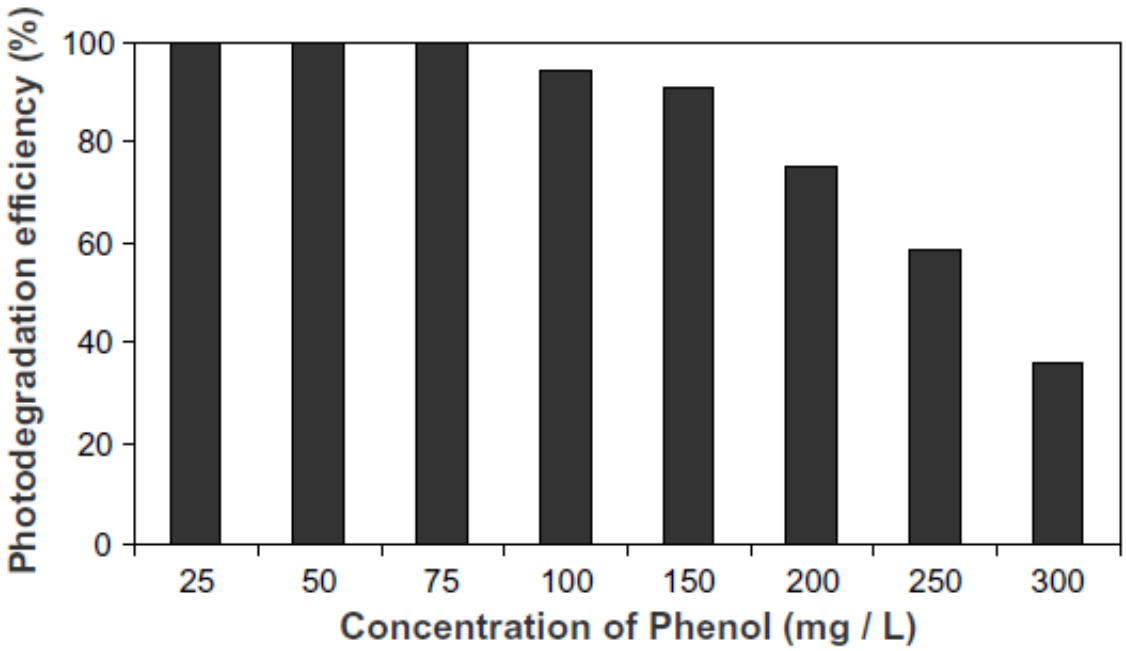

Figure 2.13: The effect of initial phenol concentration on photodegradation efficiency (Pardeshi and Patil, 2008)

The degradation efficiency was found to increase with an increase in initial concentration, however only up to a maximum initial concentration of 75 mg/L. Once this optimum concentration was exceeded, the degradation efficiency decreased considerably. Pardeshi and Patil (2008) explain that a greater phenol concentration results in more phenol adsorbed on the catalyst surface. Since reaction

time and catalyst concentration were kept constant, radical formation also remains constant and results in a decrease in OH^- and O_2 radicals attacking the phenol molecule.

A nanocomposite catalyst was used for phenol reduction and showed that the percentage removal of phenol decreased as the initial phenol concentration increased. Runs were carried out for 150 minutes and removal efficiencies of 85.18%, 83.71% , 82.5% and 77.94% were recorded for initial concentration dilution ratios of 1:3, 1:2, 1:1 and no dilution respectively (Diya'uddeen et al., 2011). When the initial concentration of a pollutant increases, for the degradation efficiency to also increase it would require a greater catalyst surface area made available (Neppolian et al., 2002).

Similar trends were observed when initial concentration of tartrazine was varied from 5 to 35 ppm and degradation efficiency decreased accordingly (Hashim et al., 2001). The degradation of COD was a focus point for Diya'uddeen et al. (2011) where it was highlighted that initial concentrations of 316.9 mg/L and 645 mg/L were used and the findings were that COD removal increased and decreased respectively under the same degradation conditions.

2.4.5. Presence of Inorganic Ions

Several inorganic ions such as magnesium, iron, zinc, copper, bicarbonate, phosphate, nitrate, sulphate and chlorides are present in most industrial wastewaters. Umar and Aziz (2013) explained that inorganic ions can affect the photodegradation rate of organic pollutants as they can be absorbed onto the surface of the catalyst. The effect of chloride, carbonate, nitrate and sulphate was investigated by Naeem and Feng (2009) and found that all the mentioned ions reduced photocatalysis as they behaved as hole scavengers and inhibited degradation. Figure 2.14 below exhibits the extent to which the ions affect degradation.

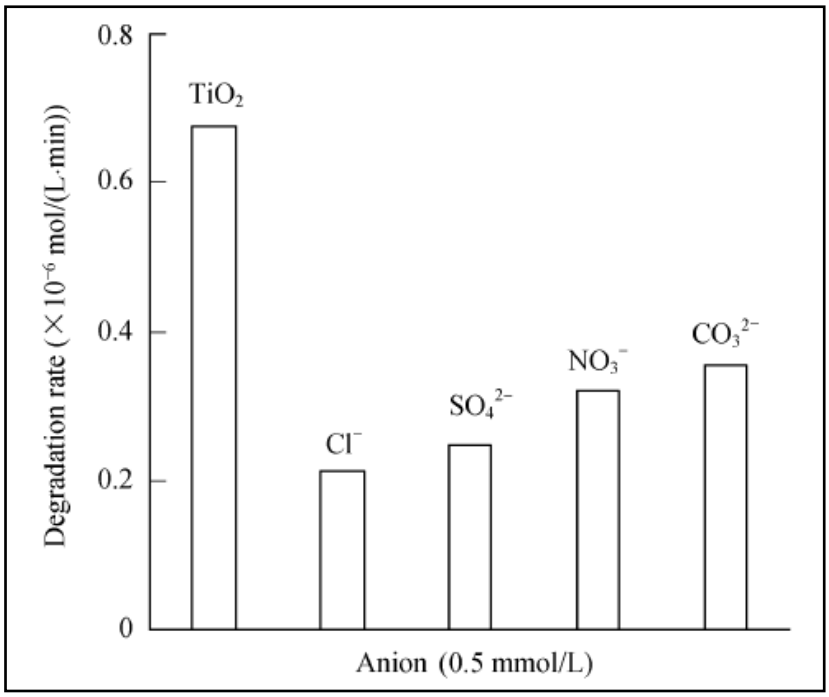

Figure 2.14: The effect of the presence of anions on phenol degradation rate (Naeem and Feng, 2009).

The figure above clearly indicates photodegradation rate is affected greatest by carbonates, nitrates, sulphates then chlorides respectively. Similar views were shared by Alrousan et al. (2009) for work aimed at reducing E.coli in surface water. Ahmed et al. (2010b) agree with the above mentioned trend, however also add that at times the sulphate radical anion can accelerate the reaction rate as well.

2.4.6. Effect of air flow rate on degradation

The air flow rate is a key component of photocatalytic degradation as it supplies oxygen for the advanced oxidation process to occur. The degradation of organic sulphides produced results indicating that as oxygen supply increased to a maximum of 5 ml/min, so did the degradation rate. It was also noted that when no oxygen supply was used, no degradation took place indicating that oxygen is of great importance (Habibi and Vosooghian, 2005). Photocatalytic oxidation of petroleum refinery wastewater was conducted by Corrêa et al. (2010) and suggests that air flow does not just enhance the oxidation process but also keeps the catalyst particles in suspension, thus allowing greater surface area for the reaction to occur.

During experimentation on the photocatalytic degradation of phenol, it was observed that the degradation rate was significantly higher with oxygen that without. Das et al. (2013) explained that oxygen acts as a photo generated electron scavenger, thus creating a superoxide radical and allowing more sites being available for electrons to be transferred to. Figure 2.15 below represents the data produced.

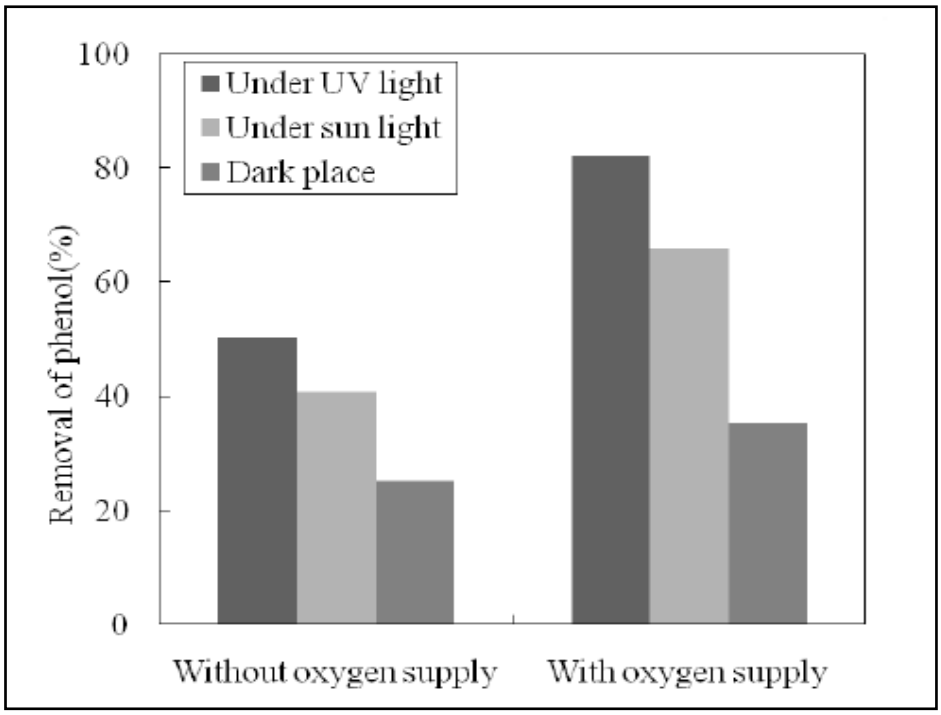

Figure 2.15: The effect of aeration on photocatalytic degradation of phenol (Das et al., 2013).

The figure above clearly indicates how important aeration is for the advanced oxidation process even in the presence of different irradiation sources.

2.4.7. Effect of Light Intensity on degradation

Light intensity is important in the photocatalytic degradation process as illuminating the catalyst particle with energy equal to or higher than its band gap, results in the lone electron being photoexcited and electron transfer then takes place (Umar and Aziz, 2013). Work carried out on phenol degradation increased light intensity from 15 W to 400 W and it was observed that the photodegradation rate increased accordingly.

Figure 2.16 below indicates the effect of light intensity on phenol degradation.

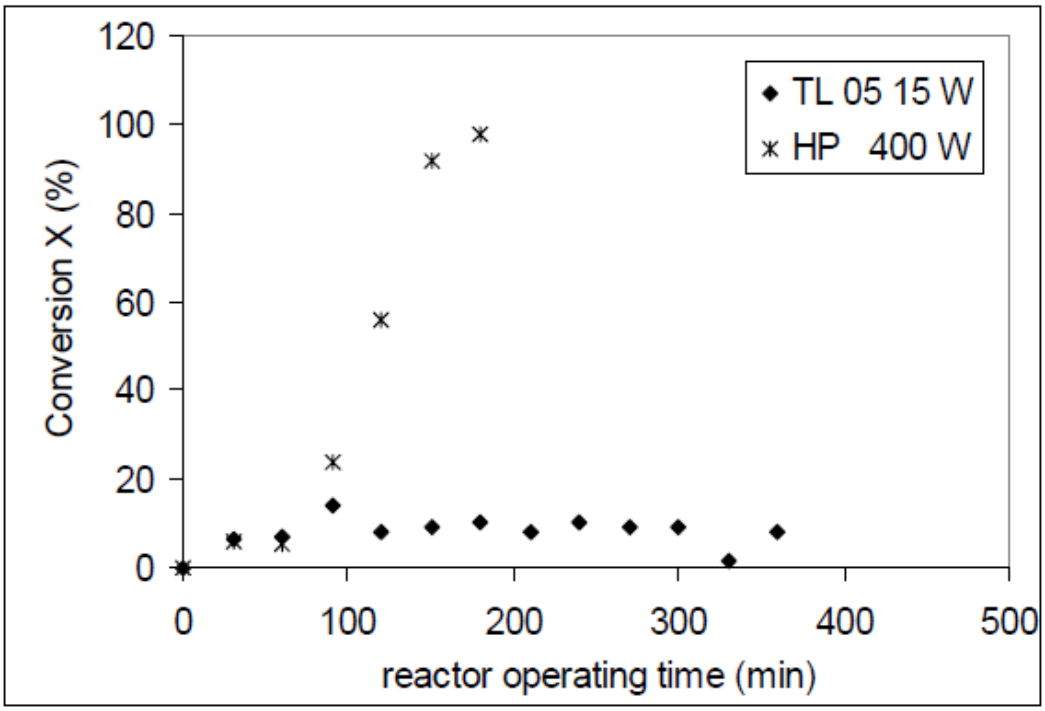

Figure 2.16: The effect of light intensity on conversion (degradation) of phenol (Laoufi et al., 2008).

It was observed at 400 W irradiation that 100% degradation was achieved in less than 4 hours as compared to 15 W yielding degradation of 15% over a very long irradiation time (Laoufi et al., 2008).

Photocatalysis can be conducted with the use of solar or UV light and Ahmed et al. (2010a) explained that with the sun producing 0.2 to 0.3 mol photons/$m^{-2}.h^{-1}$ which falls within the range of 300 to 400 mn (UV flux of 20 to 30 W/m^2) sunlight is a feasible option to drive the photocatalysis process. Vaiano et al. (2015) used UV and visible light sources for the degradation of Methyl Blue (MB).

Figure 2.17 below indicates the performance of degradation for each of the above mentioned sources.

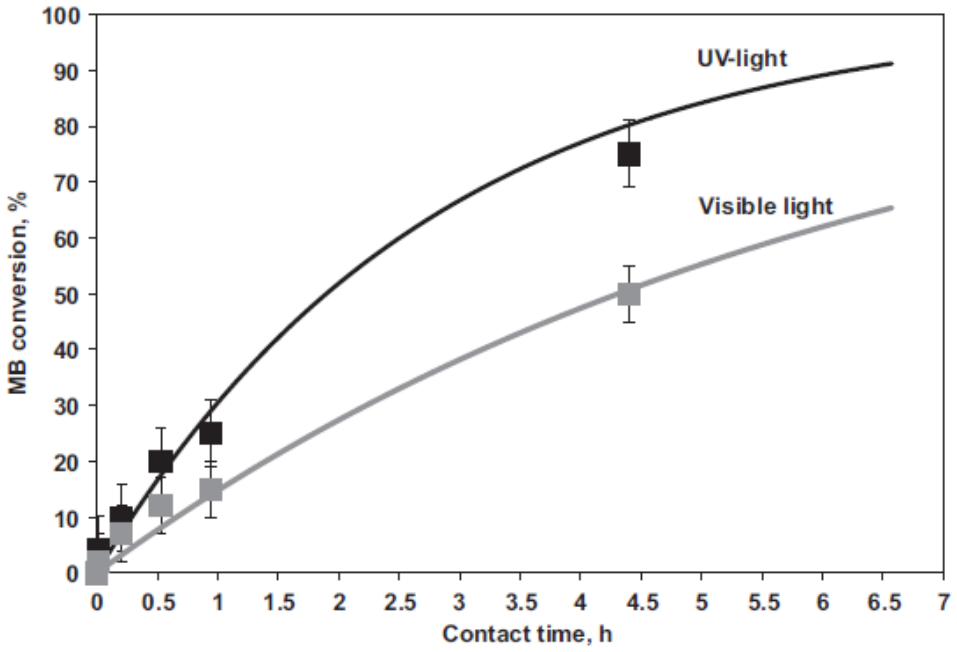

Figure 2.17: The effect of light source on conversion (degradation) of Methyl Blue (MB) (Vaiano et al., 2015)

The image above indicating the results produced yielded a much higher degradation when UV light was used compared to visible light. Diya'uddeen et al. (2011) mentioned that a non-linear relationship between light intensity and degradation exists. They further explain that an increase in degradation is associated with an increase in light intensity and this occurs as a result of an increase in the photon flux of electrons in the conduction band. Relationships highlighted in similar studies indicate that percentage degradation increased with the square root of incident light intensity (Diya'uddeen et al., 2011).

2.4.8. Effect of Reaction Time on degradation

A longer reaction time generally allows for better degradation efficiency as the oxidation reaction has enough time for greater conversion. Khan et al. (2015) conducted work on the photodegradation of organics in refinery wastewater and explained that a greater reaction time allows for more adsorption to occur. Radicals are needed to degrade the organics into intermediates which are then further degraded into CO_2 and H_2O.

Figure 2.18 below illustrates the effect of reaction time on degradation.

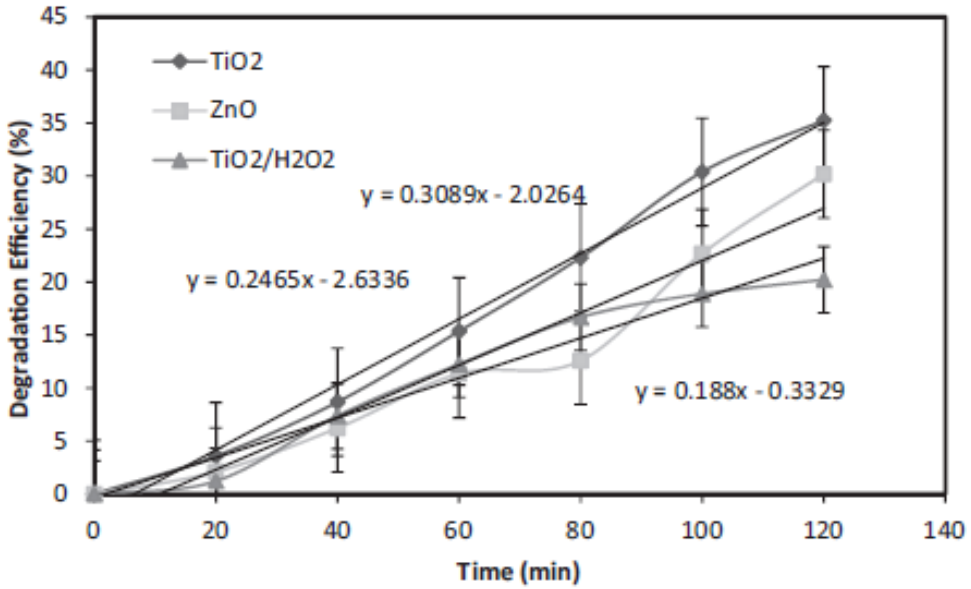

Figure 2.18: The relationship between degradation efficiency and time (Khan et al., 2015).

The result produced indicates the efficiency of TiO_2 as a photocatalyst as well as how the degradation efficiency increases over a period of time. Similar results were produced when phenol degradation was carried out. The distance of the light source from the reactor was also evaluated and the data can be observed in Figure 2.19 below.

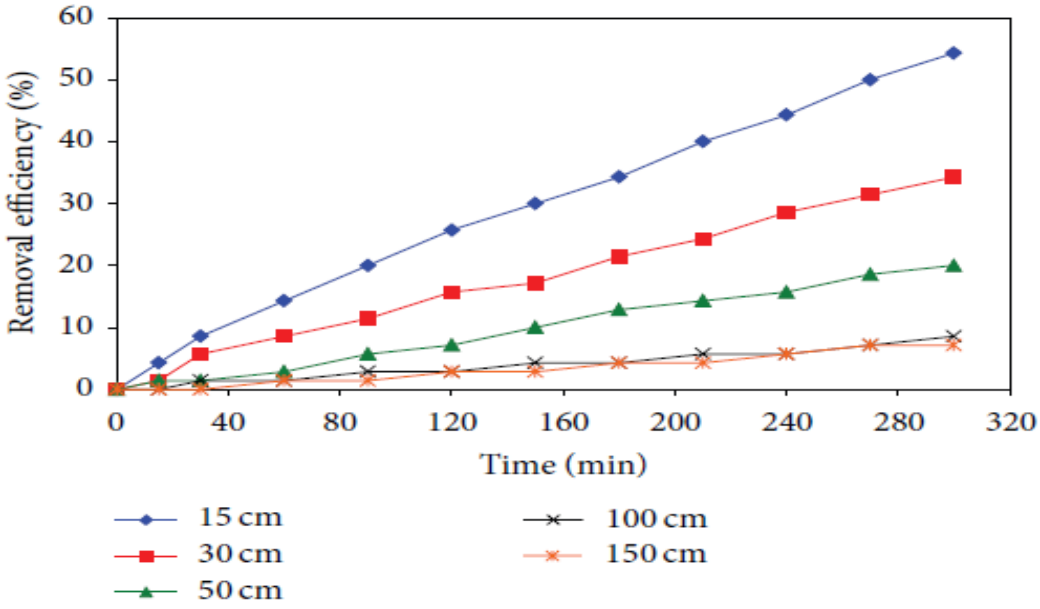

Figure 2.19: The relationship between phenol removal efficiency and time at several distances from the light source (Nickheslat et al., 2013).

The best removal efficiency was obtained with the light source being closest to the reaction vessel and this occurred at the greatest reaction time (300 min). As the light source moves further from the reaction vessel, the effect of reaction time on efficiency reduces significantly.

2.5. Design of Experiment (DOE)

Design of Experiment is a systematic approach taken by experimenters when attempting to analyse a process and determine the factors affecting the output of that process (Sunderarajan, 2000). At times it is described as a tool to identify cause-and-effect interactions where this information is used to manage process inputs with the aim of optimizing outputs (Figure 2.20). Bower (2017) explains that DOE is an important concept as strategically planned and executed experiments gives rise to a great deal of information relating the effect on a response variable to several factors.

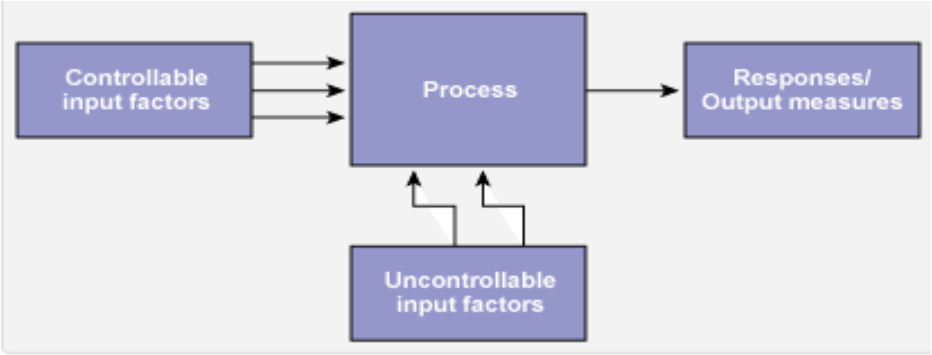

Figure 2.20: The relationship between process factors and responses (Sunderarajan, 2000)

Controllable Input factors: These are inputs that can be manipulated in an experiment or process (Bower, 2017).

Uncontrollable Input factors: These are inputs that may cause variability under normal operating conditions however may be controlled during experimentation with the use of blocking or randomization (More Steam, 2015).

Levels: The degree to which a factor is being varied (Sunderarajan, 2000)

Response or Output: Measurable outcomes that may potentially be influenced by the factors and their levels (More Steam, 2015).

DOE is applied in various aspects of engineering as it reduces the timeframe for development and design of processes, assists with current process optimisation and improves the reliability of processes by the manipulation of key variables (Dlamini, 2016, Sunderarajan, 2000). DOE allows for simple and efficient experimentation and analysis that allows the experimenter to observe simultaneous interactions of input factors on the process output (More Steam, 2015). The improvement of industrial

experimentation is crucial and should therefore consider the three principles of experimental design which are Randomization, Replication and Blocking (Antony, 2003).

Randomization: This deals with the sequence in which experimentation is conducted with the aim of eliminating the effects of unknown or uncontrolled variables (Bower, 2017).

Replication: The repetition of experiments using the same run combinations more than once, to allow the experimenter the ability to estimate the amount of random error (Sunderarajan, 2000).

Blocking: This technique assists with eliminating the effects of variation due to noise factors with the aim of improving experimental efficiency. It eliminates unwanted sources of variability (Antony, 2003)

Montgomery (2001) indicates that the key objectives of the experiment should include the following:

- Determination of which variables are most influential on the output response.
- Identifying where to set the most influential controllable inputs such that the output response is almost always near its desired value.
- Identifying where to set the most influential controllable inputs such that the variation in the output response is minimal.
- Identifying where to set the most influential controllable inputs so that the effects of the uncontrollable variables are minimized.

The table below indicates guidelines for designing an experiment.

Table 2.6: Guidelines for Designing an Experiment (Montgomery, 2001).

STEP	TASK
1	Recognition of and statement of the problem.
2	Choice of factors, levels and ranges.
3	Selection of the response variable
4	Choice of experimental design
5	Performing the experiment
6	Statistical analysis of the data
7	Conclusion and recommendations

2.5.1. One Factor at a Time (OFAT) Design

OFAT is regarded as one of the most common types of experiments (More Steam, 2015). It involves the upper and lower limits for each factor being established, then successive varying of each factor within its range while the other factors are kept constant at the baseline level (Montgomery, 2001). Once the experiments are concluded, graphs are generally produced to indicate how the response variable was influenced when varying each factor independently. Bower (2017) explains that the OFAT approach to experimentation does not give a holistic view of influential factors and how their simultaneous interactions affect the output response, thus making it an inefficient method. Dlamini (2016) indicates that an "Adaptive" OFAT design occurs when a succeeding run is devised from the outputs of all proceeding runs at their optimum condition. A representation of this approach can be seen in Figure 2.21.

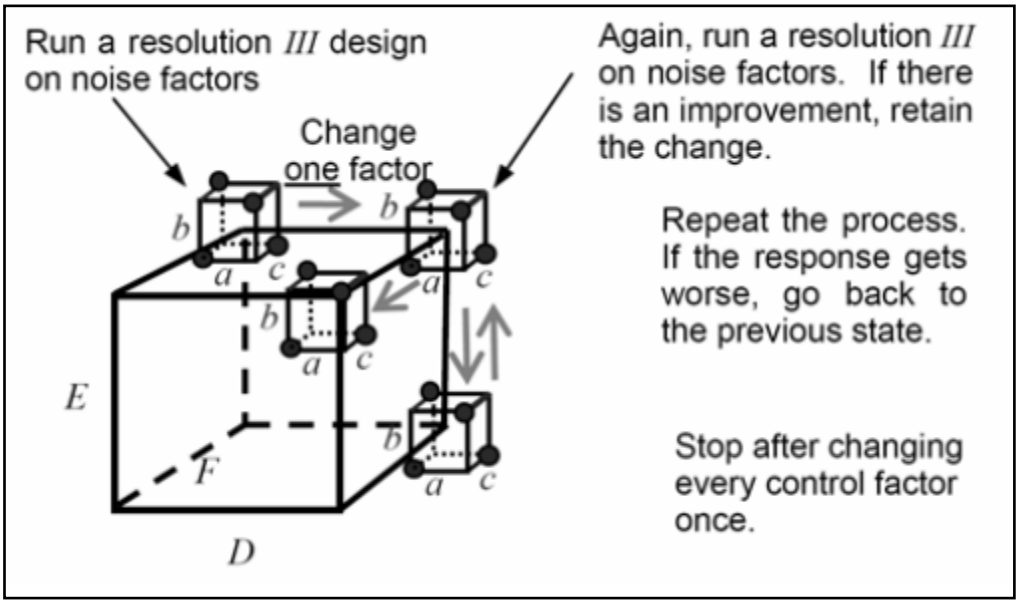

Figure 2.21: Adaptive OFAT applied to a process with three two-level factors (Frey and Sudarsanam, 2006)

Frey and Sudarsanam (2006) mention that OFAT is generally discouraged due to the following reasons:

- They require more runs to obtain the same precision as estimation.
- The interactions cannot be estimated.
- The optimal setting of factors can be missed easily.

Montgomery (2001) indicates clearly that the key disadvantage of the OFAT design strategy is that it fails to consider the possible interactions between various factors. One factor at a time experiments are less efficient as compared to methods based on a more statistical approach (More Steam, 2015).

2.5.2. Factorial Design Method

Factorial designs are a type of DOE that allows the experimenter the ability to identify several interactions in the process with the use of a minimal number of experiments (Stat-Ease, 2014). It is further indicated that using such a tool allows for a greater process understanding and the ability to identify areas where improvements can be made. More Steam (2015) mentioned that when a factorial design is conducted, each factor is tested at each level and in every possible combination simultaneously with other factors and their levels. This allows for the identification of all interactions. The N-level factorial design is a design where any factor has N levels of equal distance. The expression used is N^n where n is the number of factors (Gallina, 2009). The number of factors and number of levels determine the number of runs, as indicated in Table 2.7.

Table 2.7: The number of runs for a two and three level full factorial (More Steam, 2015)

Number of factors	Two level factorial (Runs)	Three level factorial (Runs)
2	4	9
3	8	27
4	16	81
5	32	243
6	64	729
7	128	2187
8	256	6561

As the number of factors approach 5 and beyond, the amount of experimental runs increases quite drastically and the experimenter would then need to select a fraction of the full factorial, to assist with reducing the number of runs (Dlamini, 2016). This is referred to as a fractional factorial design. The expression used for a fractional factorial design is N^{n-m} where N is the number of levels, n is the number of factors and m defines the fraction of the full factorial used.

The Two-Level factorial design is one of the most widely used DOE's as it has a simple layout with a direct analysis of the effects easily observed. The Two-level factorial is a subclass of the factorial design method. The smallest two factor factorial design is the 2^2 design, where two factors and two levels result in four treatment combinations (Gallina, 2009).

Sunderarajan (2000) mentioned that the two main advantages for the use of the Two-Factorial DOE method are:

- The experimental runs required are much smaller than most other designs.
- The interactions of factors are easily detected.

Figure 2.22 below shows the designs of Two-level factorial designs with two and three factors involved.

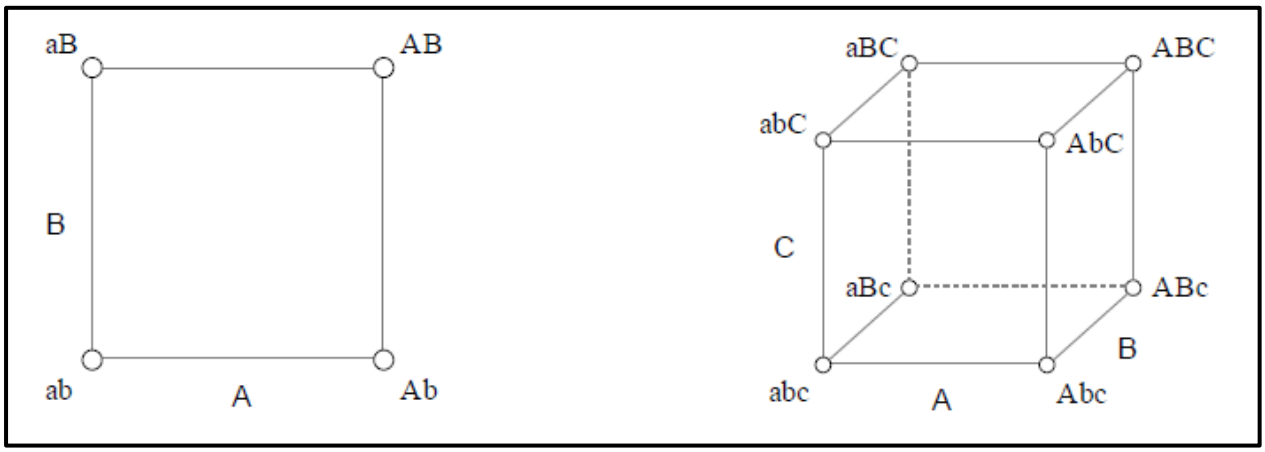

Figure 2.22: Factorial designs of 2^2 and 2^3 processes adapted from (Gallina, 2009).

Gallina (2009) further indicates that the influence of factors A and B on a two factor process can be evaluated using the following relationships:

$$A = \frac{Y_{Ab} + Y_{AB}}{2} - \frac{Y_{aB} + Y_{aB}}{2} \qquad B = \frac{Y_{aB} + Y_{AB}}{2} - \frac{Y_{Ab} + Y_{ab}}{2} \qquad (7)$$

Where Y represents the process response variable

The interaction with the simultaneous variation of factors A and B can also be evaluated using the relationship indicated below (Gallina, 2009).

$$AB = \frac{Y_{ab} + Y_{AB}}{2} - \frac{Y_{Ab} + Y_{aB}}{2} \qquad (8)$$

Another way of illustrating the relationship between a response and a set of process parameters involves the use of the regression model approach. A regression model can be used to predict the response for different process parameters at their optimum levels (Montgomery, 2001). The development of a regression model starts by determining the regression coefficients which is based on the unit change between the upper and lower level setting for a 2 Level process. Antony (2003) indicates that a regression model for factors at 2-levels is generally of the form:

$$Y = \beta_0 + \beta_1 x_1 + \beta_2 x_2 + \cdots + \beta_{12} x_1 x_2 + \beta_{13} x_1 x_3 + \cdots + \varepsilon \quad (9)$$

Where: Y is the output response

β_0 is the average response in a factorial design

β_1 and β_2 are the regression coefficients

β_{12} is the interaction between the process parameters x_1 and x_2

ε is the random error component

This response is then used to evaluate the interaction between the process variables and identify the optimum conditions for the process.

2.5.3. Response Surface Methodology

Myers et al. (2009) define Response Surface Methodology (RSM) as a collection of statistical and mathematical techniques used for the development, optimization and improvement of processes. RSM is a technique applied to several scenarios and particularly when processes with several input variables are influential on the performance of a process response (Shahrezaei et al., 2012). RSM allows for the optimization of unknown and noisy functions with the use of simpler approximating functions and designed experiments (Pakravan et al., 2015). Several methods are found under the RSM technique and Gallina (2009) explains that the three key activities of RSM involve the following:

- Design of Experiment
- Response surface approximation
- Optimization

A key component of RSM is its ability to create an approximation of a real unknown process with the use of an analytical model. Myers et al. (2009) indicates that the relationship between the process response and the controllable input variables allow for approximating the response functions as shown below:

$$Y = f(\xi_1, \xi_2, \dots, \xi_k) + \varepsilon \quad (10)$$

Where: Y represents the response

Function f depends on k input variables ξ_1 , ξ_2 ,..., ξ_k

ξ_1 , ξ_2 ,..., ξ_k are the controllable input variables

ε is the statistical error involved

Myers et al. (2009) mentioned that there is a close connection between RSM and linear regression models as polynomial models are linear functions of unknown parameters. The similarities in relationship equations are therefore inherent.

Gallina (2009) points out that a Response Surface Approximation (RSA) is created by fitting known values of a process response as indicated in Figure 2.23 below.

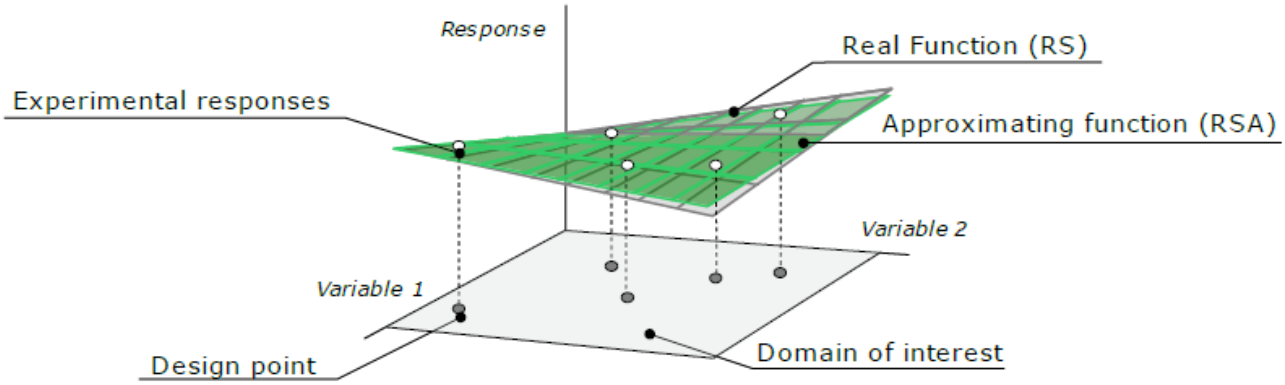

Figure 2.23: Response surface approximation for 2 input parameters (Gallina, 2009).

Once the model regression or response surface approximation is conducted, the optimization takes place and is generally referred to as steepest ascent optimization. These representations are usually in the form of a Response surface and contour plots as indicated in Figure 2.24 below for a First Order Model with interaction: $\eta = 50 + 8x_1 + 3x_2 - 4x_1x_2$

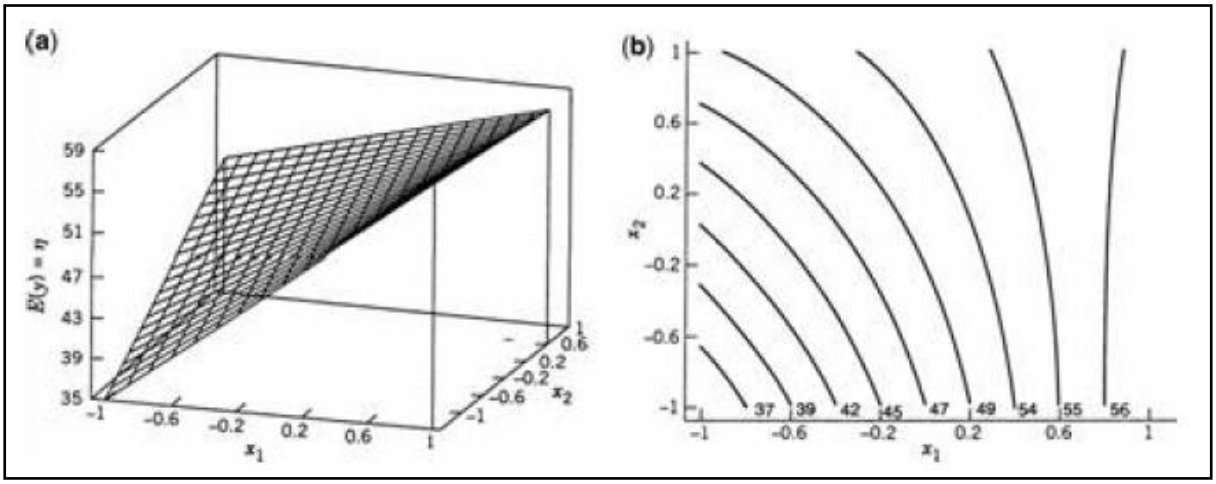

Figure 2.24: (a) Response surface for a first order model interaction. (b) Contour plot for a first order model with interaction (Myers et al., 2009).

The term of the model where variables x_1 and x_2 are multiplied, shows there interaction and brings curvature to the response function. In the case of two or more variables, a second order model is likely to be used and can be seen in Figure 2.25 for the following model: $\eta = 50 + 8x_1 + 3x_2 - 7x_1^2 - 3x_2^2 - 4x_1x_2$

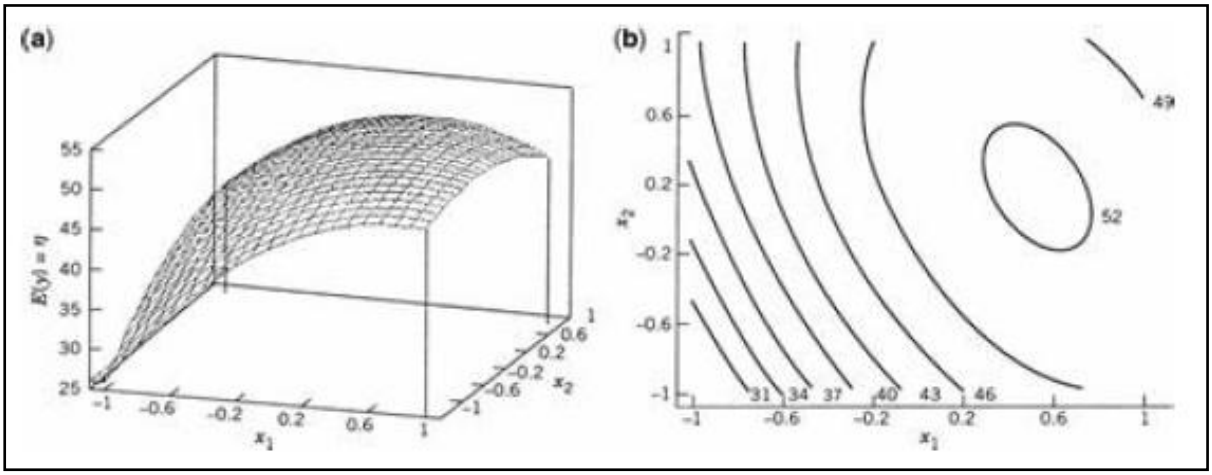

Figure 2.25: (a) Response surface for a second order model. (b) Contour plot for a second order model (Myers et al., 2009).

The response generated is flexible and is of a mount shape while the contour plot produced is of an elliptical nature. Dlamini (2016) mentions that the most commonly used RSM designs used are the Central Composite Design (CCD) and the Box-Behnken Design (BBD) and these are made possible by the addition of centre points to the first order design.

2.5.3.1. Central Composite Design (CCD)

Gallina (2009) explains that the CCD is developed on the basis of a Two factorial design with the addition of axial points which allow for the analysis of second order models. CCD has three different design points which are edge points of 2 levels (+1 and -1), star points (+α and -α) and $\alpha \geq 1$ which account for the quadratic effects and centre points (Leiviskä, 2013). Three variations of the CCD exist and these are the Circumscribed (CCC), Inscribed (CCI) and face centred (CCF). The generation of a CCD can be observed in Figure 2.26.

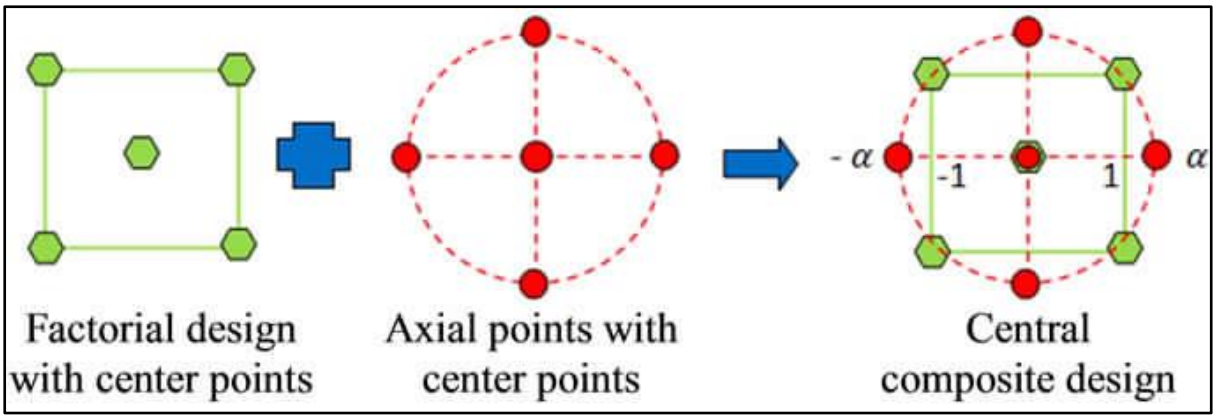

Figure 2.26: Generation of a CCD by augmentation of a factorial design and star points (Scientific Research, 2012)

Leiviskä (2013) indicates that the CCC is the original CCD and does testing at five levels. They consider the edge points, star points and centre points. For the CCI design, the star points set the design limits and the edge points are within the design range. In the CCF design, the star points are at the centre of each face of the factorial. The three variants of the CCD can be observed in Figure 2.27.

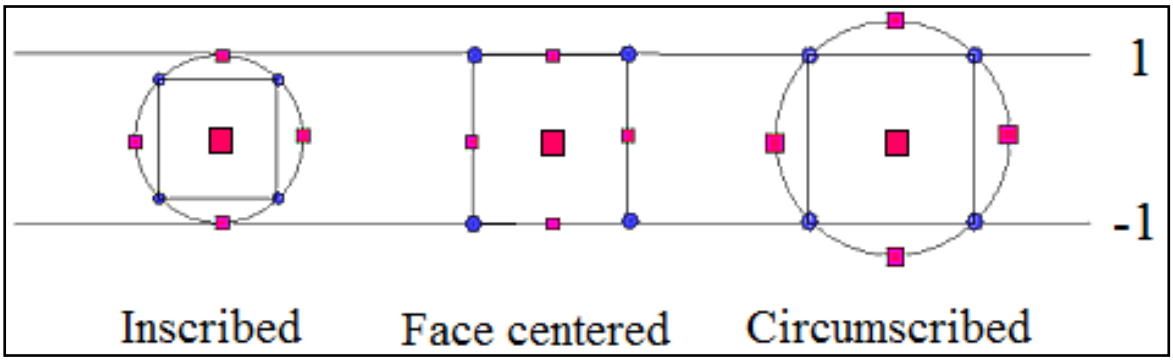

Figure 2.27: The three variants of CCD and the placement of their star points (Bajaj, 2016)

The CCD method is an efficient method as it modifies the factorial design with the addition of centre and axial points. This allows for effective optimisation when modelling the response variable (Khuri and Mukhopadhyay, 2010).

2.5.3.2. Box-Behnken Design (BBD)

The BBD is different to the CCD design as it does not have a factorial design component present. Leiviskä (2013) mentioned that the BBD is referred to as an independent quadratic design with treatment including the midpoint, centre and edges of the process plane. The BBD design is popular in industrial research as it is an economical design and allows for three levels for each factor, those being -1, 0 and 1 (Khuri and Mukhopadhyay, 2010). The BBD is known to have good design

properties namely little co-linearity as well as it being insensitive to outliers and missing data. The BBD default design aims to improve prediction by reducing the average prediction variance (Stat-Ease, 2014). A graphical representation of the BBD design can be observed in Figure 2.28 below.

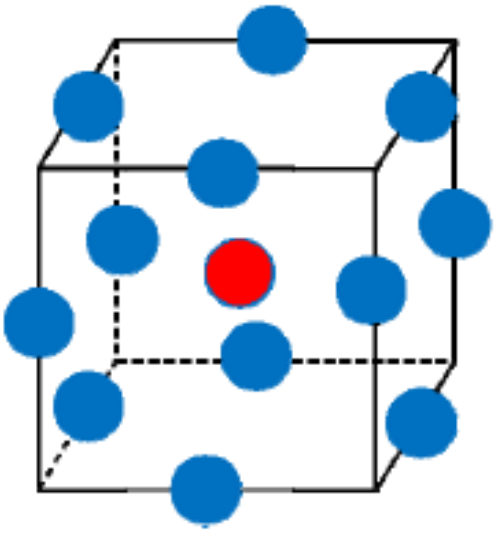

Figure 2.28: Graphical representation of the Box-Behnken design (Leiviskä, 2013)

The BBD is most commonly used for first and second order models as it does not contain a factorial design component.

2.5.4. Evaluation of Design Model

Analysis of the design allows for the determination of how adequate the process was modelled and assists with the accuracy. Myers et al. (2009) mentioned that for first order models not much curvature is present to assist with determining optimum output, however if a second order model is used this would allow easy identification of optimum conditions.

Regression adequacy testing is a key part of optimising a process and Gallina (2009) indicates that a means of efficient verification is by the analysis of residuals. The residual from an experiment is an important way of assessing the model adequacy. The residuals from a two factorial experiment are indicated below (Montgomery, 2009).

$$e_i = y_i - \hat{y}_i \quad and\ i = 1.2 \ldots . n \qquad (11)$$

Where: y_i is an observation

$\hat{y}_i$ is the corresponding fitted value from the regression model

The above indicating that the residual is the difference between the observations and the corresponding fitted values. Residuals have zero mean and determining their approximate average variance can be conducted using the equation below (Montgomery, 2009).

$$\frac{\sum_{i=1}^{n}(e_i-\bar{e})^2}{n-p} = \frac{\sum_{i=1}^{n} e_i^2}{n-p} = \frac{SS_{Res}}{n-p} = MS_{Res} \qquad (12)$$

Where n-p represents the degrees of freedom associated with the residuals.

Montgomery and Runger (2003) explain that an approximate check for normality can be done by developing a normal probability plot of the residuals. Once developed, the patterns for these residual plots are observed as indicated in Figure 2.29.

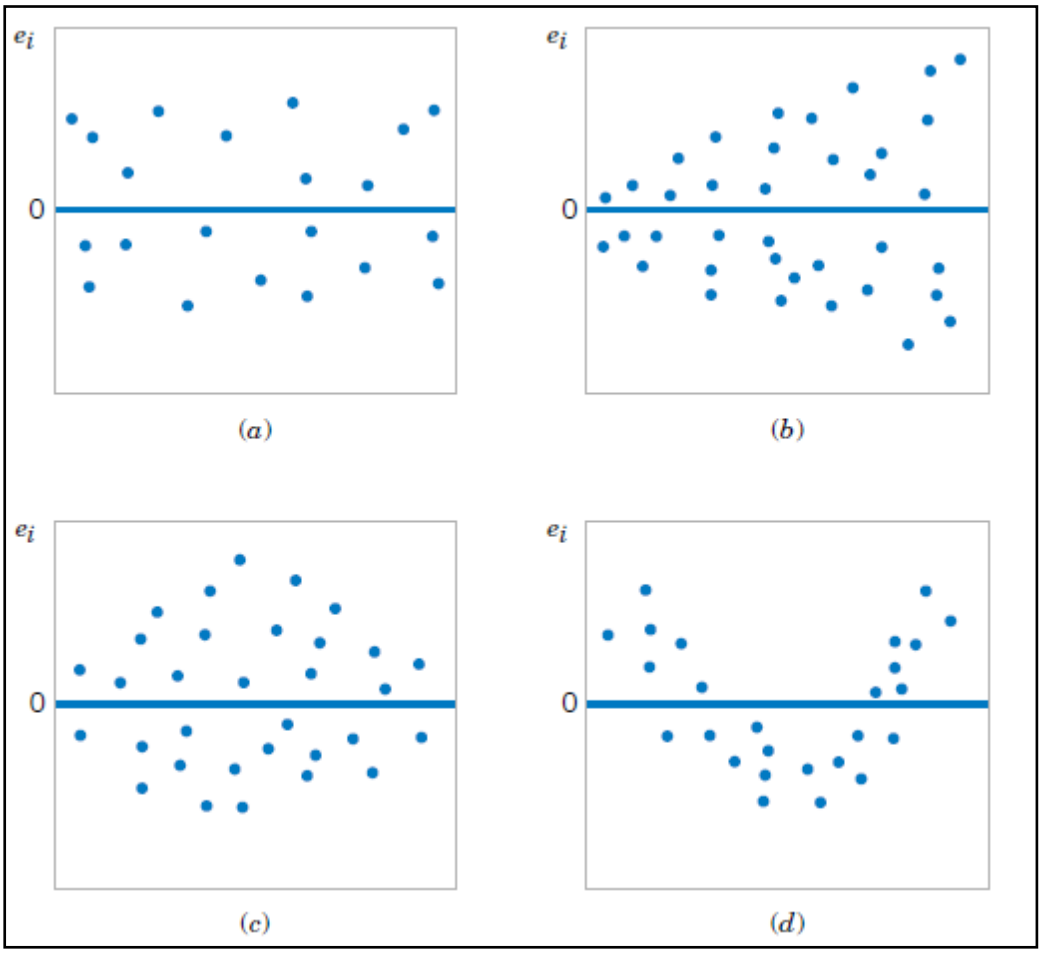

Figure 2.29: Patterns for residual plots. (a) Satisfactory, (b) Funnel, (c) Double bow, (d) nonlinear (Montgomery and Runger, 2003).

Residuals that are distinctly far outside the intervals indicate the possibility of an outlier. Montgomery (2009) mentions that outliers are important outcomes to be evaluated as they may indicate a simple data recording error or even a region where the fitted model is deemed a poor approximation of the true response surface. Normal probability plots are another means of determining error from the

distribution as a straight line is used to draw comparison. A normal probability plot can be observed in Figure 2.30.

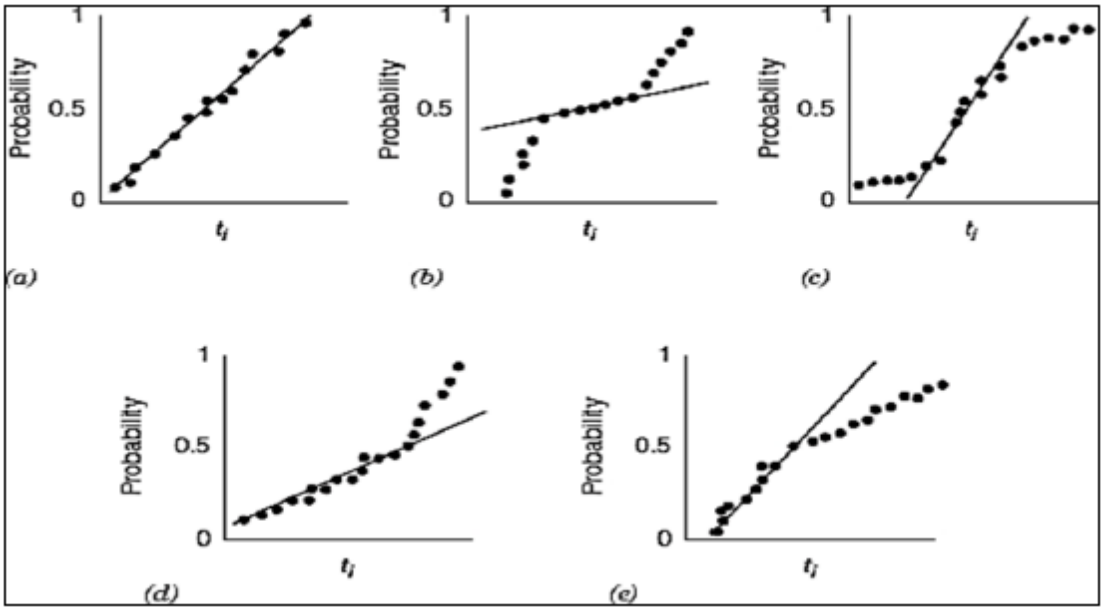

Figure 2.30: Normal Probability plots. (a) Ideal, (b) Light-tailed distribution, (c) Heavy-tailed distribution, (d) Positive skew, (e) Negative skew (Montgomery et al., 2012).

When conducting residual analysis, an important performance indicator is the residual vs. run graph and this can be observed in Figure 2.31.

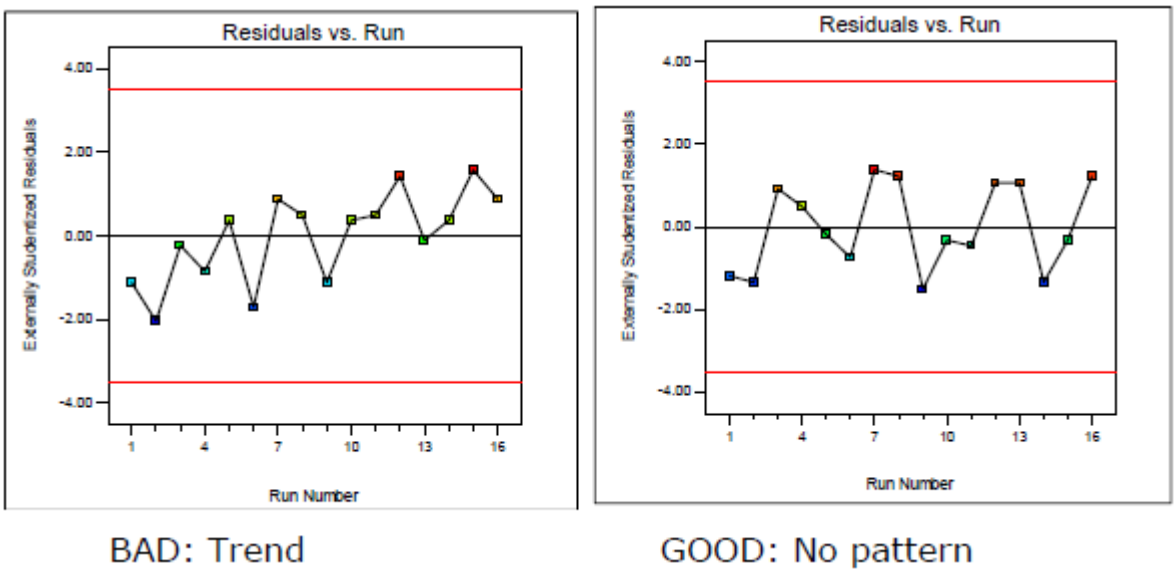

Figure 2.31: Residual vs. Run graph indicating experimental performance (Stat-Ease, 2014).

The residual vs. run graph allows for an observation of the performance of the experimental runs in its entirety. It is a key means in determining outliers as well as identifying certain runs which may be

affecting the data and model fitting. Should a run be significantly inconsistent, it can be easily identified in this plot and even redone should the need arise.

When evaluating the prediction capability of a model, the predicted vs. actual graph is a key tool (Figure 2.32).

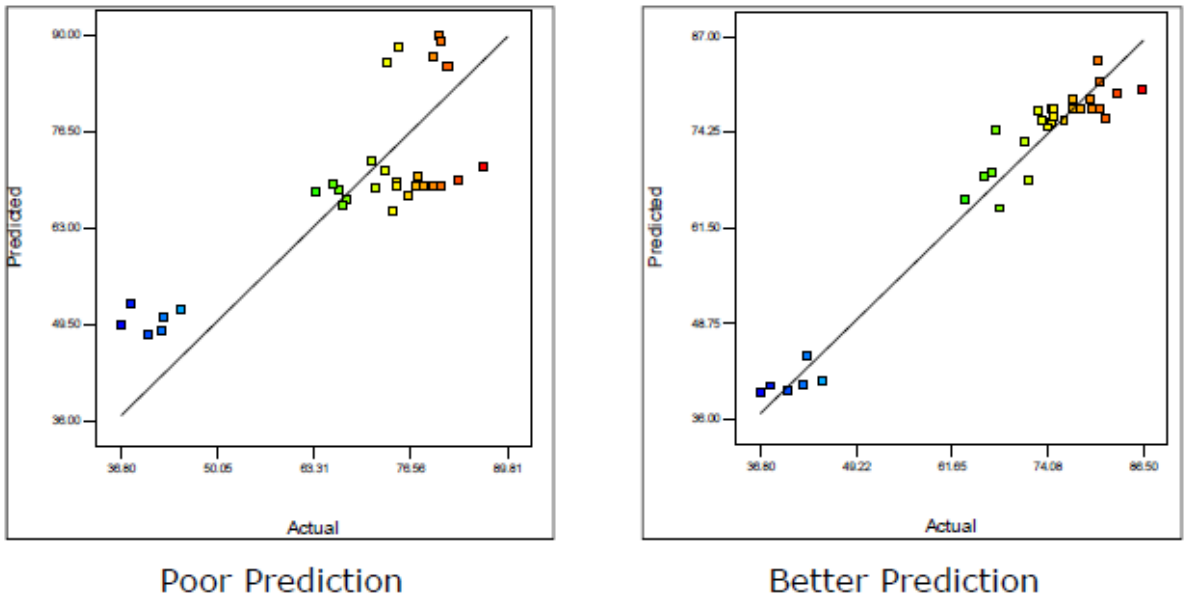

Figure 2.32: Predicted vs. actual plot for evaluation of model (Stat-Ease, 2014).

The predicted vs. actual plot allows for the evaluation of the prediction ability of the model. Based on the scatter of residuals, the analysis may highlight areas where the model is more likely to over or under predict. This plot also indicates the data range at which the model will predict well and between what ranges there are chances of over and under prediction (Stat-Ease, 2014).

When analysing results, the half-normal plot is used to assist with selection of a model. The model selected is then checked with the use of Analysis of variance (ANOVA). The model significance is determined with the use of the *F* test. For the *F* test, when a *P*-value of less than 0.05 is obtained, it indicates that the model is significant. *P*-values greater than 0.1 imply the model is not significant. The *F* test is important as it also assists with model reduction, provided it does not affect hierarchy. The adequate precision check is a signal to noise ratio that ensures the significant output result is genuine and is not greatly affected by noise.

Adequate precision can be obtained using the formula below (Stat-Ease, 2014):

$$\left[\frac{max\,(\hat{Y})-min\,(\hat{Y})}{\sqrt{\overline{V}(\hat{Y})}}\right] > 4 \qquad \bar{V}(\hat{Y}) = \frac{1}{n}\sum_{i=1}^{n} V\,(\hat{Y}) = \frac{p\sigma^2}{n} \qquad (13)$$

Where: p = Number of model parameters

σ^2 = Residual MS from the ANOVA table

n = Number of experiments

It is advisable that the adequate precision value be greater than 4, to ensure an adequate signal and the model can therefore be used to navigate the design space (Stat-Ease, 2014).

CHAPTER 3: METHODOLOGY

3.1. Introduction

A synthetic feed was developed to represent crude refinery effluent. This feed was then charged into a glass reaction vessel. Oxygen was sparged from the base of the vessel which assisted the advanced oxidation process (AOP) and allowed for the titania catalyst particles to be kept suspended in solution. Analysis was conducted on the feed and products once the reaction was completed. This was then compared to determine how efficient the degradation process was. Tests conducted included the evaluation of oil in water, phenols, pH and sulphates. A local crude refinery effluent was also tested to observe the effectiveness of photocatalytic degradation and to gauge how well it could reduce oil and phenol content.

3.2. Equipment and chemicals used

The experimental runs were conducted in a glass reaction vessel of 1 litre volume. A sparger was positioned at the base of the vessel and this was made of 4.5 mm silicone tubing. The sparger had pin holes that were 0.5 cm apart and the length of the sparger was 9 cm. The air was supplied by a DARO Twin aquarium air pump which had a double outlet and a high and low flow rate setting. Two air pumps were used to service the four reaction vessels used. All tubing used for the supply of air was 4.5 mm silicone tubing. Refer to appendix A-1 and A-2 for experimental setup.

The irradiating light source used was a radiant fluorescent T8 blacklight blue bulb of 18 W. This was used to activate the TiO_2 catalyst for the advanced oxidation reaction. The TiO_2 catalyst type used was Sachtleben RKB6 which was a rutile form of TiO_2 supplied by Huntsman Tioxide. The catalyst particles consisted of 94% TiO_2 with a particle size of 0.23 mirons.

3.3. Range Selection for variables

The key variables involved in the photocatalytic reaction were catalyst concentration, run time and air flow rate. Catalyst concentration was extensively reviewed in literature and it was observed that once Titania concentration went above 9 g/L it resulted in a downward trend on degradation. Catalyst concentrations below 2 g/L showed no significant degradation. The aim was to obtain the maximum degradation at the lowest possible catalyst concentration and the range of 2, 5 and 8 g/L was then selected. Run time generally ranged from 30 mins to 4 hours when conducting a photocatalytic reaction under UV irradiation. Given the degradation being taken on refinery effluent which continuously feeds into the effluent plant, it was not advisable to go above 90 minutes reaction time as a larger reaction time is not able to be achieved given the large effluent flow rates. The range of 30, 60 and 90 minute reactions were then conducted. Air flow is responsible for feeding the AOP with oxygen and allowing the catalyst particles to remain fluidised and provide maximum surface contact

for degradation. The aquarium air pump selected had a high and medium setting. The high and low flow rates were used and the medium was obtained by restricting flow at the high rate with a control valve. Drop rates using the inverted cylinder method were conducted to ensure flow was accurate. The air flow was then ranged from 0.768, 1.11 and 1.48 L/min.

3.4. Calibration of the air pump

The inverted cylinder method was used to determine the high and low air flow rates. These flow rates together with a control valve were used to obtain the medium air flow rate. The details for determining the flow rates can be found below:

Pump Setting - High (Control valve fully opened- 12 turns)

Air flow rate = 24.6 ml/sec = 1.48 L/min

Pump Setting - Low (Control valve fully opened- 12 turns)

Air flow rate = 12.8 ml/sec = 0.768 L/min

Medium flow rate

Midpoint = 12.8 + 5.9 = 18.7 ml/sec = 1.12 L/min (target value)

The control valve was then manipulated to obtain a flow close to the midpoint value:

Table 3.1: Valve position selection of air flow rate

Attempt	Valve Position Open	Flow rate ml/sec	Flow rate L/min
1	2 turns	12.5	0.75
2	3 turns	19.8	1.19
3	2.5 turns	18.5	1.11 Selected

Attempt 3 produced a flow rate very close to that of the medium flow rate and was then selected.

The diagram below indicates the setup for the inverted cylinder method.

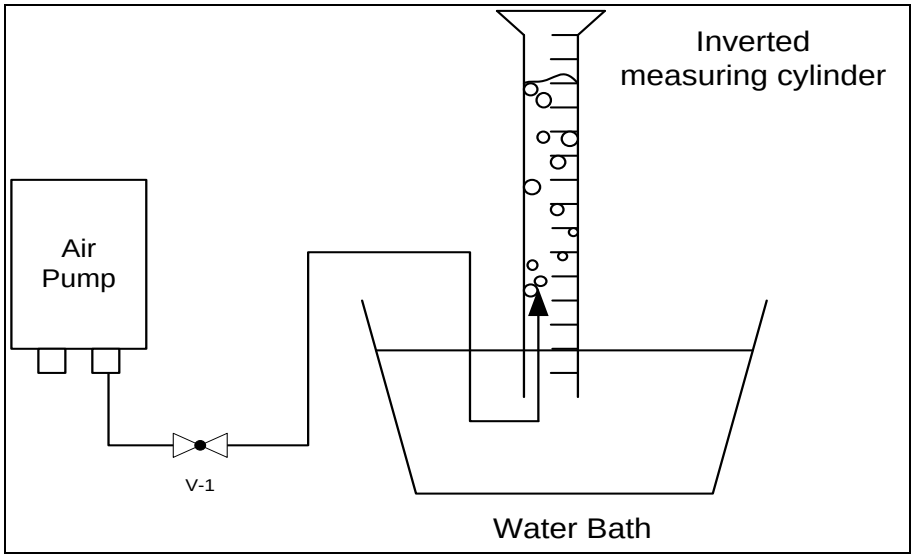

Figure 3.1: Diagram of equipment setup for the inverted cylinder method.

3.5. Making up of the synthetic feed

The refinery effluent matrix comprises of largely water with contaminants present in it. Municipal water was used and spiked with 3 ppm phenol and 40 ppm motor vehicle oil. Phenol crystals and Powerglide SAE40 Motor oil was used and stock solutions of 10000 ppm were prepared. These stock solutions were then spiked into the municipal water to prepare the synthetic feed of 3 ppm phenol and 40 ppm. Municipal water already contains approximately 22 ppm of sulphates and this was monitored during the degradation process. Refer to appendix B-1 for expected feed composition prior to mixing.

Analysis of municipal water supply from the 1st February to the 22 March 2017 was used to determine the other components in the water that would contribute to making up the synthetic effluent. Once the feed was developed, analysis of the feeds took place and there compositions determined. Two feeds were made as they were produced in 20 litre batches. The compositions of the feeds are indicated in Tables 3.2 and 3.3.

Table 3.2: Composition of feed 1

Component	Value
Oil in water (ppm)	40.13
Phenol (ppm)	3
Phosphate (ppm)	0.6
Calcium hardness (mg/L as $CaCO_3$)	37
M-Alkalinity (mg/L as $CaCO_3$)	77

Total Dissolved Solids (TDS) (ppm)	233
pH	7.13
Iron (ppm)	0.06
Chlorides (ppm)	99
Sulphates (ppm)	28
Silica (ppm)	6

Table 3.3: Composition of Feed 2

Component	Value
Oil in water (ppm)	39.6
Phenol (ppm)	3
Phosphate (ppm)	0.6
Calcium hardness (mg/L as $CaCO_3$)	37
M-Alkalinity (mg/L as $CaCO_3$)	77
Total Dissolved Solids (TDS) (ppm)	233
pH	7.13
Iron (ppm)	0.06
Chlorides (ppm)	99
Sulphates (ppm)	28
Silica (ppm)	6

3.6. Chemical Analysis Procedure

3.6.1. Oil in water (OIW) Test Method

The industrial effluent is agitated with Dichloromethane. The extract is then collected in a weighed flask and the solvent is evaporated on a water bath. The oil residue is then weighed and calculated based on the volume of sample taken.

Apparatus

- Separating funnel of 1 litre volume
- 250 ml flat bottom flask
- 100 ml measuring cylinder
- Glass funnels
- Steam bath

- 250 ml conical flasks
- Oven
- Aluminium foil
- Desiccator

Reagents used

- Dichloromethane
- Sodium Sulphate (Anhydrous)

Procedure

- 250 ml of sample was transferred into the separating flask (Figure 3.2).
- The sample bottle was resealed and shaken vigorously before transferring the remaining sample into the separating flask.

Figure 3.2: Separating flasks with industrial effluent during dichloromethane extraction.

- 25 ml of the dichloromethane was then added into the empty sample bottle, resealed with the bottles original cap and was then shaken. Pressure was released as required and any oil adhering to the bottle was then rinsed out.

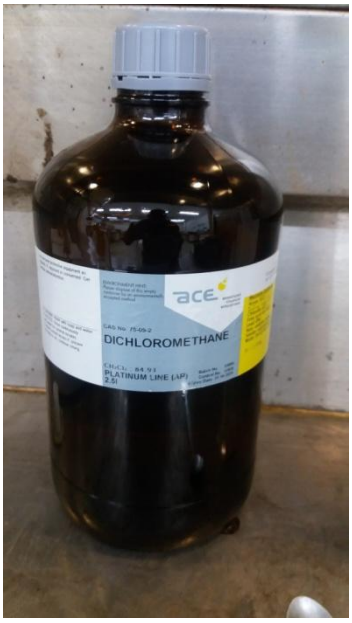

Figure 3.3: Dichloromethane used for extraction of oil from water.

- This dichloromethane (Figure 3.3) from the original sample bottle was then added to the separating flask.
- The rinsing procedure was then repeated with a further 25 ml of dichloromethane and this was also added to the separating flask.
- Stopper the separating funnel and shake for 2 minutes, releasing pressure as required.
- The solvent layer was allowed to separate and run off carefully into the dry 250 ml conical flask.
- The extraction step was then repeated once again by adding 25 ml of dichloromethane, stopper the funnel and shaking it and releasing pressure as needed. Once again the solvent layer was run off into the conical flask.
- The final extraction step was then done with the use of 20 ml of dichloromethane and the solvent layer then transferred to the conical flask.
- About 2 grams of granular anhydrous sodium sulphate (Figure 3.4) was then added to the combined extracts in the conical flask, swirled and the neck of the flask then covered with aluminium foil and allowed to stand for 30 minutes.

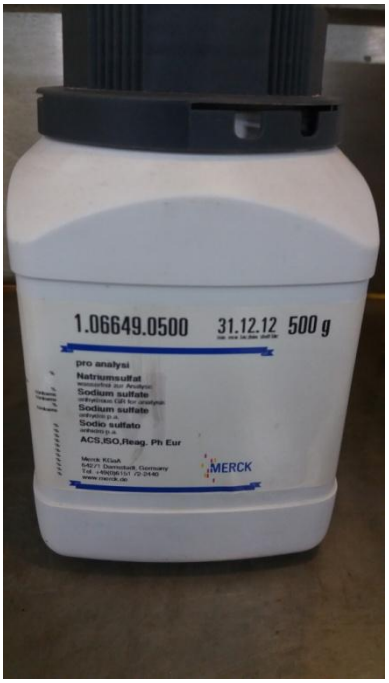

Figure 3.4: Anhydrous sodium sulphate added to the combined extract.

- The extract was then filtered into a weighed flask with the use of a Phase Separator (GE Silicone treated filter paper) and a glass funnel. Figure 3.5 presents the phase separator used.

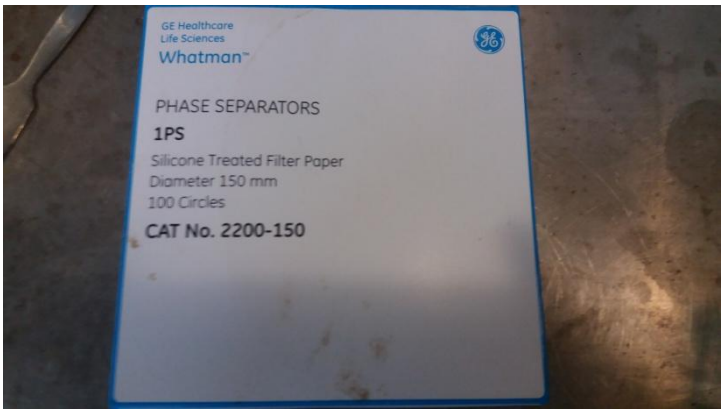

Figure 3.5: GE Whatman phase separators used to filter the extract for boiling.

- The conical flask was then rinsed with 10 ml of dichloromethane and passed though the filter.
- The flask containing the filtered extract was then placed on a boiling water bath under the fume hood to evaporate the solvent (Figure 3.6).

Figure 3.6: Evaporation of Solvent in the fume hood.

- Once evaporation was completed, the solvent vapour blanket was blown out with the use of compressed air.
- The exterior of the flask was then wiped with a dry cloth and then placed in a desiccator for 30 minutes before it is weighed (Figure 3.7).

Figure 3.7: Desiccator used to cool the flask with oil.

Calculation Procedure

The amount of oil present in water is determined by the formula below with the outcome being ppm of oil in water.

$$ppm\ Oil\ \left(\frac{mg}{L}\right) = \frac{(Mass\ of\ flask + Oil\ extract - Mass\ of\ flask) \times 1000}{Volume\ of\ sample\ (L)} \qquad (14)$$

3.6.2. Phenol content Test Method

Phenol was tested with the use of the ThermoFisher- Gallery Discrete Analyser.

Figure 3.8: ThermoFisher Gallery Discrete Analyser used for phenol testing (Thermo Fisher SCIENTIFIC, 2017)

Procedure

Operation

- Switched the computer on and switched power on to the Gallery machine.
- Logged onto the computer as a routine user.
- Loaded cuvettes and then performed a start up from the home screen.
- Inserted reagents (F3). There were 3 Reagent racks available. Defined the reagent positions from the drop down window.
- Test Methods were then selected (F3).
- To see what was required on the analyser to run a method, the test status was checked and this gave details as to what needed to be inserted into the machine eg. reagents, standards and QC's.
- QC's and standards were loaded on the same rack. It was required that QC's be loaded in 7 ml tubes.

Programming the sample rack

- There were three sample racks. The calibrator and control ID's were then entered.
- The rack was then selected on screen and placed into the analyser when opened.

- Selection of analysis (F2) for each sample took place. The specific tests as well as desired dilutions were selected as required.
- Then returned back to the home page (F1) and prepared to start a run.

Programming the reagent rack

- Selected one of the three racks to be used as a reagent rack.
- Clicked on the empty rack position and then selected the desired reagent from a drop down menu.
- Inserted reagent into the analyser, pressed the button on the front of the analyser under the right side green draw. The button flashed blue followed by a click.
- The lid was then lifted, the reagent rack inserted and the lid clicked closed.

Calibration of the method used

- F4 was clicked to initiate calibration
- Clicked Cal or QC selection.
- For the Calibration, the tests to be calibrated were selected amd then click calibrate on screen.
- Then click (F1) and return to home page and prepare to start a run.

Conducting a run on the sample rack

- Clicked (F2) to identify the rack for testing. Filled the gallery with approx 5 ml of sample and position on the sample rack.
- Clicked on each sample in the onscreen gallery provided. Then added identity tags so the actual sample rack sample positions match the on screen display.
- Once the sample was selected, clicked New and added the test method to be used to test that specific sample.
- For test duplicates, select the same test twice for the specific sample requiring a duplicate result.
- To perform a re-calibration press Re-run.
- Then clicked (F2) for a report and selected Report all for the final results to be displayed.

Shut down Procedure

- Highlighted the desired racks then clicked remove rack until all racks are removed.
- Clicked removed all reagents (F3), selected racks and removed them.
- Inserted wash water onto a sample rack, then insert this rack into the analyser and clicked (F1) to return to the home page.

- Clicked standby and started the standby procedure. Once this was completed, the rack of wash water was removed.
- Clicked (F5) for maintenance options, then selected the action tab.
- The data was then saved, inserted a storage device and saved onto device. Cleared out the daily file which then moves this data into the archives folder.

3.6.3. Sulphates Test Method

Sulphates were tested with the use of a HACH DR890 Colorimeter (Figure 3.9). The colorimeter, a 25 ml vial and a powder pillow of reagent called SulfaVer 4 was used.

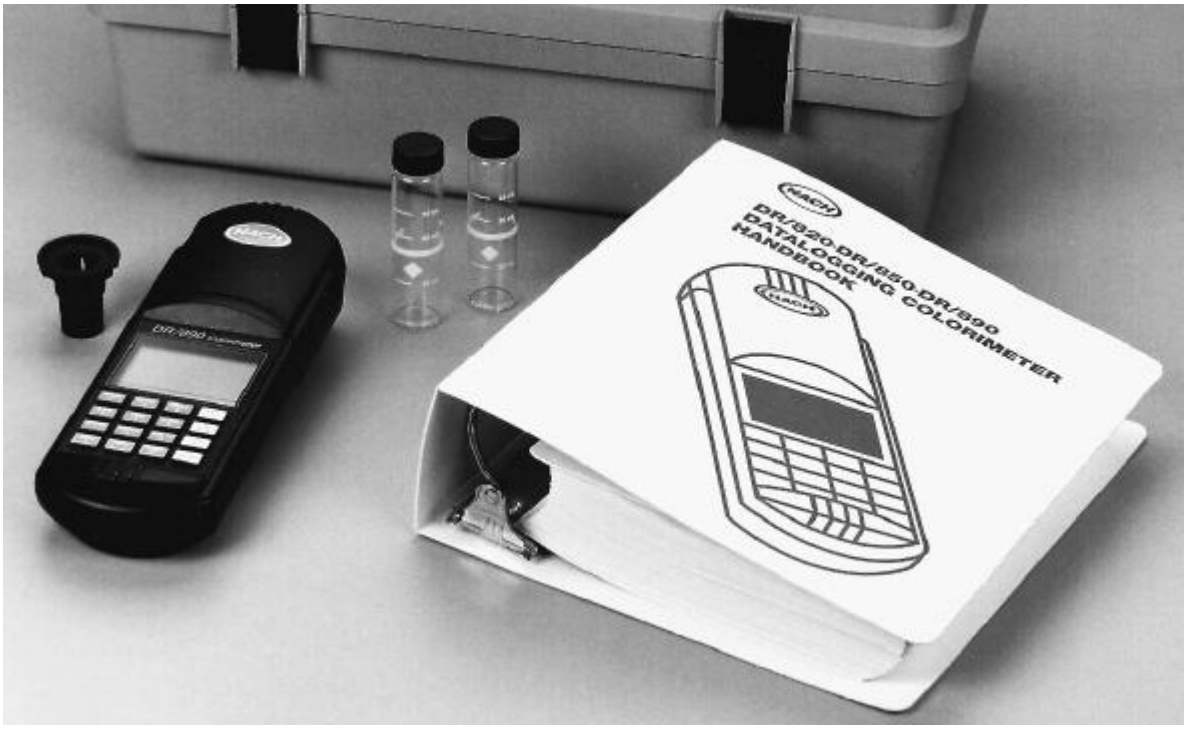

Figure 3.9: HATCH DR890 Colorimeter.

Procedure (HATCH DR 890 Colorimeter procedures handbook)

- Switch the DR890 colorimeter on and the PRGM button followed by 91 which is the sulphate program number.
- The display then shows mg/L, SO_4 and the ZERO icon.
- Fill a clean sample cell with 10 ml of sample.
- Add the contents of one SulfaVer 4 Sulphate reagent powder pillow into the sample cell, fasten the cap onto the cell and then invert the cell to mix the sample and reagent.
- Press the TIMER button and a 5 minute timer is shown on the screen. Then click ENTER to start the timer which times the 5 minute reaction period. Allow the vial to stand while being timed.

- After the timer beeps, fill a second vial with 10 mL of the sample and this is used as the blank.
- Place the blank into the sample folder and tightly cover the sample cell with the cap.
- Then press ZERO and the curser then moves to the right and will display 0 mg/L SO_4.
- Within 5 minutes after the sample beeps, place the prepared sample into the cell holder and tightly cover the vial with the cap.
- Press READ and the curser moves to the right then displaying the result in mg/L SO_4.

3.6.4. pH Test Method

pH of the feed and outputs of the Photocatalytic reactor were tested to ensure they do not exceed environmental limits as well as to evaluate the effectiveness of the treatment. A HANNA HI8314 pH meter was used (Figure 3.10).

Figure 3.10: HANNA pH meter.

Calibration Procedure (Instrument Manual)

It was important that the instrument be calibrated frequently. The instrument should be recalibrated whenever the electrode is replaced, a minimum of once a month, after intensive chemical testing and where extreme accuracy is required.

Preparation

Pour out small quantities of pH 7.01 and pH 4.01 buffer solutions into clean beakers. To ensure accurate calibration, two beakers were used for each buffer solution as one would be for rinsing and the other for calibration. This helped minimise contamination of buffers. To obtain accurate readings, pH 7.01 and pH 4.01 buffers were used when the sample being tested was of acidic nature and pH 7.01 and pH 10.01 buffers were used for alkaline measurements. All samples were of alkaline nature.

Procedure

- Connected the pH electrode and switched the meter ON.
- Removed the protective cap from the electrode, rinsed the tip with some pH 7.01 buffer, stirred gently and waited until thermal equilibrium was reached.
- Pressed CAL. The calibration buffer was recognised and the menu for offset and slope calibration was then displayed.
- Adjusted the OFFSET trimmer on the lower left corner of the instrument until the pH value shown matched that of the buffer at the specific temperature.
- Then pressed pH when the values match.
- Rinsed and immersed the pH electrode into pH 10.01 buffer for the second calibration point, and stirred gently.
- Waited a few minutes then adjusted the SLOPE trimmer on the lower right corner of the instrument until the pH matched that of the buffer for that specific temperature.
- Once the pH values matched, pressed CAL and the pH meter was now calibrated.

Testing Procedure

To take a pH measurement, the electrode was rinsed with the sample and then submerged into 4 cm of the sample to be tested. The pH mode was selected and the electrode swirled briefly before allowing it to sit and stabilize in the solution. The display then showed the pH value which was automatically compensated for temperature variations. Recorded the pH displayed once stabilization occurred.

3.7. Experimental Design and Analysis

The design of experiment involved the use of Design Expert software package (Version 10). The multilevel factorial, central composite design and Box-Behnken designs were conducted. Design matrices for each of the above mentioned designs were developed. This allowed for randomisation of experiments as each design gave a random order in which runs must be conducted. The analytical tests were conducted to evaluate the outputs and comparison of the output and input for each design indicted how good the designs were. The performance of each of the models and their degradation efficiencies were compared to select the best model for oil in water and phenol degradation. Model

verification was conducted by using an unfamiliar set point for a variable, to observe how well the models are able to navigate the design space with regard to prediction capability. Optimisation was then carried out with the aim of achieving the greatest degradation efficiency with the lowest possible catalyst concentration and run time. These optimum conditions were then identified.

CHAPTER 4: RESULTS AND DISCUSSION

4.1. Introduction

This chapter presents the results obtained from the photocatalytic degradation of synthetic crude refinery effluent. The effluent was exposed to micro TiO_2 photocatalyst under ultraviolet lighting and aeration conditions. The main contaminants were oil in water, phenols and sulphates. The contaminant levels before and after degradation was used to evaluate how efficient the process was. Sulphates when exposed to an advanced oxidation reaction can react in three major ways; firstly they could retard the degradation process; secondly combine with the catalyst and produce super oxide radicals that enhance degradation or should they be organo-sulphate in nature, they will degrade. Finally sulphates may not be affected at all by advanced oxidation. It was observed that during the experimental runs conducted, sulphates were not affected by the oxidation process. All runs were conducted in randomized order and repeated three times. Refer to appendix C-1 and C-4.1 for degradation outputs.

4.2. Photocatalytic Degradation Process

4.2.1. The effect of Catalyst Concentration on degradation efficiency

The catalyst concentration present during an advanced oxidation reaction is a key element as it has direct influence on the degradation efficiency. The catalyst concentration was varied at 2 g/L, 5 g/L and 8 g/L and the effect was observed on the degradation of the contaminants. The runs were conducted in a randomized order to assist with the elimination of any biased results. The graph below depicts the effect of catalyst concentration on the degradation process.

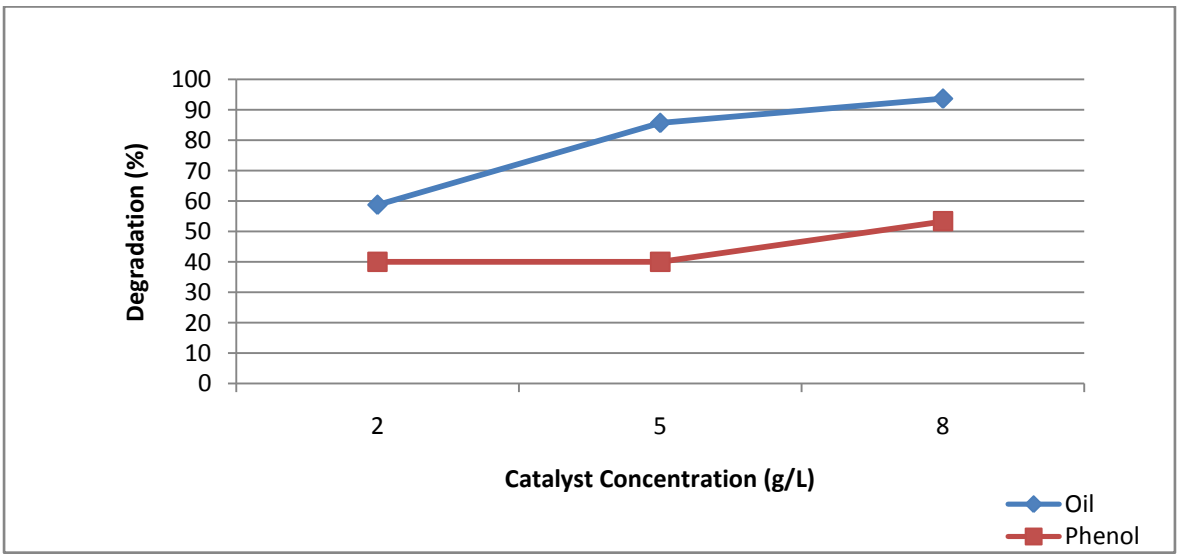

Figure 4.1: The effect of catalyst concentration on degradation (Run time and air flow rate kept constant at 60 minutes and 1.11 L/min respectively).

The data points represented in Figure 4.1 were obtained from the outputs of randomized runs conducted. It is observed that oil in water degradation took place to a much greater extent than phenol degradation. The average oil in water degradation at catalyst concentrations of 2 g/L, 5 g/L and 8 g/L was found to be 58.80%, 85.71% and 93.69% respectively. An increase in degradation of 26.91% was seen when catalyst concentration increased from 2 g/L to 5 g/L, however an increase in degradation of 7.98% was observed with a catalyst concentration increase from 5 g/L to 8 g/L. The maximum oil in water degradation occurred at 8 g/L; however, it is important to take into account the magnitude of the industry process as well as the catalyst cost at the time, to ensure it is feasible to move from 5 g/L to 8 g/L for a degradation increase of 7.98%.

Several researchers mention that when catalyst concentration exceeds its optimum, a significant decrease in degradation is observed (Saien and Nejati, 2007, Saien and Shahrezaei, 2012). The very slight increase in degradation from 5 g/L to 8 g/L could imply that the catalyst concentration is approaching its optimum, hence the levelling off in degradation efficiency. This would mean that the degradation would slowly level out; reaching its optimum and then once exceeding the optimum, degradation would decrease (Habibi and Vosooghian, 2005, Diya'uddeen et al., 2011).

The average phenol degradation at catalyst concentrations of 2 g/L, 5 g/L and 8 g/L was found to be 40%, 40% and 53.33% respectively. Increasing catalyst loading from 2 g/L to 5 g/L yielded no degradation increase. This finding implies that at constant run time and air flow rate, the movement from 2 g/L to 5 g/L had no effect on phenol degradation. Given no increase in degradation and the cost implication, it is therefore not advisable to use 5 g/L of catalyst loading. The move from catalyst loading of 5 g/L to 8 g/L brought on a degradation increase of 13.33%. On average the phenol degradation was 34.96% lower than that of oil degradation.

The literature on photocatalytic degradation, on several accounts, indicate that when catalyst concentration exceeds its optimum value it results in a decrease in degradation efficiency (Hashim et al., 2001, Laoufi et al., 2008). The advanced oxidation process takes place in the presence of light. As the concentration of catalyst increases above its optimum, it results in the scattering of light resulting in the light not being able to penetrate to the effluent due to the large amount of particles in solution (Das et al., 2013, Ahmed et al., 2010a). Refer to appendix D-1 and D-4 for more trend graphs.

4.2.2. The effect of Run Time on degradation efficiency

Advanced oxidation reactions generally require great run times to allow for more efficient degradation. This occurs because light irradiation in the presence of catalyst is over a much longer time. Applying photocatalytic degradation to industrial applications does not easily permit large run times; hence it is vital that the maximum degradation be attained in the shortest possible space of time. Figure 4.2 below indicates the effect of run time on the degradation of oil and phenol contaminants. The run times investigated were 30, 60 and 90 minutes.

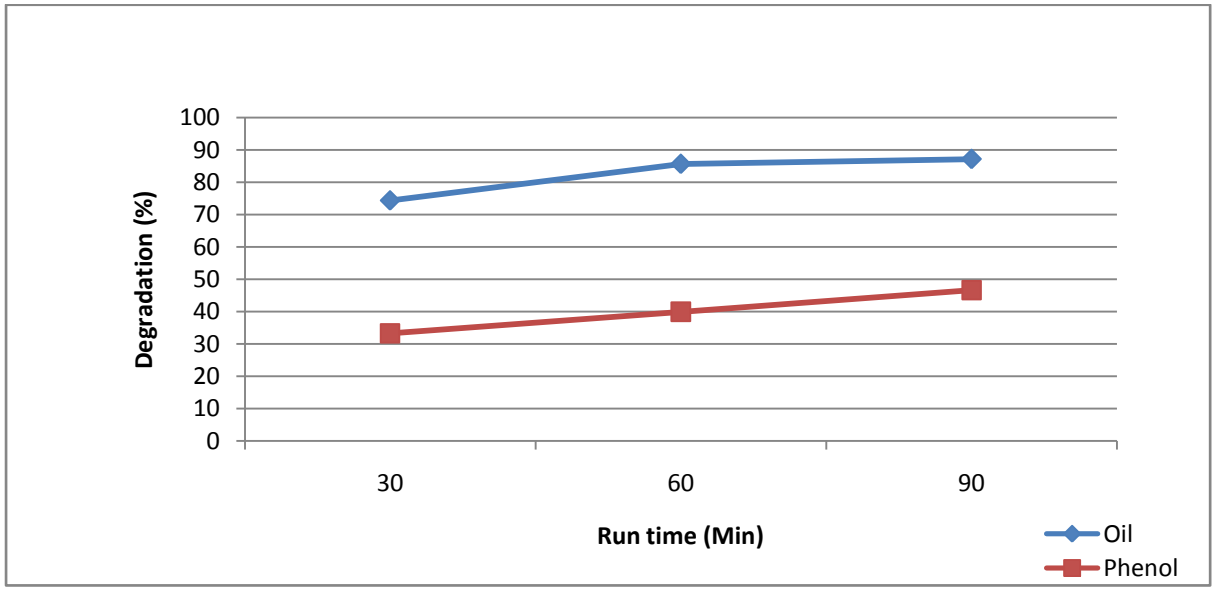

Figure 4.2: The effect of run time on degradation (Catalyst concentration and air flow rate kept constant at 5 g/L and 1.11 L/min respectively).

The average oil in water degradation at 30, 60 and 90 minutes were 74.42%, 85.71% and 87.21% respectively. The increase in run time from 30 to 60 minutes showed an increase in degradation of 11.29%. A further increase in run time from 60 to 90 minutes improved the degradation by 1.5%. These increases in degradation are quite significant. This is vital information, especially when applying the photocatalytic degradation process to industry. For industrial applications, it is challenging to cater for high run times as effluent streams exit the units into the effluent plants continuously, hence the selection of an upper limit of 90 minutes run time.

The average phenol degradation at 30, 60 and 90 minutes were observed to be 33.33%, 40% and 46.67% respectively. The increase in run time from 30 to 60 minutes yielded an increase in degradation of 6.67%, which is a decent increase, however the run time has doubled. The increase in run time from 60 to 90 minutes showed an increase in degradation of 6.67%. This is a significant increase in degradation. Selection of the appropriate run time needs to take into consideration what

the industrial application allows and if the degradation increase is significant enough. On average phenol degradation was noted to be 42.45% lower than that of oil.

The above results clearly indicate that the greater the run time, the greater the degradation efficiency as the oxidation reaction has more time for conversion of the organic contaminants. Khan et al. (2015) mentioned a similar occurrence when conducting photocatalytic degradation of organics in refinery waste water. Nickheslat et al. (2013) indicated that the greatest degradation efficiency will be obtained when the irradiating light source is closest to the reaction vessel and for the longest reaction time. The results obtained from this study follow similar trends as it was also noted that the greatest degradation occurred at the maximum time. Refer to appendix D-2 and D-5 for more trends.

4.2.3. The effect of Air flow rate on degradation efficiency

The addition of oxygen is a vital component to advanced oxidation reactions. Not only does the supply of oxygen aid the reaction, it also assists in keeping the particles fluidized and enhances the interaction of catalyst particles with effluent. The oxygen was sparged from the base of the photocatalytic reactor through pin holes. The oxygen flow was varied and supplied at 0.768, 1.11 and 1.48 L/min. The graph below indicates the effect of air flow rate on the degradation process.

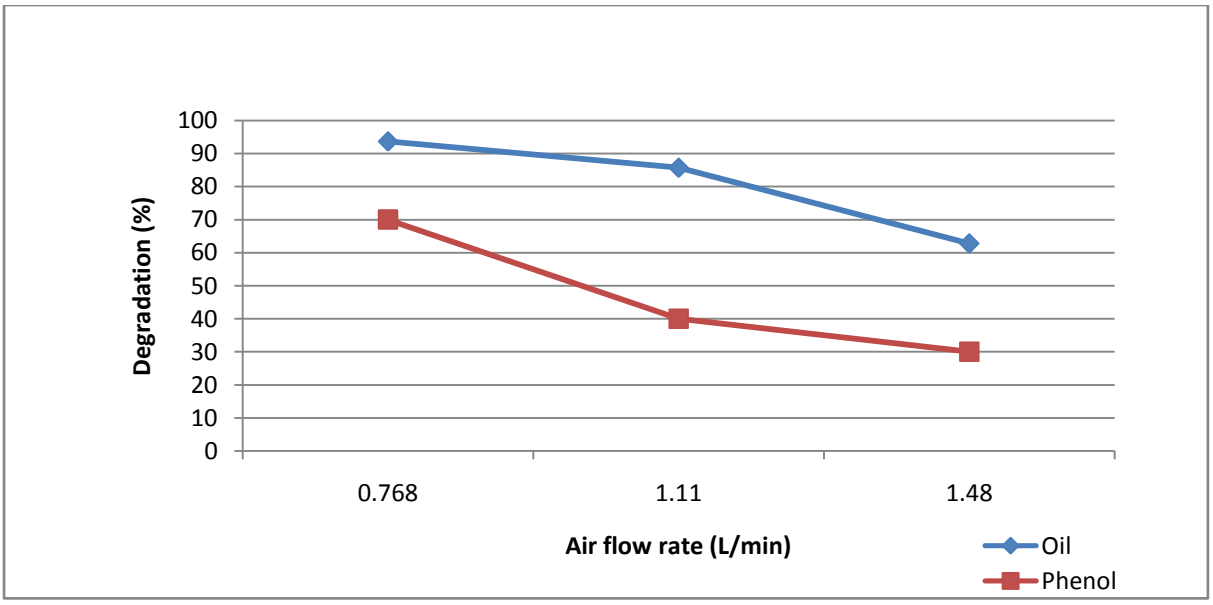

Figure 4.3: The effect of air flow rate on degradation (Catalyst concentration and run time kept constant at 5 g/L and 60 minutes respectively).

The air flow to the base of the reactor was supplied at 0.768, 1.11 and 1.48 L/min. The degradation of oil in water at these air flow rates were found to be 93.69%, 85.71% and 62.79% respectively. When air flow was increased from 0.768 L/min to 1.11 L/min, a degradation decrease of 7.98% was observed. When air flow rate increased from 1.11 L/min to 1.48 L/min, it was noted that degradation

decreased further and lowered by a value of 22.92%. This is a very significant decrease in the performance of the photocatalytic process. This clearly indicating that the best air flow rate (within the range investigated) for the degradation of oil is 0.768 L/min and going beyond this will only pose negative results.

The degradation of phenol at 0.768, 1.11 and 1.48 L/min was found to be 70%, 40% and 30% respectively. On average the degradation of phenol was found to be 34.06% lower than that of oil. It is clearly observed that the best degradation occurs at the lowest air flow rate for both oil and phenol degradation.

The above mentioned results and trends indicate that increasing the air flow rate does not improve the advanced oxidation process. Similar trends were shared by Das et al. (2013). The optimum air flow rate must be selected based on the targeted contaminant for degradation. For oil in water degradation and in the case of phenol degradation, the best results were achieved at an air flow of 0.768 L/min for the range investigated here. Refer to appendix D-3 and D-6 for further graphical trends.

4.2.4. The change in pH after photocatalytic degradation

It was of great importance that pH before and after degradation is monitored. The treated effluent is to be sent to the municipal treatment works, which still has stringent specifications even for pH. The specification for pH is that it must be greater than 6. pH was therefore monitored to ensure after photocatalytic degradation, the effluent was still safe to be sent to the municipal water works. Figure 4.4 indicated the pH of the feeds and how they changed for each of the respective runs.

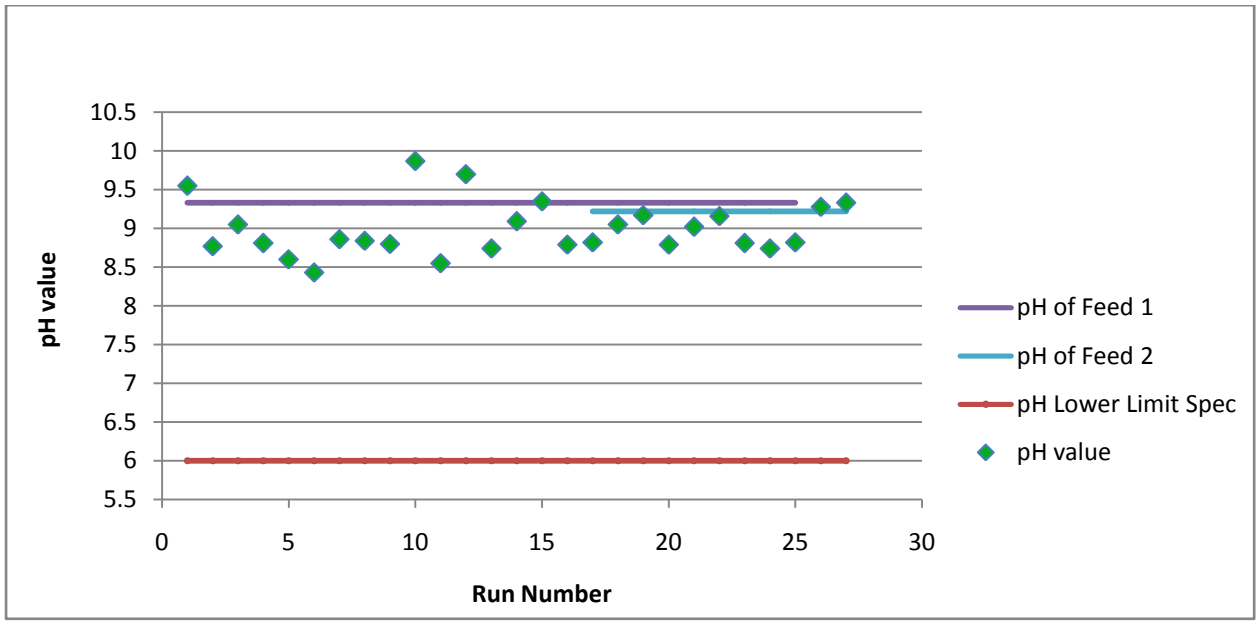

Figure 4.4: The effect of degradation on pH for Feed 1 and 2.

Two synthetic effluent feeds were developed and the pH of both noted. The change in pH for each experimental run was then monitored to be sure that no run exceeded the pH limit and that the effluent was safe to send to the municipality. The pH of synthetic feed 1 and 2 for the photocatalytic degradation process was 9.33 and 9.22 respectively.

When testing a local crude refinery effluent, the runs were conducted using the optimum conditions of the CCD and BBD models. The CCD conditions degraded oil from 126 ppm to 29 ppm and degraded phenol from 19 ppm to 3ppm. The BBD conditions were also positive and degraded oil from 126 ppm to 21 ppm and lowered phenol from 19 ppm to 4 ppm. The pH monitoring indicated that most of the pH values decreased after the advanced oxidation reaction had occurred, however they did not go below 6. This implied that the pH was still within the effluent limit specifications provided by the local municipality. Refer to appendix E-1 for more pH trends.

4.2.5. Summary

Currently crude refineries are finding it difficult to meet the oil in water and phenol specifications of 50 ppm and 10 ppm respectively. The results above clearly indicate that photocatalytic degradation has lowered effluent contaminants well below the 50 ppm oil and 10 ppm phenol specification. The photocatalytic degradation carried out was able to degrade oil and phenol by up to 96.39% and 70% respectively. The photocatalytic degradation process is therefore deemed acceptable and can be used for industrial application as specifications by government are not exceeded. The photocatalytic degradation process was able to achieve degradation outputs of up to 2.53 ppm oil and 0.9 ppm phenol, hence further indicating that it is a feasible method for improving crude refinery effluent quality.

When testing local crude refinery effluent using the CCD and BBD optimum conditions, it was noted that the CCD conditions degraded oil and phenol by 76.98% and 84.21% respectively. The BBD conditions also provided favourable results and degraded oil and phenol by 83.33% and 78.95% respectively. Figure 4.4 indicated that the lowest pH attained was 8.43 and this occurred at run 6 with a catalyst concentration of 8 g/L. Even with the maximum catalyst concentration the pH specification was still not violated, thus making photocatalytic degradation feasible for degrading organics in crude refinery effluent.

CHAPTER 5: OPTIMISATION USING RESPONSE SURFACE METHODOLOGY (RSM)

5.1. Introduction

This chapter deals with the design of experiment using the software package called Design Expert. Based on the dependant and independent variables and constraints identified, models are selected to depict the outputs of the advanced oxidation process. These models were then verified against new unfamiliar data and the prediction capability of the model then tested. The aim was to determine good models to predict the response of oil in water and phenol degradation. Once identified, these models would be used to optimise the process to achieve the desired outcomes. This chapter discusses the multilevel factorial design, Central composite design and Box-Behnken designs. These designs were considered for optimisation of the photocatalytic degradation process as they best take into account the number of factors and levels at which the factors were required to be tested.

5.2. Design Information

The three factors involved were catalyst concentration, run time and air flow rate and the three responses to the process were the percentage removal of oil in water, phenol and sulphates. As mentioned in chapter 4, focus is placed on oil in water and phenol degradation as the degradation had no effect on sulphates. The above mentioned factors were tested at low, medium and high levels. The table below indicates the three factors and the levels at which they were tested when trying to obtain the best degradation responses.

Table 5.1: The factors and levels at which the factors were tested.

	Levels Tested		
Factors (Coded)	**Low (-1)**	**Medium (0)**	**High (1)**
Catalyst Concentration (g/L)	2	5	8
Run Time (min)	30	60	90
Air Flow Rate (L/min)	0.768	1.11	1.48

5.3. The Multilevel Factorial Design

Factorial design is one of the most commonly used design of experiment methods. The most common being the two factorial design, generally represented as 2^2. The factorial design conducted in this study consisted of three factors tested at three levels (3^3). This meant that 27 experimental runs were required. The Design Expert software package was used to develop a run matrix for randomised runs to be conducted. The experimental run matrix can be observed in Table 5.2.

Table 5.2: Multilevel factorial design run matrix

		Factor 1	Factor 2	Factor 3
Std	Run	A:Catalyst Concentration (g/L)	B:Run Time (min)	C:Air Flow rate (L/min)
14	1	5	60	1.11
6	2	8	60	0.768
1	3	2	30	0.768
8	4	5	90	0.768
13	5	2	60	1.11
3	6	8	30	0.768
21	7	8	30	1.48
2	8	5	30	0.768
27	9	8	90	1.48
7	10	2	90	0.768
5	11	5	60	0.768
9	12	8	90	0.768
15	13	8	60	1.11
23	14	5	60	1.48
16	15	2	90	1.11
22	16	2	60	1.48
17	17	5	90	1.11
25	18	2	90	1.48
12	19	8	30	1.11
24	20	8	60	1.48
10	21	2	30	1.11
11	22	5	30	1.11
19	23	2	30	1.48
4	24	2	60	0.768
26	25	5	90	1.48
20	26	5	30	1.48
18	27	8	90	1.11

5.3.1. Evaluation of the model for Oil in water

Once the runs indicated in the design matrix were conducted, the outputs were used to determine the performance of the photocatalytic degradation process. Figure 5.1 below indicates the normal plot of residuals.

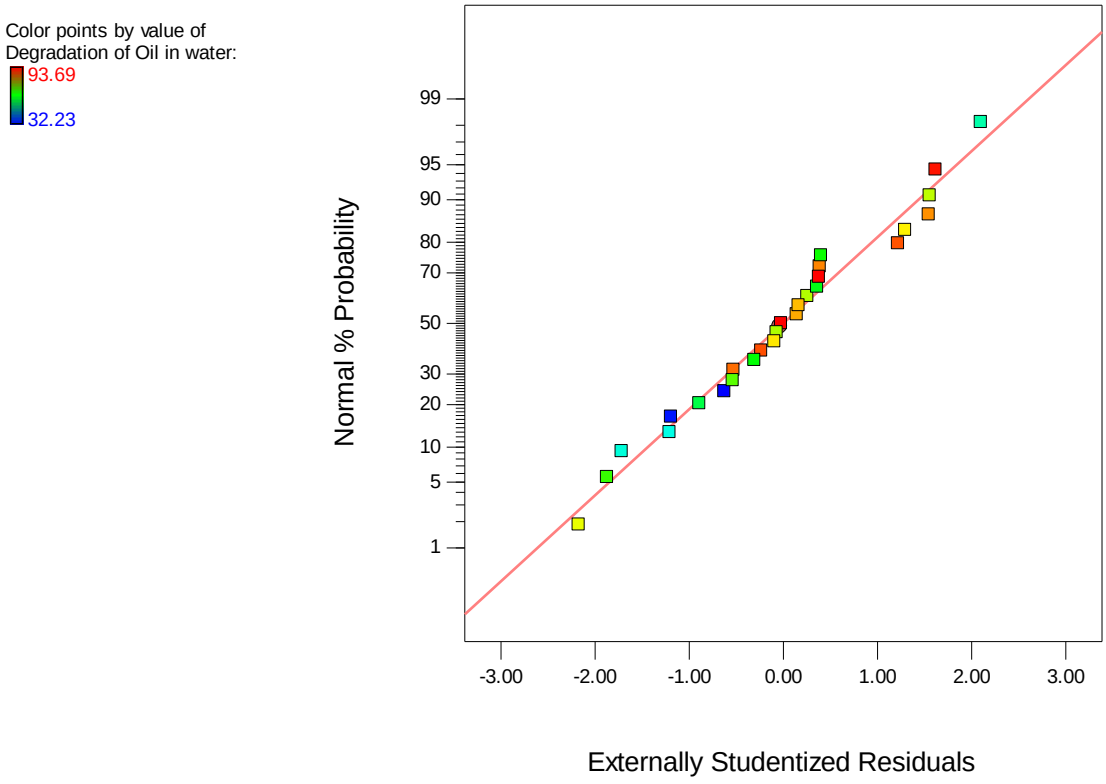

Figure 5.1: Normal plot of residuals for the multilevel factorial design for oil in water.

The graph above indicates a good fit as the residuals are of a normal or linear pattern. Residuals in a straight line are desired as they show good correlation between the data and model. This implies the model for oil in water degradation is of a good fit.

The residuals vs. predicted plot can be observed in Figure 5.2 below:

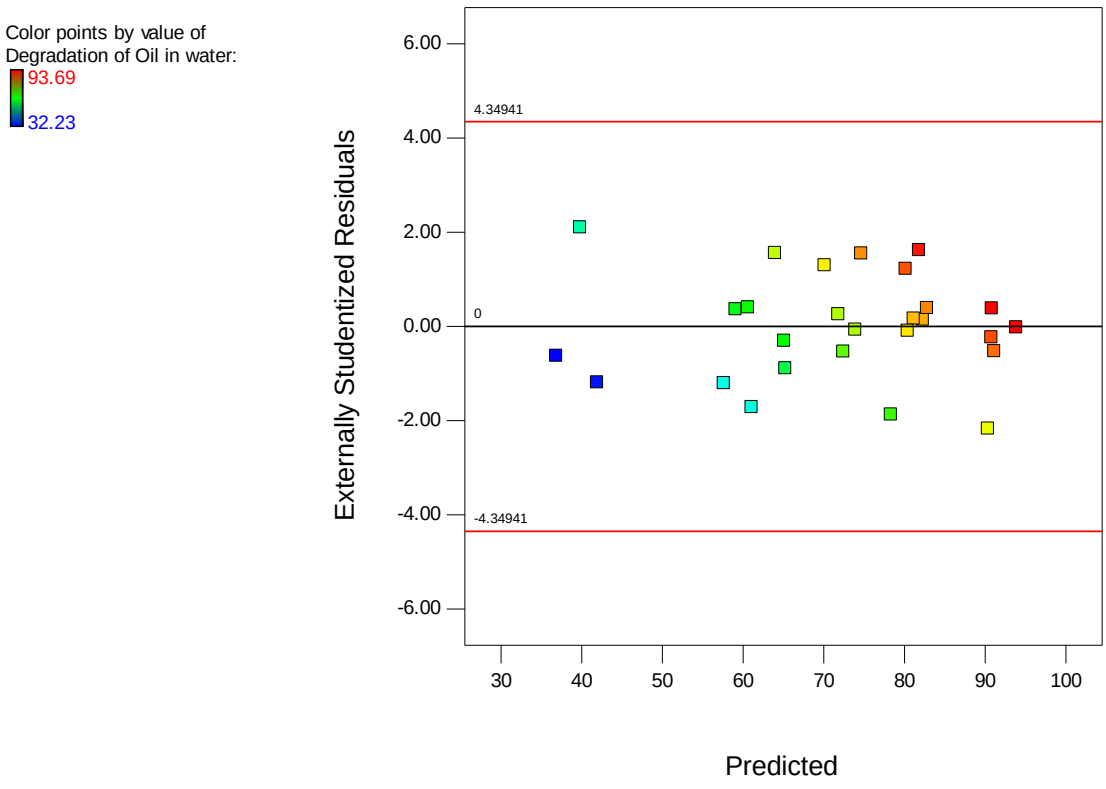

Figure 5.2: Residuals vs. Predicted plot for oil in water degradation (Multilevel factorial design).

It is desired to observe a random and scattered plot of residuals. This ensures the prediction will produce strong results within the design space. The plot starts with good random scatter, however from central to the right of the plot the residuals start to become less random, thus indicating the prediction ability of the plot is not good.

The residuals vs. run plot can be seen in Figure 5.3.

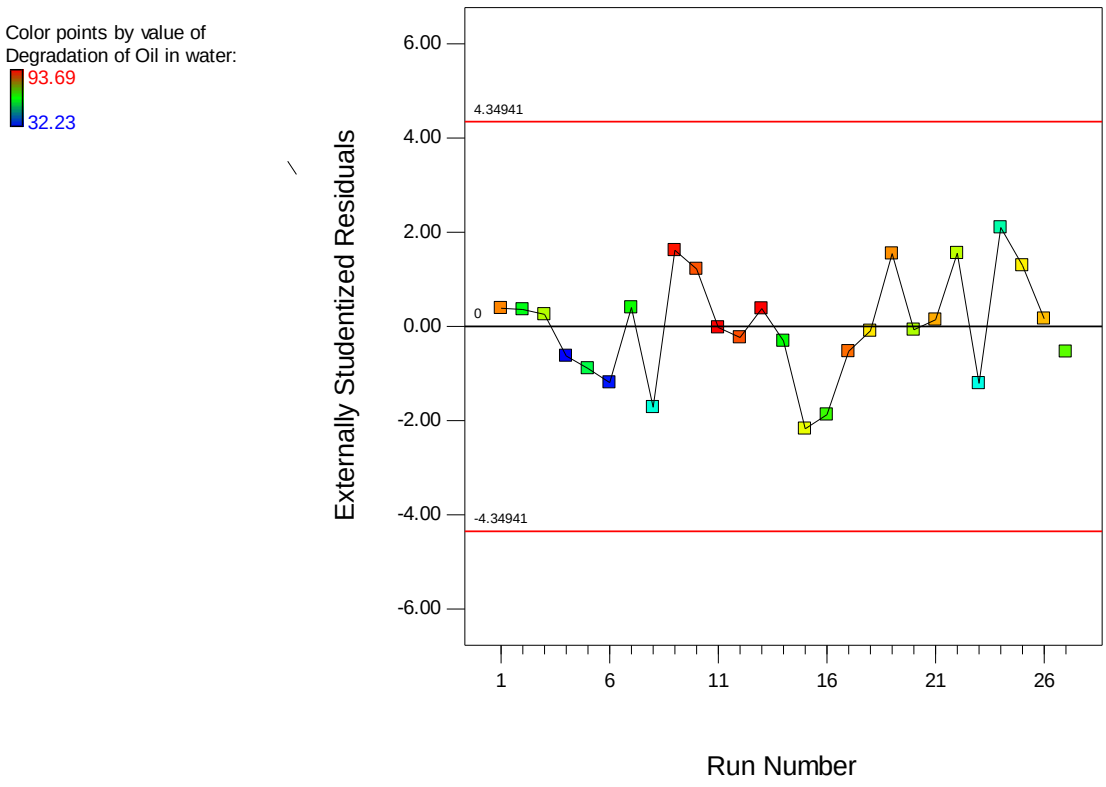

Figure 5.3: Residual vs. run plot for oil in water degradation (Multilevel factorial design).

Figure 5.3 starts from run 1 on a very positive note as no trend can be observed for the residuals. From run 18 it is observed that more of a trend has formed, indicating the latter experimental run residuals are very much predictable. It is advisable to have no trends as this would assist with developing a much better fitted model.

The prediction vs. actual plot can be seen below:

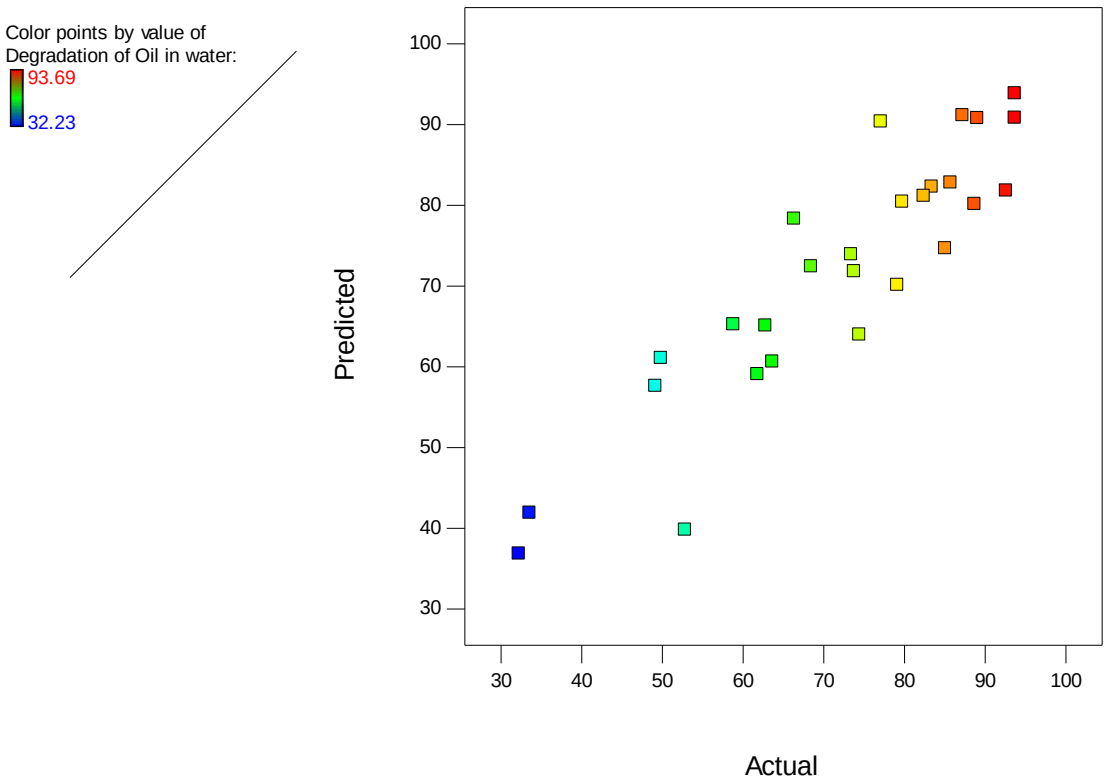

Figure 5.4: Predicted vs. actual plot for oil in water degradation (Multilevel factorial design).

The graph above indicates a random scatter along the 45 degree line. The slight grouping of points indicate various areas of over and under prediction occurring. This indicates an average prediction ability of the model.

Table 5.3 indicates the outputs obtained from the multilevel factorial design for oil in water degradation. Refer to appendix F-1 for attempt 1 results.

Table 5.3: Response outputs for multilevel factorial degradation of oil in water (A is catalyst concentration, B is run time and C is air flow rate)

Response	**1**	**Degradation of Oil in water**			
ANOVA for selected factorial model					
Analysis of variance table [Classical sum of squares - Type II]					
	Sum of		Mean	F	p-value
Source	Squares	df	Square	Value	Prob > F
Model	6439.281	16	402.4551	2.901216	0.046128 significant
B-Run Time	545.4682	2	272.7341	1.966084	0.190505
C-Air Flow rate	1065.525	2	532.7627	3.840577	0.057869
AB	1383.797	4	345.9493	2.493877	0.109951
ABC	3444.491	8	430.5614	3.103829	0.048512
Residual	1387.194	10	138.7194		
Cor Total	7826.476	26			

Std. Dev.	11.77792	**R-Squared**	0.822756
Mean	71.79037	**Adj R-Squared**	0.539166
C.V. %	16.40599	**Pred R-Squared**	-0.29211
PRESS	10112.65	**Adeq Precision**	6.099426
-2 Log Likelihood	182.9811	**BIC**	239.0104
		AICc	284.9811

The model for the degradation of oil in water:

Degradation of Oil in water = 71.79 -7.86C + 7.52C^2 + 9.10ABC +0.20A^2BC - 13.46AB^2C + 21.13A^2B^2C + 4.20ABC^2 - 12.28A^2BC^2 - 3.4AB^2C^2-5.3$A^2B^2C^2$ (15)

The model data can be regarded as significant as the F-value is 2.90 implying there can only be a 4.61% chance that an F value this large could occur as a result of noise. When considering the terms it is advisable that Prob>F should be less than 0.05 for terms to be significant. It is observed that ABC is a significant term in the model. Run time and the AB term have a Prob>F value of more than 0.1 and

are therefore not significant. A R^2 value of 0.82 indicates that the data is fairly closely fitted to the regression line. The predicted R^2 value is negative and this indicates that the model would not be able to predict the response well. When the predicted R^2 is negative, the mean value is usually tried out and in this case the mean value did not provide a significant model and could not be used. This model was therefore disregarded as it was not a reliable means of predicting oil in water degradation response.

5.3.2. Evaluation of the model for phenol degradation

Figure 5.5 displays the normal plot of residuals:

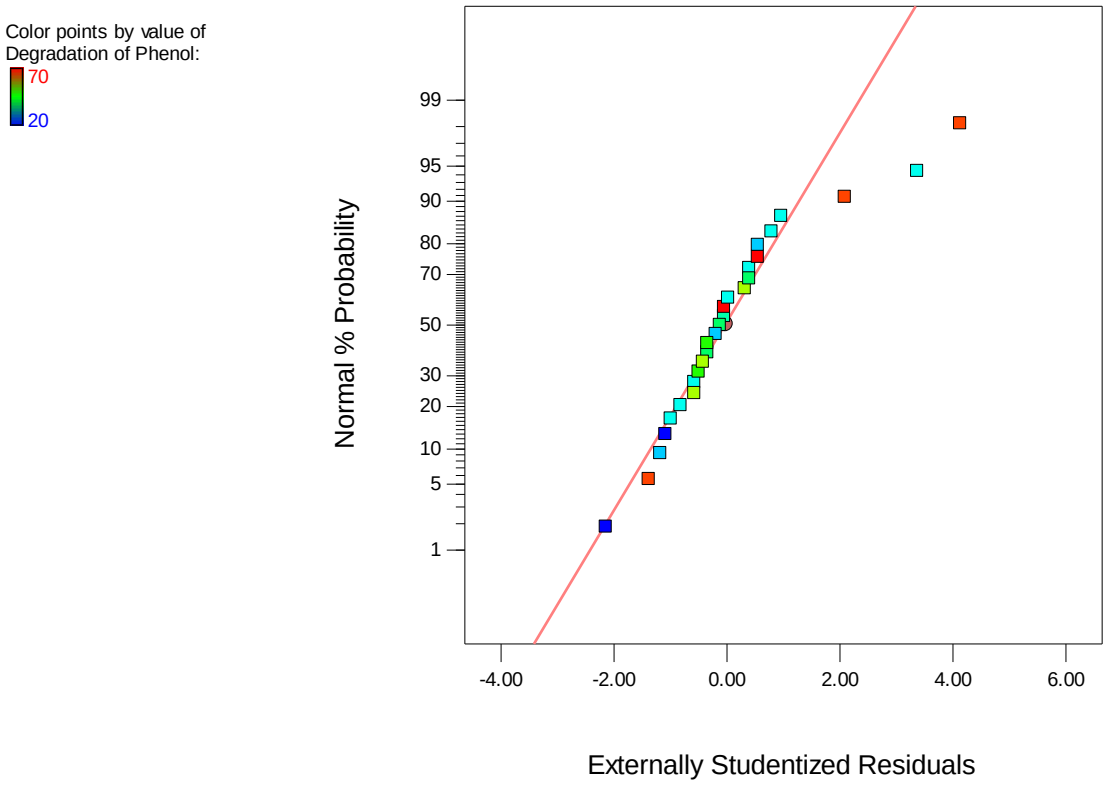

Figure 5.5: Normal plot of residuals for the degradation of phenol (factorial design).

The residual plot above shows most points lie very closely if not on the regression line and this indicates a good model fit. There are just three points that sit below the 45 degree line and are not linear in nature.

Figure 5.6 depicts the residuals vs. predicted for the phenol degradation:

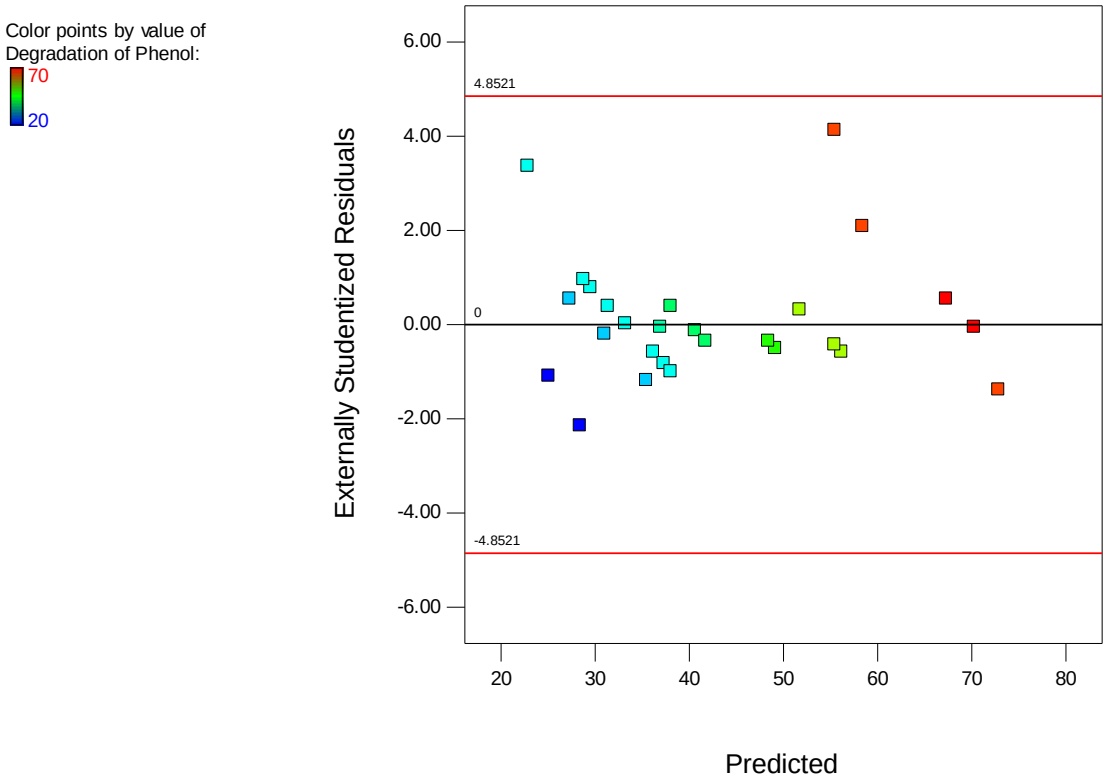

Figure 5.6: Residuals vs. predicted plot for phenol degradation (factorial design).

The figure above initially indicated particles very closely grouped indicating a very low prediction ability of the model. From a predicted value of 50% and up, the graph displays very good random scatter thus indicating a much more accurate prediction for this range of the data.

Figure 5.7 displays the residual vs. run plot

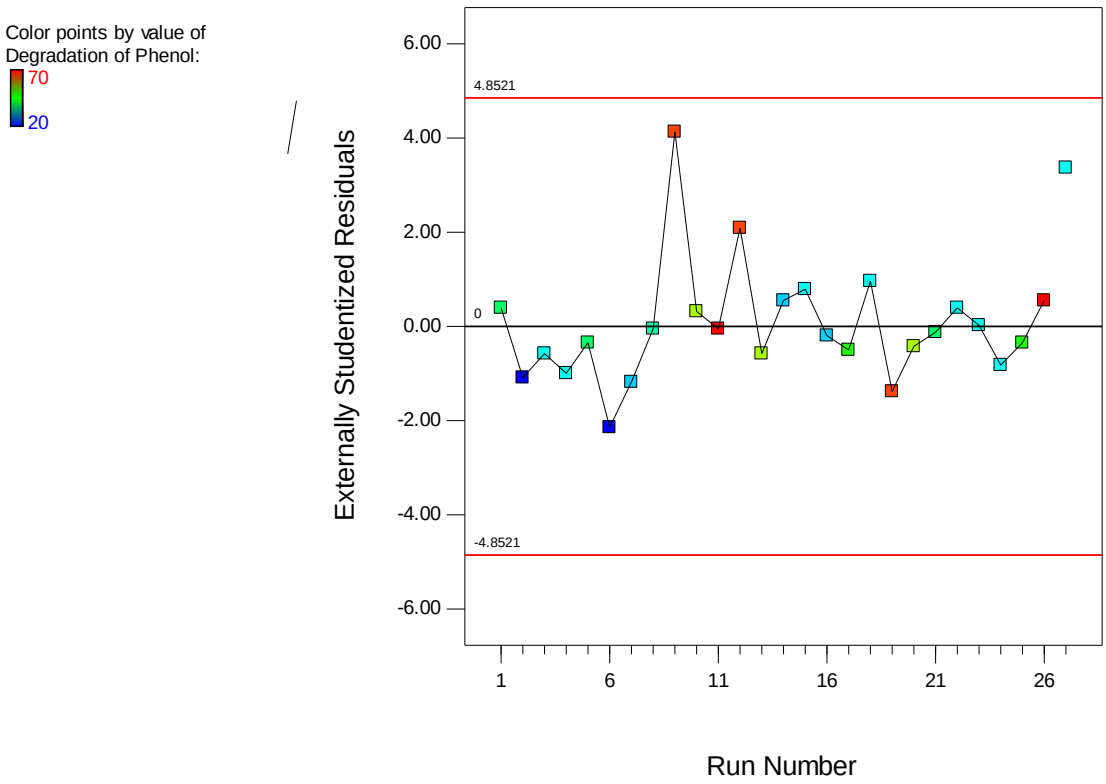

Figure 5.7: Residuals vs. run for the degradation of phenol (Multilevel factorial design).

From the figure above, it can be observed that run 1 to run 6 displays a trend in output and this is not good when evaluating the model. From run 7 upwards the outputs for each run are quite erratic and this is favourable in a good model. There are no observable outliers as no residuals lie outside the limits.

Figure 5.8 displays the predicted vs. actual plot which shows residuals along a 45 degree line:

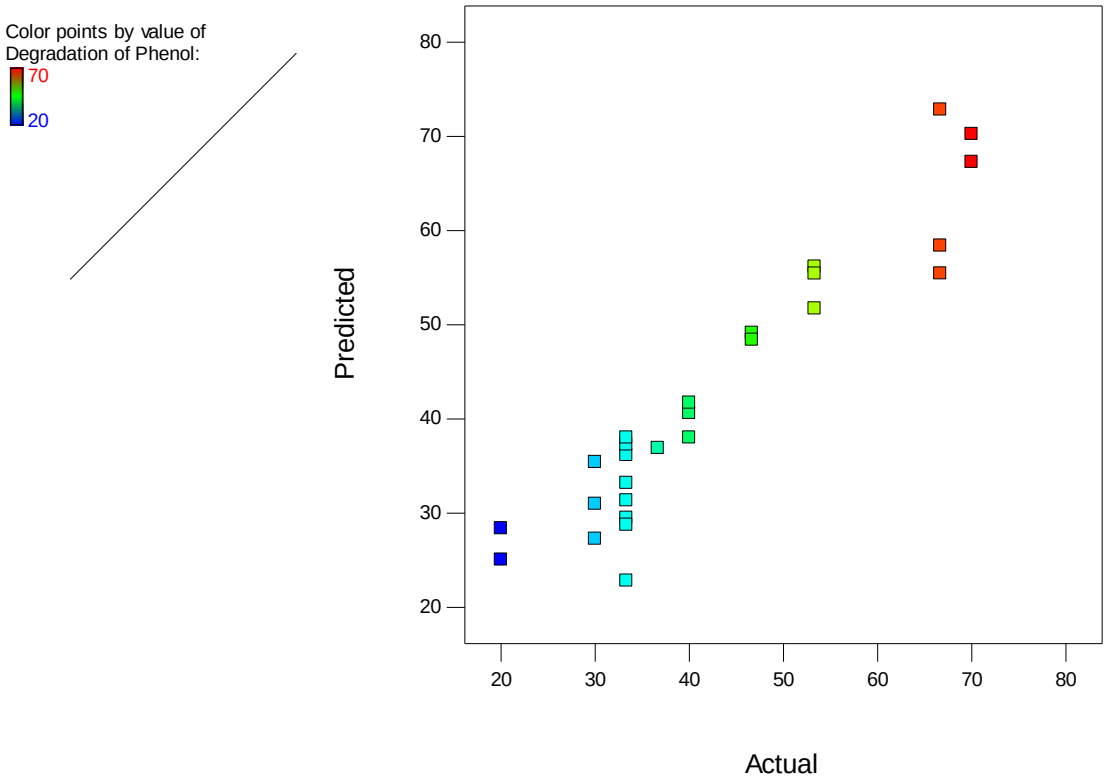

Figure 5.8: Predicted vs. actual data for the degradation of phenol (Multilevel factorial design).

The actual percentage degradation data from 20% up to 40% displays a grouping of data with a significant amount below the 45 degree line being under predicted. This indicates poor prediction capability of the model for the degradation of phenol. This trend is similar to the plot of residuals vs. run number which also indicates that the model is unable to predict the initial data well.

Table 5.4 displays the response outputs for the degradation of phenol.

Table 5.4: Response outputs for the degradation of phenol (A is catalyst concentration, B is run time and C is air flow rate). Refer to appendix F-2 for attempt 1 results.

Response	**2**	**Degradation of Phenol**			
ANOVA for selected factorial model					
Analysis of variance table [Classical sum of squares - Type II]					
	Sum of		Mean	F	p-value
Source	Squares	df	Square	Value	Prob > F
Model	5257.543	18	292.0857	3.889024	0.02788 significant
A-Catalyst Concentration	455.3943	2	227.6971	3.031711	0.104712
AC	633.6428	4	158.4107	2.109186	0.171334
BC	821.4033	4	205.3508	2.734178	0.105436
ABC	3347.103	8	418.3879	5.570695	0.01275
Residual	600.8412	8	75.10515		
Cor Total	5858.385	26			

Std. Dev.	8.666323	**R-Squared**	0.897439
Mean	42.46852	**Adj R-Squared**	0.666677
C.V. %	20.40646	**Pred R-Squared**	-0.16823
PRESS	6843.957	**Adeq Precision**	6.87857
-2 Log Likelihood	160.39	**BIC**	223.0109
		AICc	306.9614

The model for the degradation of phenol in water

Degradation of Phenol in water = $42.47 - 5.80A + 2.72A^2 + 3.09ABC - 2.84A^2BC - 6.17AB^2C + 20.12A^2B^2C - 2.47ABC^2 - 13.95A^2BC^2 + 1.60AB^2C^2 - 4.32A^2B^2C^2$ (16)

The above model can be regarded as significant as can be seen by an F-value of 3.89. There is only a 2.79% chance of an F value this large occurring as a result of noise. The Prob>F value is less than 0.05 for term ABC, implying this term is a significant model term. All values greater than 0.1 indicate terms are not significant, however not all terms could be removed from the model as they were required to support hierarchy. An R^2 value of 0.89 indicates that the data is closely fitted to the model. The predicted R^2 value is negative and this indicates that the model has very poor prediction ability

and the overall mean may most likely be a better predictor. The mean was selected, however this did not yield a significant model and the model was therefore disregarded.

5.4. The Central Composite Design (CCD)

The Central Composite Design makes use of the two factorial framework with the addition of axial points. The CCD is a very effective design as it allows for effective optimisation since it takes into account centre points and axial points. The circumscribed CCD was used and this takes into account points slightly beyond the parameters of the process. The Design expert software package was used to develop the design matrix for the CCD and the run matrix can be seen in Table 5.5. Refer to appendix C-2 for CCD outputs.

Table 5.5: CCD experimental run matrix.

		Factor 1	Factor 2	Factor 3
Std	**Run**	**A:Catalyst Concentration (g/L)**	**B:Run Time (min)**	**C:Air Flow rate (L/min)**
9	1	2	60	1.11
6	2	8	30	1.48
15	3	5	60	1.11
3	4	2	90	0.768
5	5	2	30	1.48
13	6	5	60	0.768
8	7	8	90	1.48
14	8	5	60	1.48
10	9	8	60	1.11
18	10	5	60	1.11
4	11	8	90	0.768
16	12	5	60	1.11
12	13	5	90	1.11
20	14	5	60	1.11
7	15	2	90	1.48
17	16	5	60	1.11
11	17	5	30	1.11
2	18	8	30	0.768
1	19	2	30	0.768
19	20	5	60	1.11

5.4.1. Evaluation of the model for oil in water degradation

Once the experimental runs were conducted as per the run matrix above, the output data graphs were generated to evaluate the CCD model. Figure 5.9 below displays the normal plot of residuals for the degradation of oil in water.

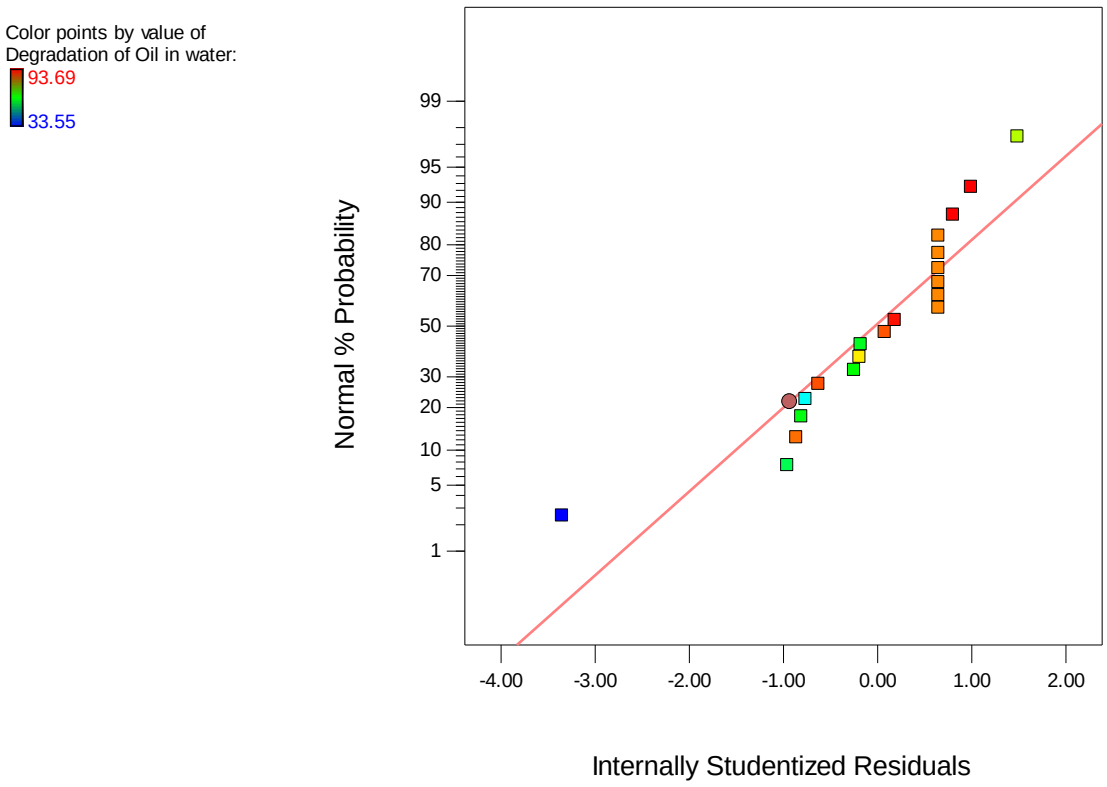

Figure 5.9: Normal plot of residuals for the degradation of oil (CCD).

The plot above indicates very few residuals sitting on the line which indicates that the model is not a very good fit. Many points sit below the line with no linear trend of residuals. The greatest performance of the model is observed when the normal percentage probability lies between 5% and 50%. It is within this range that most residuals sit on the regression line.

Figure 5.10 displays the residuals vs. predicted values for the degradation of oil.

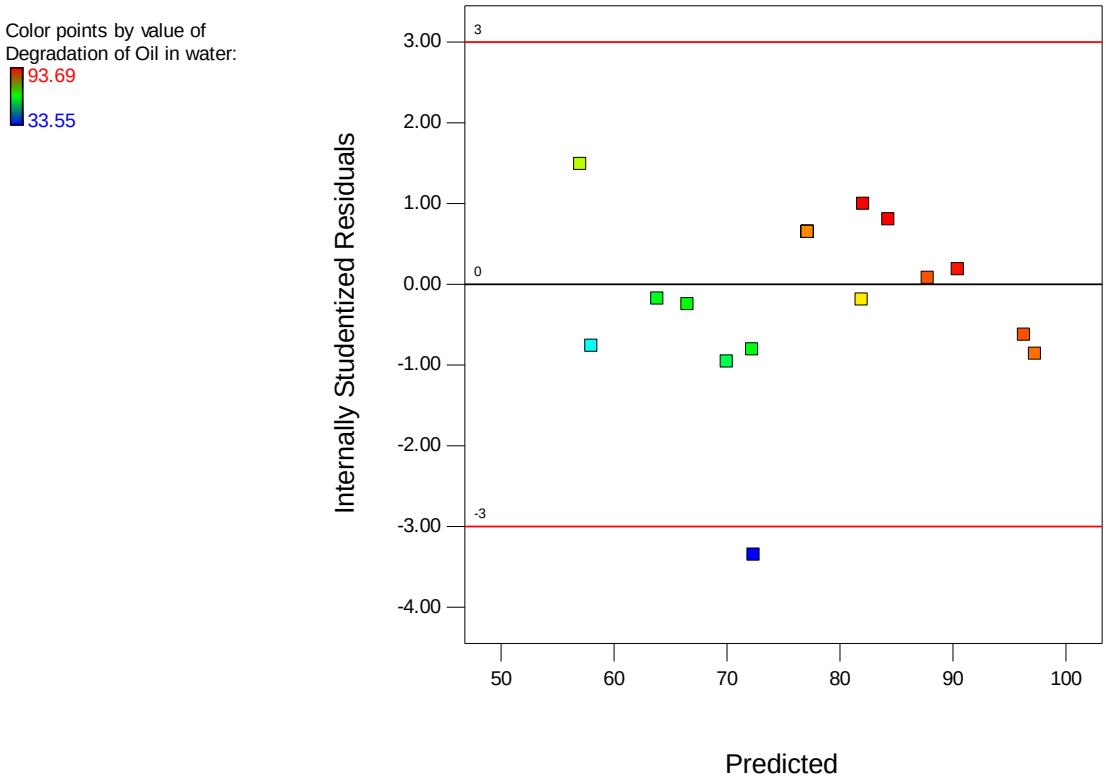

Figure 5.10: Residuals vs. predicted for the degradation of oil (CCD).

The graph above displays a very good random scatter of residuals and this indicates the model fits the data well. There are no distinct trends observed and this shows good prediction ability of the model. An outlier was observed just beyond the predicted 70% degradation of oil. This outlier occurred at run 18 which took place at the maximum catalyst concentration, however with the minimum air flow rate and run time. This was then compared to the only other random run which took place with a minimum catalyst concentration and air flow rate (Run 19) and the result obtained was also degradation lower than most other runs. This therefore indicated there is no issue with the data or that specific run as a similar occurrence had taken place.

Figure 5.11 below indicates the residuals vs. runs and displays how the outputs of degradation vary with the run order observed in the run matrix.

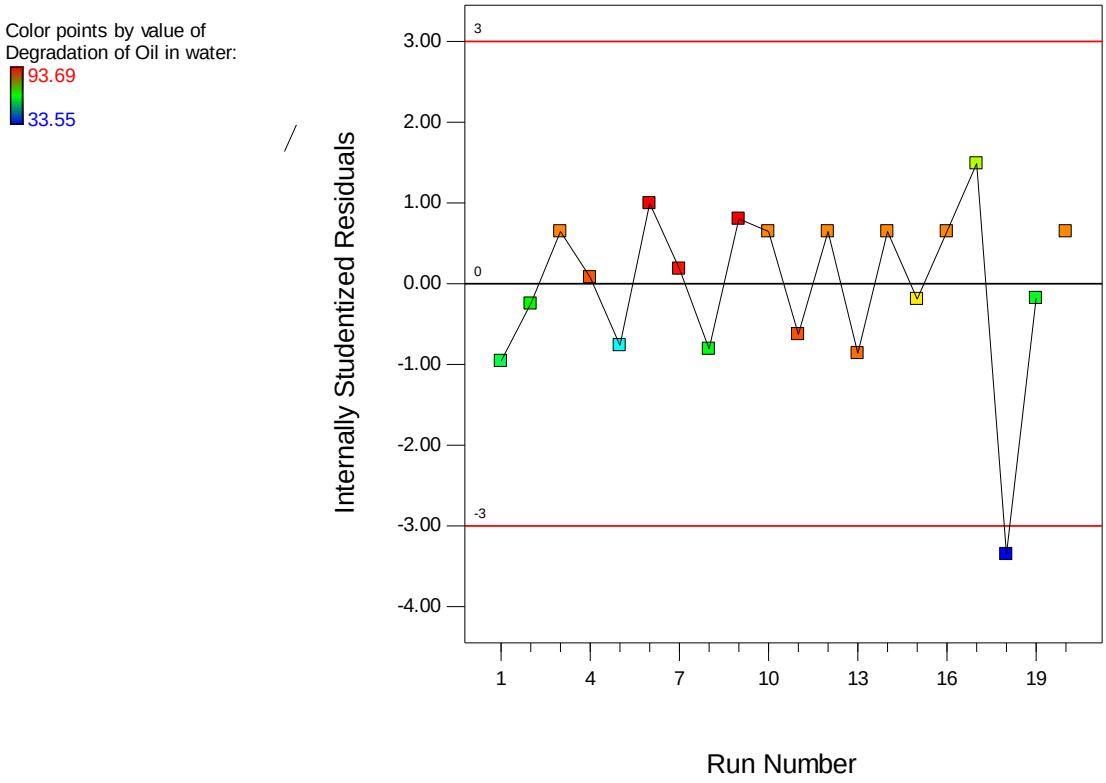

Figure 5.11: Residuals vs. runs for the degradation of oil in water (CCD).

The analysis of residual vs. run above shows a clear trend of increasing and decreasing output and is quite predictable. This indicates that the model is a bad fit as it is desirable to observe a random scatter in residuals for runs carried out since this allows for the development of a more robust model with greater prediction accuracy. The outlier which occurred during run 18 is due to the combination of minimal run time and minimal air flow rate and was found to have a similar effect during other runs.

Figure 5.12 displays the predicted vs. actual plot with output data scattered across a 45 degree line.

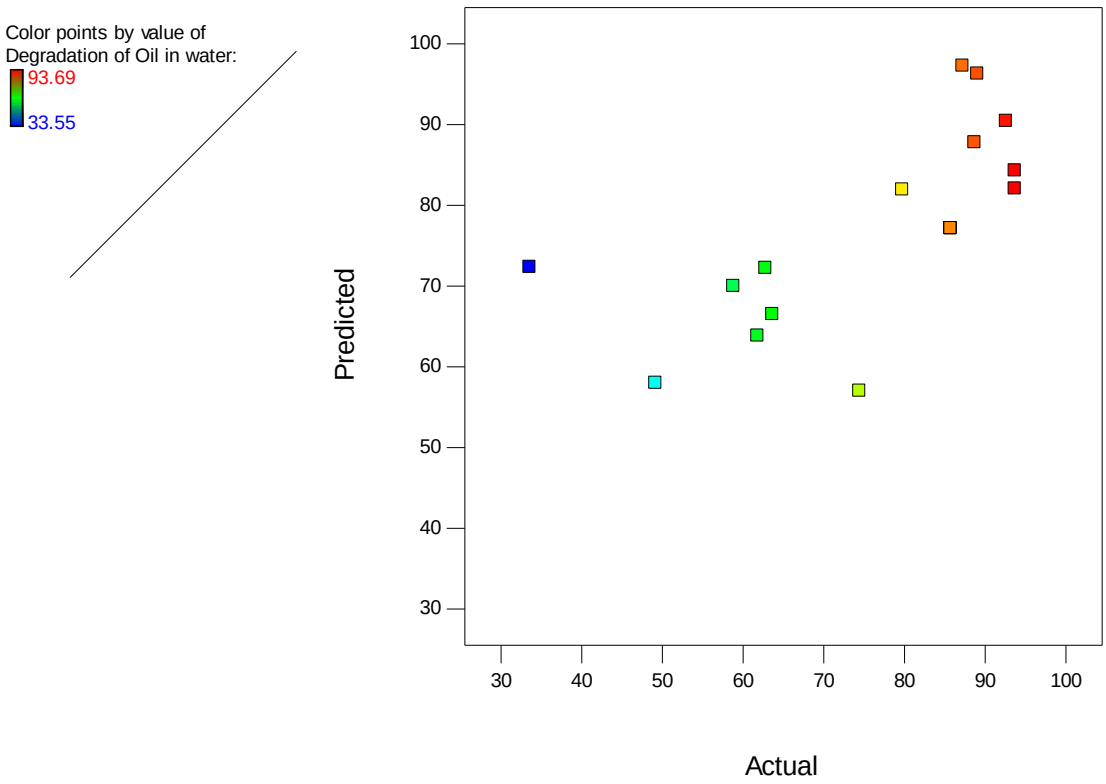

Figure 5.12: Predicted vs. actual plot for the degradation of oil (CCD).

The graph above shows good scatter across the 45 degree line for the actual degradation range of 30% to 80% degradation. Above 80% actual degradation, a grouping occurs indicating the model has a tendency to under predict at this range.

Table 5.6 displays the response outputs for the degradation of oil (A is catalyst concentration, B is run time and C is air flow rate). Refer to appendix F-3 for attempt 1 data.

Table 5.6: CCD response outputs for the degradation of oil

Response	**1**	**Degradation of Oil in water**			
ANOVA for Response Surface Linear model					
Analysis of variance table [Partial sum of squares - Type III]					
	Sum of		Mean	F	p-value	
Source	Squares	df	Square	Value	Prob > F	
Model	2319.808	3	773.2693	4.206494	0.022563	significant
A-Catalyst Concentration	247.3244	1	247.3244	1.345416	0.263098	
B-Run Time	1955.751	1	1955.751	10.63906	0.004898	
C-Air Flow rate	116.7324	1	116.7324	0.635011	0.437189	
Residual	2941.24	16	183.8275			
Lack of Fit	2941.24	11	267.3854			
Pure Error	0	5	0			
Cor Total	5261.048	19				

Std. Dev.	13.5583	**R-Squared**	0.44094
Mean	77.153	**Adj R-Squared**	0.336117
C.V. %	17.57326	**Pred R-Squared**	0.025948
PRESS	5124.534	**Adeq Precision**	6.638405
-2 Log Likelihood	156.5746	**BIC**	168.5576
		AICc	167.2413

The CCD model for degradation of oil in water is given by

Degradation of Oil in water = 77.15 + 4.2556A + 11.967B - 2.92C (17)

A significant model is developed as can be seen by the F-value of 4.21. This indicates that there is a 226% chance that the F value could occur as a result of noise. When focussing on the terms, it is seen that B is a significant term as it has a Prob>F value of less than 0.05. Terms above 0.1 are not significant, however were not removed when reducing the model as they were required to maintain model hierarchy. The R^2 value of 0.44 does not show a very good fit of the model to the data as it is quite low. The predicted R^2 is extremely small and given that the predicted r-squared is not as close to

the adjusted r-squared value indicates the models prediction capability is poor. The signal to noise ratio as indicted by adequate precision is 6.638. This is good as it is above the desired ratio of 4. Even though there isn't much influence from noise, the model is unable to make accurate prediction.

5.4.2. Evaluation of the model for phenol degradation

On completion on randomized experimental runs, the following graphs were generated based on the outputs for phenol degradation. Figure 5.13 below displays the normal plot of residuals.

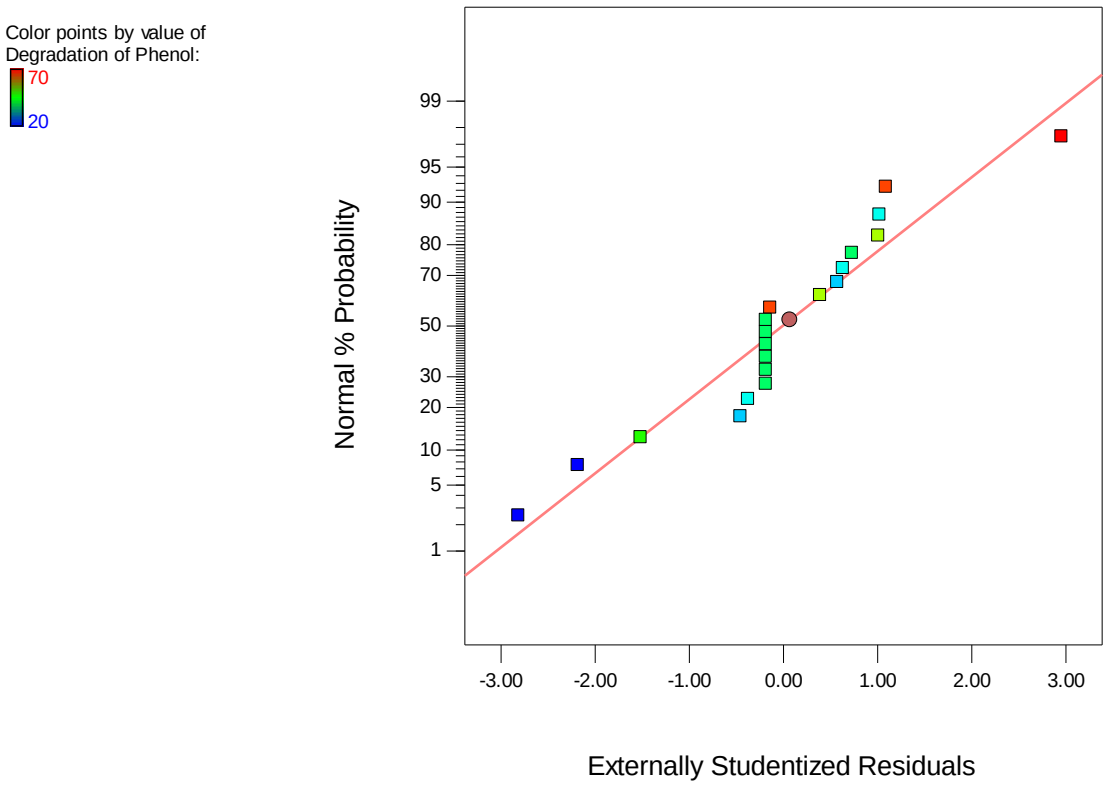

Figure 5.13: Normal plot of residuals for degradation of phenol (CCD).

The graph above shows a decent amount of residuals placed very closely to the regression line. Most points are in close proximity to the model and this can be observed throughout the degradation range. This may indicate that the model could navigate the design space well along most of the degradation spectrum. During the normal percentage probability range of 20% to 50%, formation of an almost vertical gathering of residuals is observed. This is the only region where there may be difficulty in the model predicting as the residuals are not well fitted. All the maximum and minimum degradation points also fall closely to the model indicating a good fit even at boundary conditions of the process.

Figure 5.14 depicts the residuals vs. predicted values for phenol degradation.

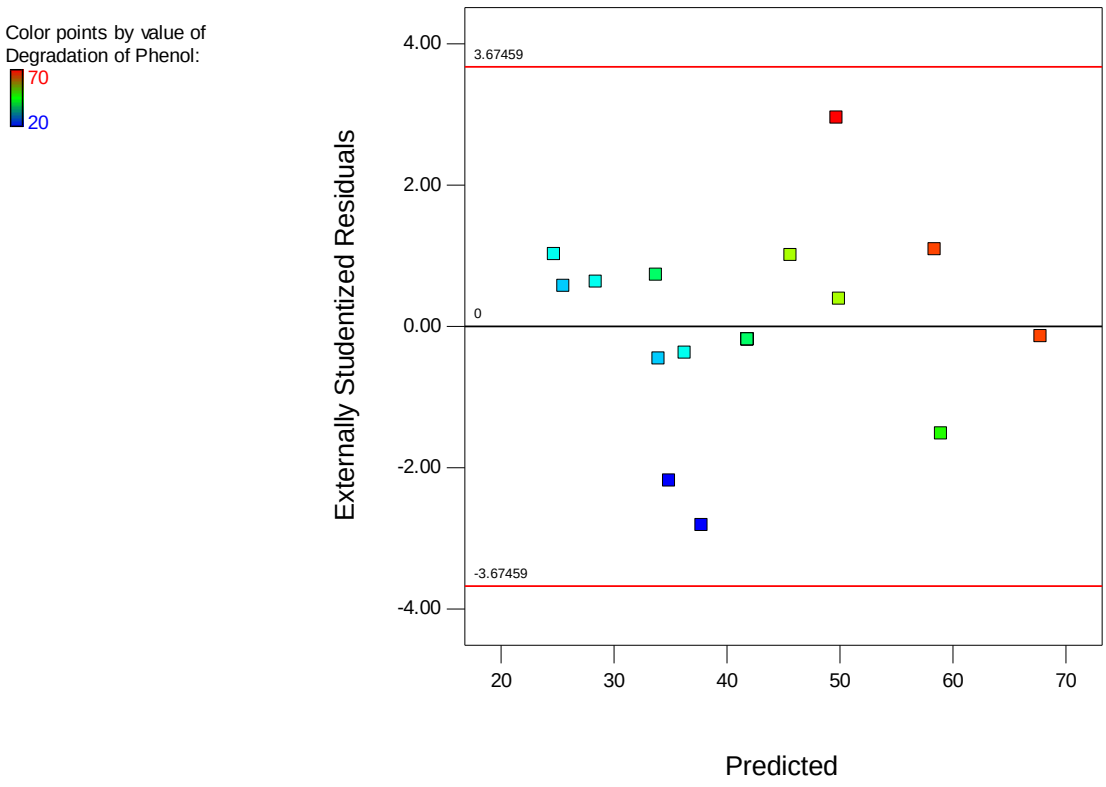

Figure 5.14: Residuals vs. predicted values for the degradation of phenol (CCD).

The figure above shows a very random scatter of points and this favours good prediction ability of the model. No distinct trends can be observed hence the data points used to fit the model would result in the development of a significantly robust model.

Figure 5.5 displays the residuals vs. runs and allows for the evaluation of output performance based on the sequence of experiments conducted.

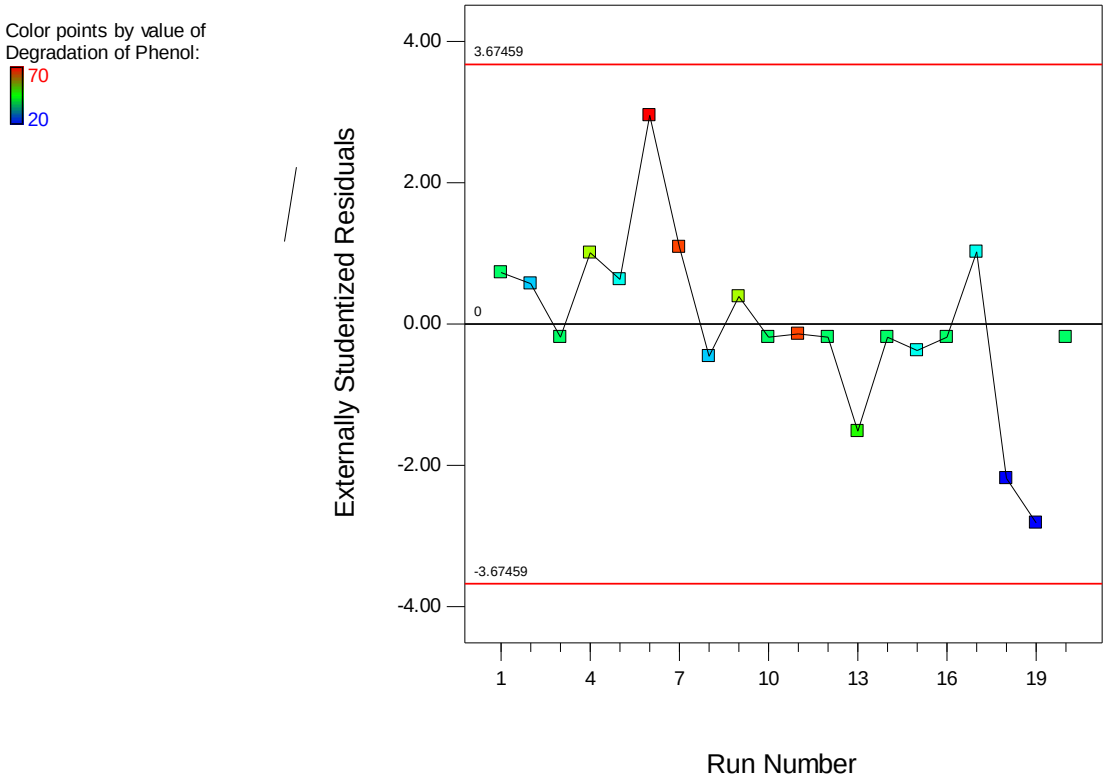

Figure 5.15: Residuals vs. runs for the degradation of phenol (CCD).

The data above indicates very erratic, unpredictable degradation outputs throughout the experimental run sequence and this is generally known for producing well fitted and robust models. With no distinct pattern observed this implies there is a great chance this model would provide good prediction ability. All data points fall within the limits and the model would take into account all experimental runs conducted.

Figure 5.16 of predicted vs. actual values can be observed below.

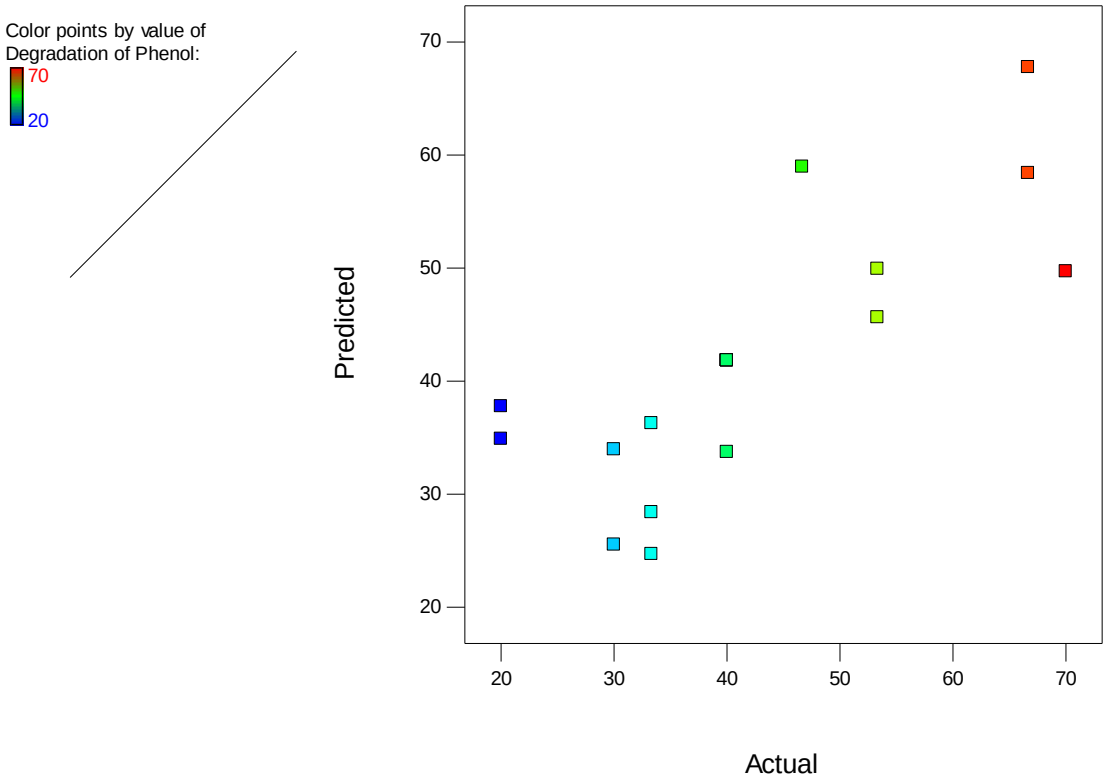

Figure 5.16: Predicted vs. actual values for the degradation of phenol (CCD).

The graph above shows a very random scatter of residuals along the 45 degree line and this scatter occurred throughout the degradation range. This indicates a high possibility that the model is well fitted and would be a good predictor of the design space. In the actual degradation range of 30% to 40% a small grouping occurs which indicates the likelihood of under prediction within this range. Similar explanation can be used for the actual degradation range of 60% to 70% as the majority of residuals sit below the 45 degree line.

Table 5.7 indicates the response output data for the degradation of phenol. Refer to appendix F-4 for attempt 1 data.

Table 5.7: CCD response output data for phenol degradation

Response	**2**	**Degradation of Phenol**			
ANOVA for Response Surface Reduced 2FI model					
Analysis of variance table [Partial sum of squares - Type III]					
	Sum of		Mean	F	p-value
Source	Squares	df	Square	Value	Prob > F
Model	2345.615	4	586.4037	6.095256	0.004051 significant
A-Catalyst Concentration	316.7251	1	316.7251	3.292136	0.089661
B-Run Time	1416.888	1	1416.888	14.72756	0.001614
C-Air Flow rate	299.3766	1	299.3766	3.11181	0.098076
AB	312.625	1	312.625	3.249518	0.091569
Residual	1443.099	15	96.20657		
Lack of Fit	1443.099	10	144.3099		
Pure Error	0	5	0		
Cor Total	3788.713	19			

Std. Dev.	9.808495	**R-Squared**	0.619106
Mean	41.833	**Adj R-Squared**	0.517534
C.V. %	23.44679	**Pred R-Squared**	0.139512
PRESS	3260.143	**Adeq Precision**	8.78118
-2 Log Likelihood	142.3339	**BIC**	157.3125
		AICc	156.6196

Degradation of phenol = 44.833 + 4.816A + 10.19B - 4.68C + 6.25AB (18)

The table above displays analysis of the output data and it can be observed that a significant model is developed since the model has an F-value of 6.10. There is only a 0.41% likelihood that an F value this large could occur due to noise. Where Prob>F is less than 0.05, it indicates significant model terms, therefore term B is significant. All other terms are below 0.1 and this indicates they are significant for the model. A R^2 value of 0.62 is noted and this indicates the model is a decent fit to the

data, however not extremely well fitted. There is also a notable difference between the predicted R^2 value and adjusted R^2 value which may be an indication that the model prediction ability is not as great as one would expect from the above residual analysis. A noise ratio of 8.78 was obtained and this is good as values above 4 are desirable. This gives an indication that the model can be used to navigate the design space well.

5.5. The Box-Behnken Design (BBD)

The Box-Behnken Design is a quadratic design approach which makes use of the midpoint, centre points and edges of the process. In this design each factor can be tested at only three levels. This design model has many positives as it is insensitive to outliers and missing data. The BBD default setting is aimed at reducing average prediction variance, thus resulting in the development of a robust model with very good prediction capabilities. Refer to appendix C-3 for BBD output data.

The design matrix indicating the experimental run order for the BBD can be seen below.

Table 5.8: BBD experimental run matrix

		Factor 1	Factor 2	Factor 3
Std	**Run**	**A:Catalyst Concentration (g/L)**	**B:Run Time (min)**	**C:Air Flow rate (L/min)**
8	1	8	60	1.48
10	2	5	90	0.768
15	3	5	60	1.11
9	4	5	30	0.768
2	5	8	30	1.11
6	6	8	60	0.768
5	7	2	60	0.768
14	8	5	60	1.11
11	9	5	30	1.48
4	10	8	90	1.11
13	11	5	60	1.11
12	12	5	90	1.48
16	13	5	60	1.11
17	14	5	60	1.11
3	15	2	90	1.11
1	16	2	30	1.11
7	17	2	60	1.48

5.5.1. Evaluation of the model for oil in water degradation

The following figures were developed from the degradation outputs using the BBD model. Figure 5.17 of the normal plot of residuals can be observed below.

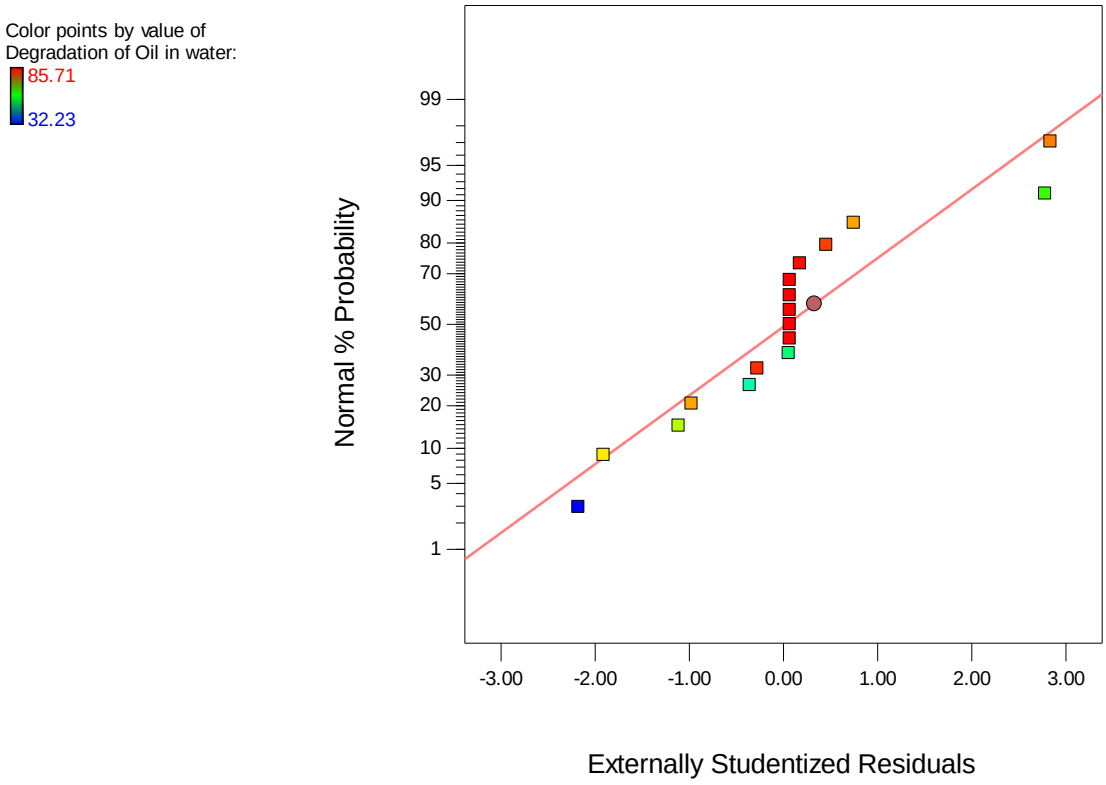

Figure 5.17: Normal plot of residuals for the degradation of oil (BBD).

The graph above displays the scatter of residuals in a linear manner. Several points lie very close to as well as on the regression line and this indicates a good fit of the model to the data. The upper and lower normal percentage probabilities also sit close to the line implying even at the boundary points the model still has a good fit. A vertical line of residuals is observed in the normal percentage probability region between 35% and 70% and in this region the model would therefore not be as good a predictor as other areas.

Figure 5.18 below displays the residuals vs. predicted data.

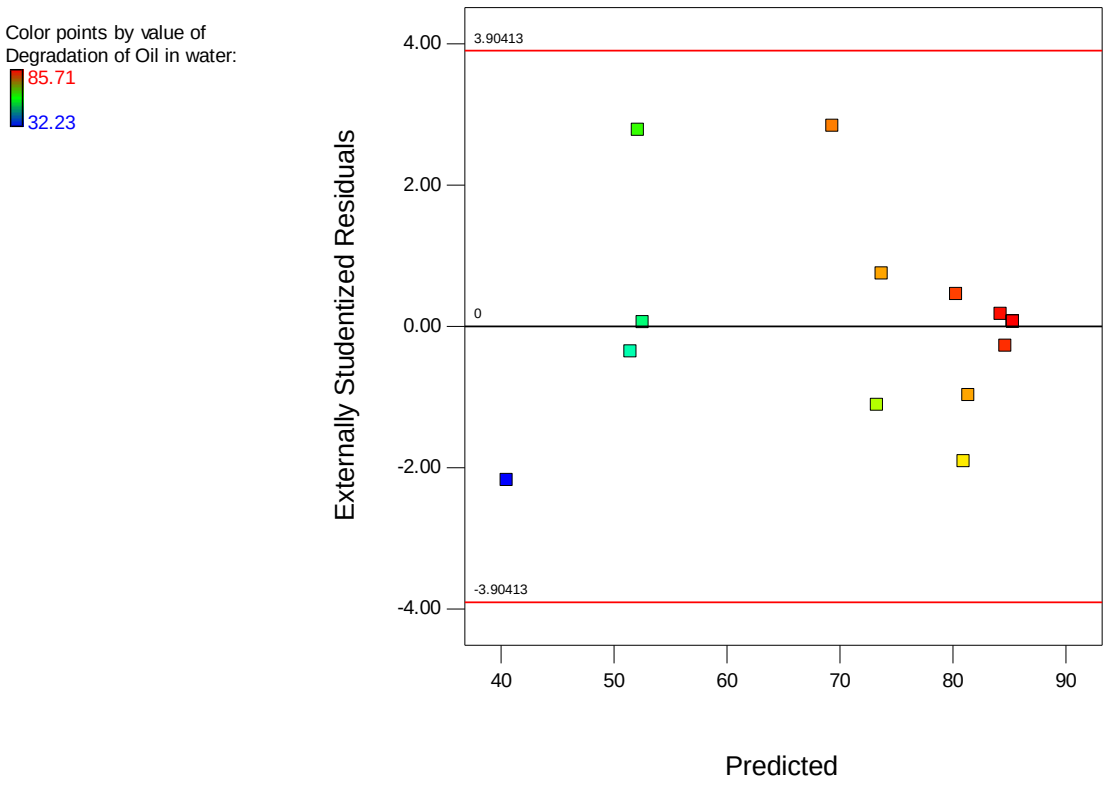

Figure 5.18: Residuals vs. predicted data for the degradation of oil (BBD).

The residuals above don't seem to be following any distinct pattern or trend. They are scattered very randomly and this is highly desirable. This ensures the development of a much more robust model which can navigate the design space with much greater accuracy.

A graph of the residuals vs. runs can be observed below:

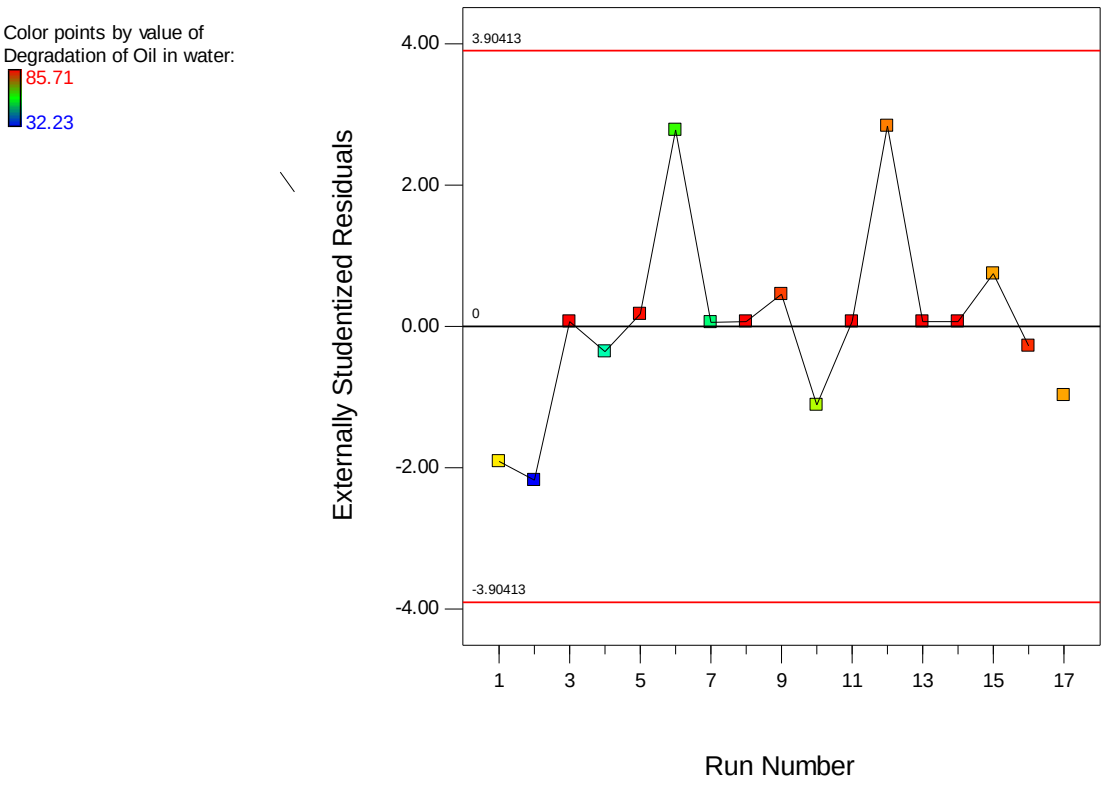

Figure 5.19: Residuals vs. runs for the degradation of oil (BBD).

When examining the residuals and the experimental run sequence it can be noted that no clear trend is present. The outputs are very random and allows for a much better model to be developed as the model would take into account all factors and not just be based on an observable trend which is unreliable. All residuals fall within the limits and with no outliers present, it reinforces a good model and representative data for the process.

Figure 5.20 depicts the predicted vs. actual data for the process outputs:

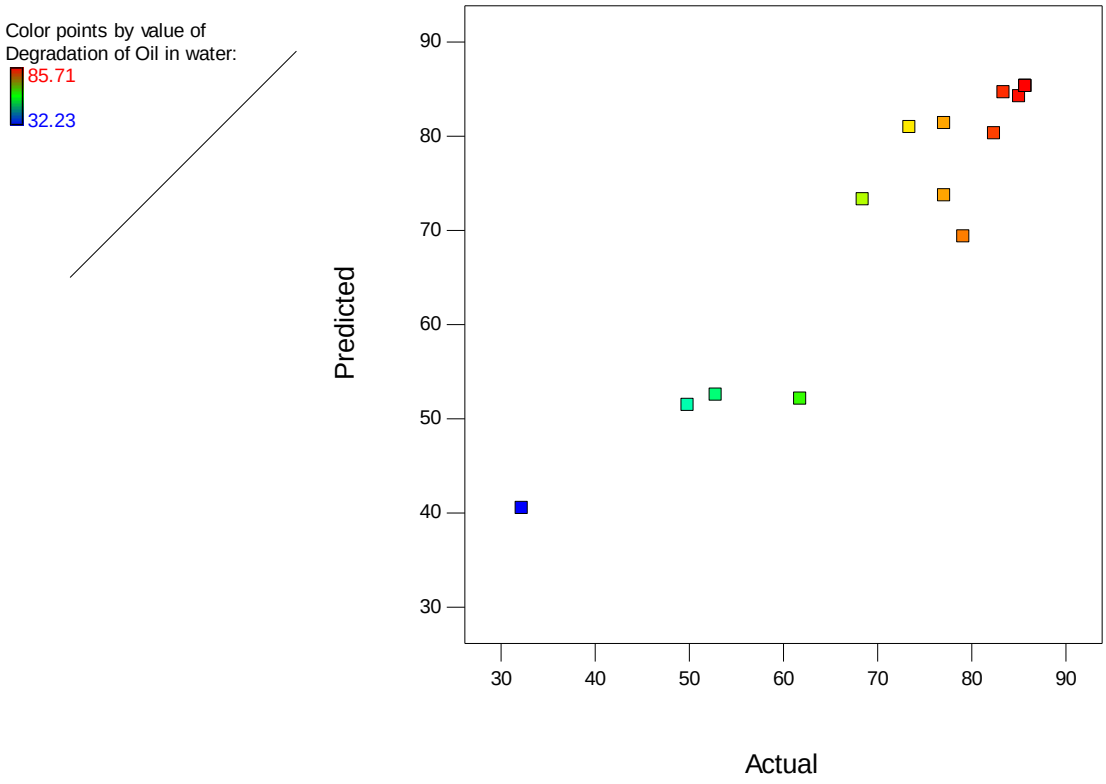

Figure 5.20: Predicted vs. actual data for the degradation of oil (BBD).

The graph above displays a good scatter of residuals with no distinct shape formed. The lowest percentage degradation is quite high above the 45 degree line implying at low percentage degradation the model may have the tendency to over predict. At higher percentage degradation values there is no distinctly larger grouping above or below the 45 degree line thus resulting in a much better prediction. From the graph is can be observed that at the maximum percentage degradation, the model is able to predict very well as the actual values and predicted values are in very close proximity to each other and the 45 degree line.

Table 5.9 presents an analysis of the process outputs for the degradation of oil (A is catalyst concentration, B is run time and C is air flow rate). Refer to appendix F-5 for attempt 1 data.

Table 5.9: BBD response output data for the degradation of oil

Response	**1**	**Degradation of Oil in water**			
ANOVA for Response Surface Reduced Quadratic model					
Analysis of variance table [Partial sum of squares - Type III]					
	Sum of		Mean	F	p-value	
Source	Squares	df	Square	Value	Prob > F	
Model	3588.427	5	717.6853	20.87532	2.82373E-05	significant
A-Catalyst Concentration	0.357013	1	0.357013	0.010384	0.92066673	
B-Run Time	239.6955	1	239.6955	6.972027	0.022974337	
C-Air Flow rate	1662.338	1	1662.338	48.35245	2.41161E-05	
B^2	170.1659	1	170.1659	4.949618	0.047963102	
C^2	1455.372	1	1455.372	42.33243	4.38947E-05	
Residual	378.1756	11	34.3796			
Lack of Fit	378.1756	7	54.02509			
Pure Error	0	4	0			
Cor Total	3966.602	16				

Std. Dev.	5.863412	**R-Squared**	0.90466
Mean	73.59824	**Adj R-Squared**	0.861324
C.V. %	7.966784	**Pred R-Squared**	0.702496
PRESS	1180.078	**Adeq Precision**	12.86194
-2 Log Likelihood	100.9804	**BIC**	117.9797
		AICc	121.3804

Model for the degradation of oil is as follows

$$Degradation\ of\ Oil = 85.32 - 5.47B + 14.42C - 6.35B^2 - 18.57C^2 \quad (19)$$

The above model is significant and has an F-value of 20.88. This implies that there is only a 0.01% likelihood that an F-value this high could be as a result of noise. Significant model terms are indicated by values less than 0.05, therefore B, C, B^2 and C^2 are all significant model terms. The

model produces an R^2 value of 0.9 which is very good. This indicates a good fit of the model to the data, thus the model is well representative of the process. The difference between the predicted R^2 and adjusted R^2 values is less that 0.2 indicating reasonable agreement. This means that the ability of the model to provide good prediction is high. A noise ratio of 12.86 is obtained indicating the model can be used to navigate the design space well.

5.5.2. Evaluation of the model for phenol degradation

The graphs below are obtained from the degradation outputs for phenol. The normal plot of residuals for phenol degradation can be seen in Figure 5.21 below:

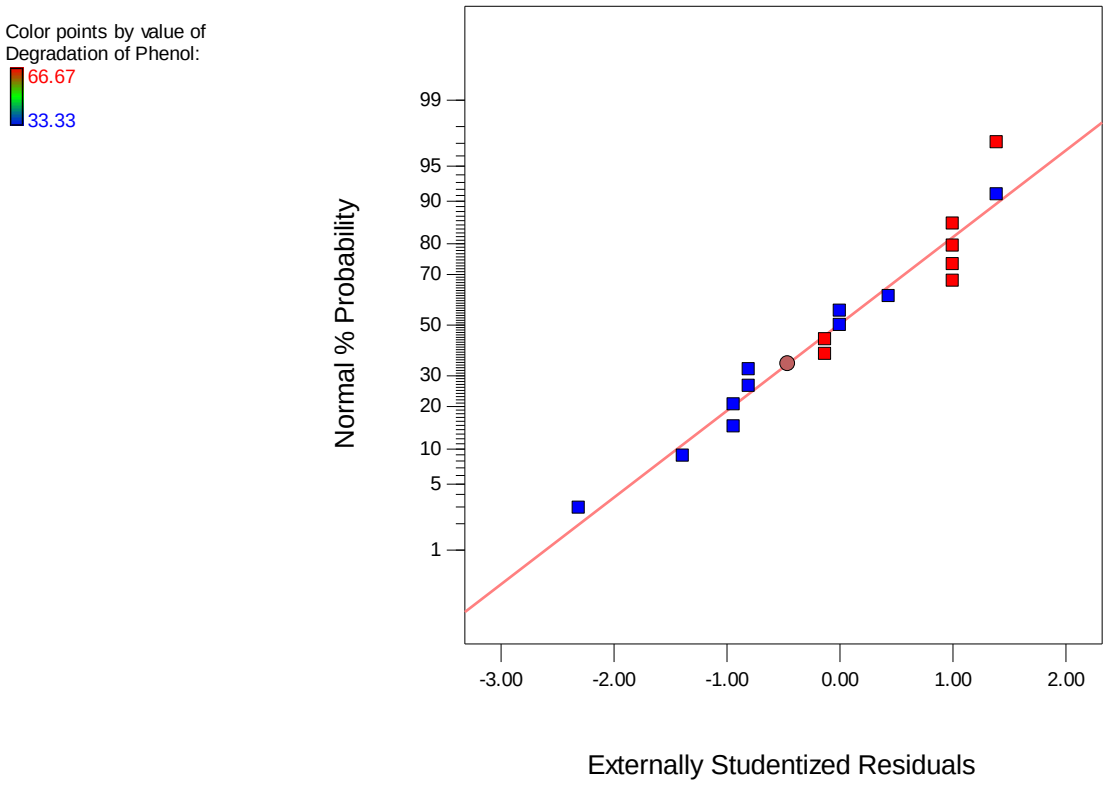

Figure 5.21: Normal plot of residuals for the degradation of phenol (BBD).

The residuals above are scattered in a very linear manner and are in close proximity to the regression line. This indicates a good fit of the model to the output data. The normal percentage probability range of 60% to 85% shows a vertical line of residuals and may result in the model not being very accurate within this range. It can be noted that the lower percentage degradation values are a better fit to the model.

Figure 5.22 below displays the residuals vs. predicted data:

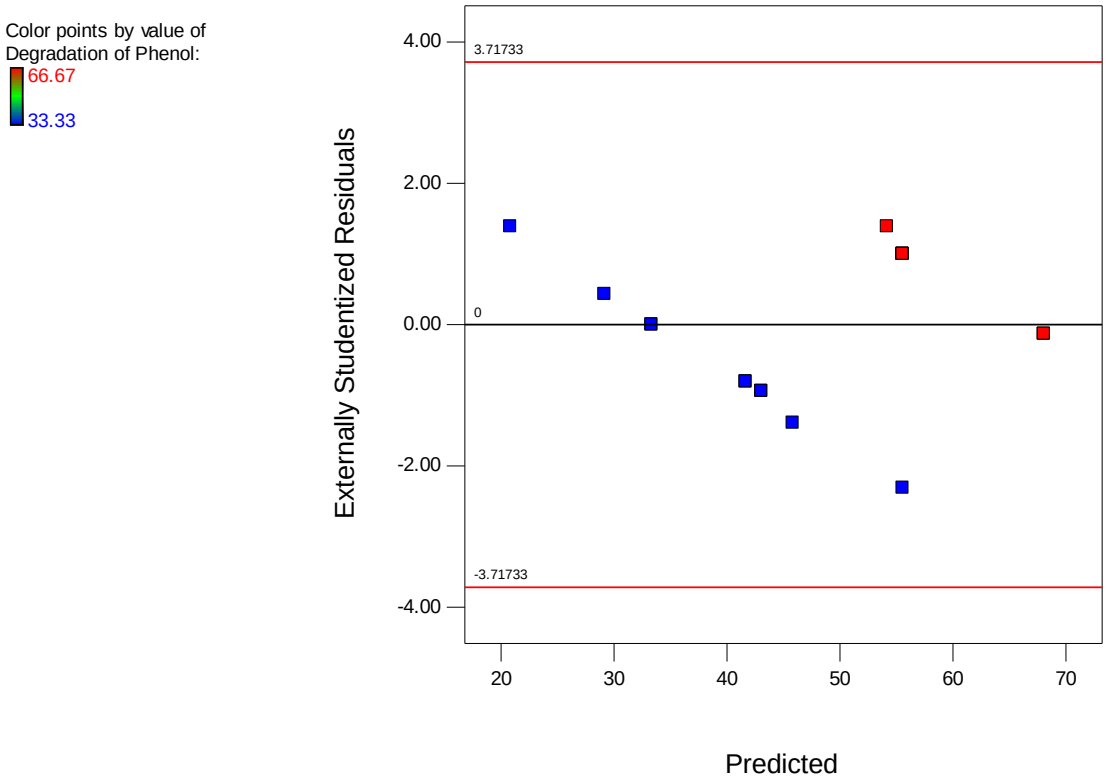

Figure 5.22: Residuals vs. predicted for the degradation of phenol (BBD).

The graph above displays residuals which tend to be spread in a very linear formation. This linear trend is very likely to result in a model unable to provide much prediction ability. For a more robust model to be developed, it is advisable to observe a random scatter of residuals.

Figure 5.23 displays the residuals vs. runs:

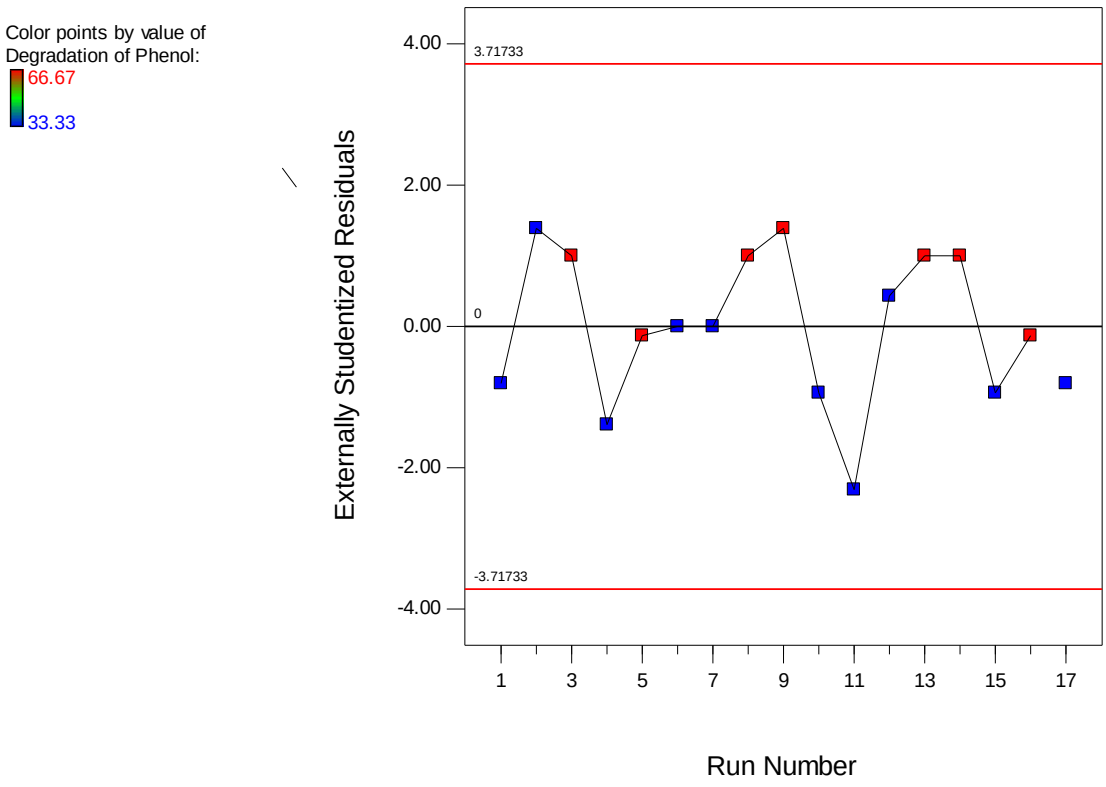

Figure 5.23: Residuals vs. run for the degradation of phenol (BBD).

The graph above shows no distinct trend of residual distribution for the sequence of experimental runs carried out. This random distribution of residuals is positive and indicates the model developed will be well fit to account for any process variation and that the model is not based on a trend in data. All data points sit within the limits and imply that all data was used for model development.

The predicted vs. actual data graph can be observed in Figure 5.24 below:

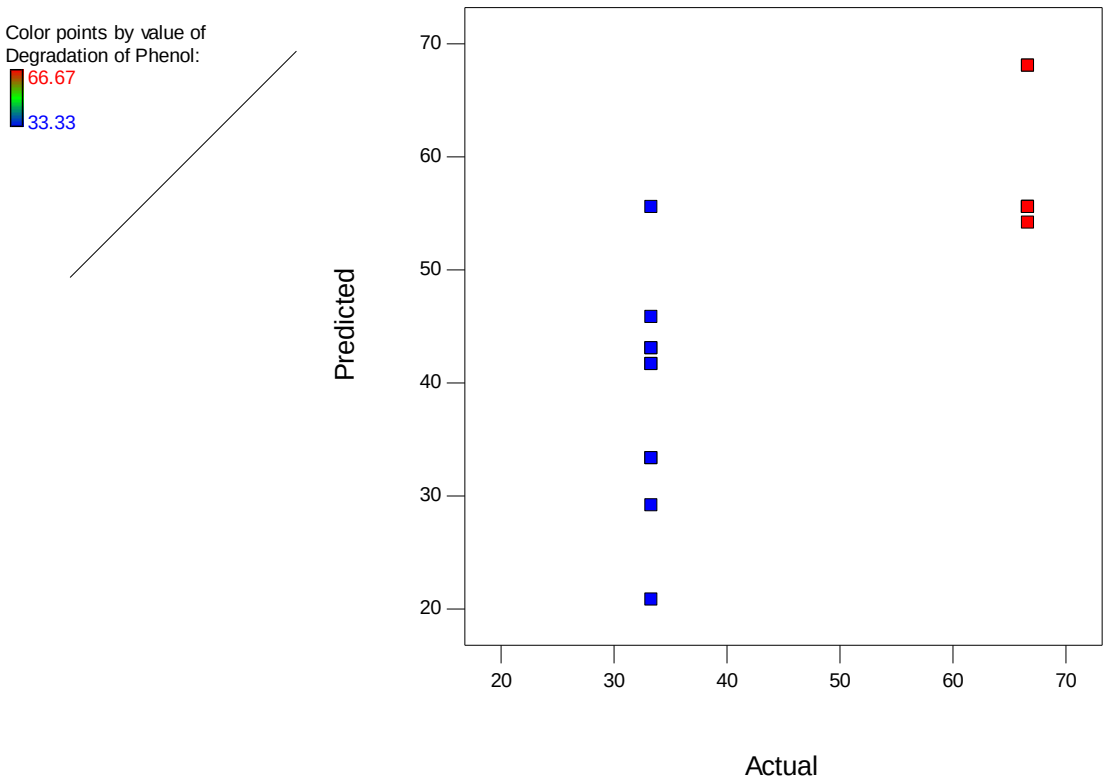

Figure 5.24: Predicted vs. actual data for the degradation of phenol (BBD).

The data above only shows one low percentage degradation and one high percentage degradation value that lie on and very close to the 45 degree line. In the percentage actual degradation range of 30% to 40% a grouping is observed above the 45 degree line indicating that within this range, the model is very likely to under predict outcomes. A similar trend occurs in the percentage actual degradation range of 60% to 70% as most data sits below the 45 degree line. Overall, this model will result in poor prediction of the process and is not a good fit to the process.

Table 5.10 below presents an analysis of the output data for the degradation of phenol. Refer to appendix F-6 for attempt 1 data.

Table 5.10: BBD response output data for the degradation of phenol

ANOVA for Response Surface Reduced Quadratic model						
Analysis of variance table [Partial sum of squares - Type III]						
	Sum of		Mean	F	p-value	
Source	Squares	df	Square	Value	Prob > F	
Model	2770.72	3	923.57	6.65	0.0058	significant
B-Run Time	1250.50	1	1250.50	9.00	0.0102	
C-Air Flow rate	138.94	1	138.94	1.00	0.3356	
C2	1381.27	1	1381.27	9.94	0.0076	
Residual	1806.28	13	138.94			
Lack of Fit	917.03	9	101.89	0.46	0.8478	not significant
Pure Error	889.24	4	222.31			
Cor Total	4576.99	16				

Std. Dev.	11.79	**R-Squared**	0.6054
Mean	47.06	**Adj R-Squared**	0.5143
C.V. %	25.05	**Pred R-Squared**	0.3286
PRESS	3073.17	**Adeq Precision**	8.261
-2 Log Likelihood	127.56	**BIC**	138.90
		AICc	138.90

Model for the degradation of phenol is given as follows:

Degradation of Phenol = 55.56 - 12.5025B - 18.06C^2 (20)

The mode F-value of 6.55 implies that the model is significant and there is only 0.58% likelihood that this large an F value could be due to noise. Prob>F values less than 0.05 indicate significant terms and therefore B and C2 are significant terms. Lack of Fit F-value of 0.46 indicates that the lack of fit is not significantly relative to the error. This means there is an 84.78% chance that a lack of fit value this large could be as a result of noise. A non-significant lack of fit is good as it is desirable that the model fits. An R^2 value of 0.61 is not the greatest fitted model. The predicted R^2 and adjusted R^2 values are in reasonable agreement with each other as the difference between these values is less than 0.2. A noise ratio of 8.26 is obtained indicating the model will navigate the design space well, however due

to the low R^2 and poor fit of the model its prediction capabilities would not be a true representation of the process.

5.6. Verification of the design models

Verification of the design models involved exposing the models already developed to unfamiliar data in order to observe how well they navigate the design space and how capable they are at prediction. The verification involved introducing a new level for one factor and this was catalyst concentration. The new level was 7 g/L of catalyst loading. This new initial run conditions would be fed to the model to determine a predicted output response. This new initial run conditions would then be used to carry out the experimental run and get an actual output response. Evaluation of the model was done by drawing a comparison between the actual and predicted data and the model with the smallest variation would be the best fit. The table below indicates the new initial run conditions for verification.

Table 5.11: New initial run conditions for model verification

Catalyst Concentration (A)	**7 g/L**
Run Time (B)	60 mins
Air Flow rate (C)	1.11 L/min

This was then used to conduct an experimental run and the outcome from that run is found in Table 5.12 below:

Table 5.12: Calculation of oil and phenol degradation from experimental results

Oil in water calculation					
Verification Run	Weight of beaker before sample (g)	Total weight of oil and beaker (g)	Difference in weight (g)	PPM of Oil present in the 0.75 L sample	Percentage degradation of oil in water (%)
FEED	131.6170	131.6467	0.0297	39.60	
Verification Run	137.3320	137.3357	0.0037	4.93	87.54

Phenol Calculation		
Verification Run	Phenols (PPM)	Percentage degradation of Phenols (%)
FEED	3	
Verification Run	1.6	46.67

All six design models were then used to evaluate the new conditions and to provide predicted percentage degradation of oil and phenol. This was then compared to the above actual percentage degradation values calculated. Table 5.13 below compares actual and predicted results.

Table 5.13: Comparison of model prediction to actual results for oil and phenol degradation

Model selected	Predicted Degradation (%)	Actual degradation (%)	Difference (%)
Factorial Design			
Degradation of oil in water	71.79	87.54	15.75
Degradation of Phenol	39.83	46.67	6.84
Box-Behnken Design			
Degradation of oil in water	85.18	87.54	**2.36**
Degradation of Phenol	55.56	46.67	8.89
Central Composite Design			
Degradation of oil in water	79.96	87.54	7.58
Degradation of Phenol	48.01	46.67	**1.34**

From the above data which compares the actual degradation obtained from experimentation and the predicted degradation by design models, it can be observed how the models have performed. The best degradation of oil in water was obtained from the Box-Behnken design model. The best phenol degradation was predicted by the central composite design. Refer to appendix G-1, G-5 and G-6 for model selection details.

5.7. Determining the optimum conditions for photocatalytic degradation

The best design models for oil and phenol degradation were obtained from the comparison done during design verification. These models were then optimised to obtain the best operating conditions for oil and phenol degradation. Since degradation of oil and phenol occurs simultaneously in an experimental run, optimisation of the CCD and BBD will be done to determine which design model is able to produce the greatest combined degradation of both oil and phenol. These optimum conditions will then be identified.

5.7.1. Optimisation of CCD for oil and phenol degradation

The Design expert software package was used to optimise the CCD model. The optimisation was conducted with the aim of minimizing catalyst concentration and air flow rate while varying run time. This was selected as it allowed for the most economical operation of the process. The following outputs were produced in Table 5.14 below:

Table 5.14: Optimisation of the CCD model

Constraints						
		Lower	Upper	Lower	Upper	
Name	**Goal**	**Limit**	**Limit**	**Weight**	**Weight**	**Importance**
A:Catalyst Concentration	minimize	-1	1	1	1	3
B:Run Time	is in range	-1	1	1	1	3
C:Air Flow rate	minimize	-1	1	1	1	3
Degradation of Oil in water	maximize	33.55	100	1	1	3
Degradation of Phenol	maximize	20	100	1	1	3

Solution							
Number	**Catalyst Concentration**	**Run Time**	**Air Flow rate**	**Degradation of Oil in water**	**Degradation of Phenol**	**Desirability**	
1	-0.978	1.000	-1.000	87.880	45.874	0.715	Selected
2	-0.977	1.000	-1.000	87.887	45.891	0.715	
3	-0.985	1.000	-1.000	87.851	45.797	0.715	
4	-0.960	1.000	-1.000	87.958	46.076	0.715	
5	-0.997	1.000	-1.000	87.802	45.670	0.715	

Goals were set for the catalyst concentration and air flow rate to be minimized as this is most economical. The goal for run time was to be kept within range. The objective was set to maximize oil and phenol degradation. Based on the goals set, the solutions were produced. The default optimum solution was selected and Figures 5.25 and 5.26 developed. Refer to appendix G-2 and G-3 for optimisation diagrams.

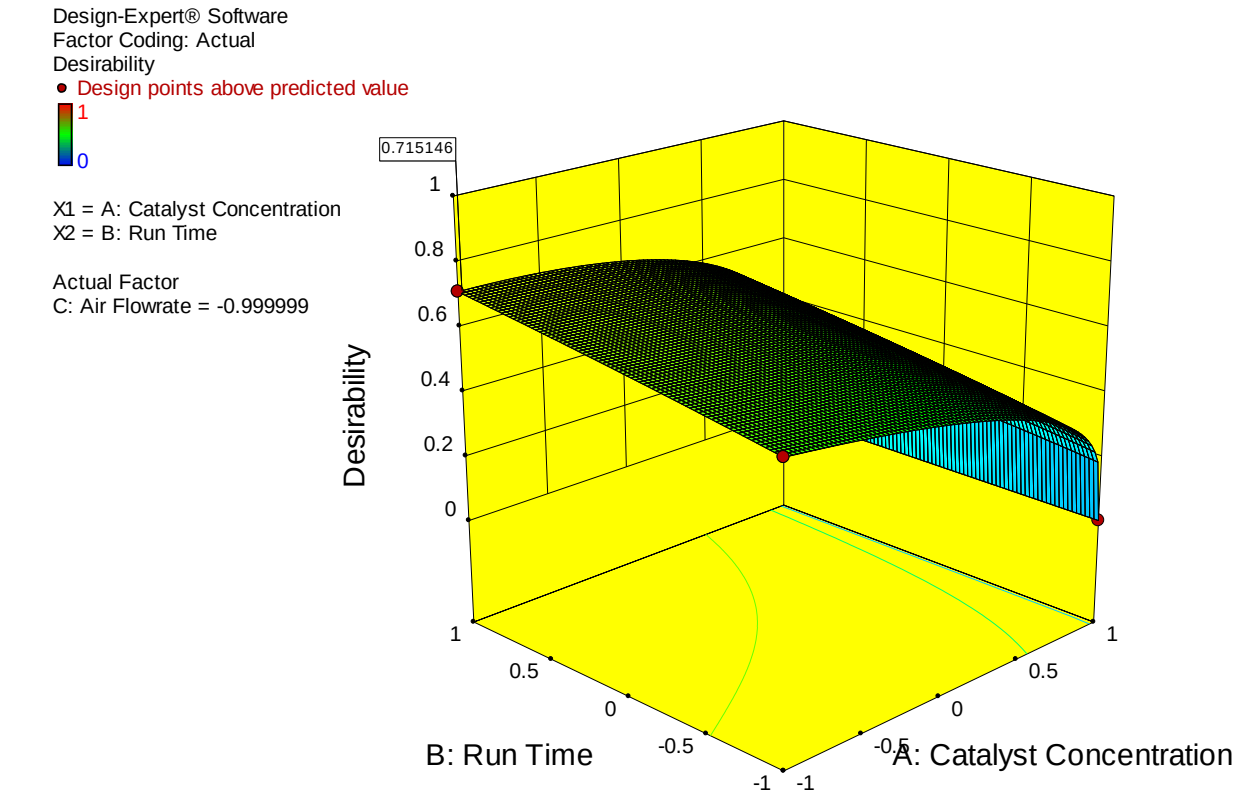

Figure 5.25: Response surface plot indicating the optimum points for photocatalytic degradation.

Figure 5.26 indicates the contour plots developed when optimising the degradation

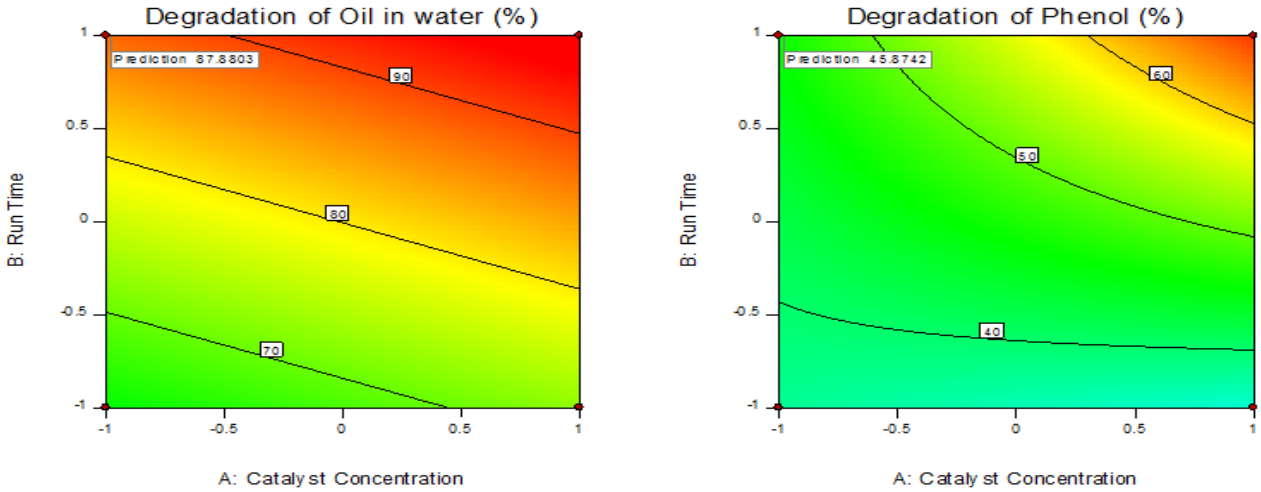

Figure 5.26: Contour plots indicating desirability of oil and phenol degradation.

The figures above both indicate the best desirability for maximum degradation of both oil and water using the CCD model is 71.5%. This occurs at a coded catalyst concentration of -0.978, a run time of 1 and an air flow rate of -1. Therefore the optimum conditions to achieve a desirable combined

degradation of 71.5% is with a catalyst concentration of 2.07 g/L, a run time of 90 minutes and an air flow rate of 0.768 L/min.

5.7.2. Optimisation of BBD for oil and phenol degradation

Optimisation of the BBD model occurred using Design expert and response surface methodology techniques. The optimisation was conducted with the aim of minimizing catalyst concentration and air flow rate while varying run time. This was selected as it allowed for the most economical operation of the process. The table below displays the output data for the optimisation study.

Table 5.15: Optimisation of the BBD model

Constraints						
		Lower	**Upper**	**Lower**	**Upper**	
Name	**Goal**	**Limit**	**Limit**	**Weight**	**Weight**	**Importance**
A:Catalyst Concentration	minimize	-1	1	1	1	3
B:Run Time	is in range	-1	1	1	1	3
C:Air Flow rate	minimize	-1	1	1	1	3
Degradation of Oil in water	maximize	32.23	100	1	1	3
Degradation of Phenol	maximize	33.33	100	1	1	3

Solutions							
Number	**Catalyst Concentration**	**Run Time**	**Air Flow rate**	**Degradation of Oil in water**	**Degradation of Phenol**	**Desirability**	
1	-1.000	-1.000	-0.214	80.716	66.336	0.681	Selected
2	-1.000	-1.000	-0.222	80.535	66.239	0.681	
3	-1.000	-1.000	-0.201	81.001	66.486	0.681	
4	-1.000	-1.000	-0.234	80.261	66.090	0.681	
5	-1.000	-1.000	-0.243	80.072	65.986	0.681	

Goals were set for the catalyst concentration and air flow rate to be minimized as this is most economical. The goal for run time was to be kept within range. The objective was set to maximize oil degradation within the range of 32.23 and 100%. The objective was to also degrade phenol in the range of 33.33 and 100%. Based on the goals set, the solutions were produced where a desirability of 0.681 was achieved. The default optimum solution was selected and Figures 5.27 and 5.28 developed.

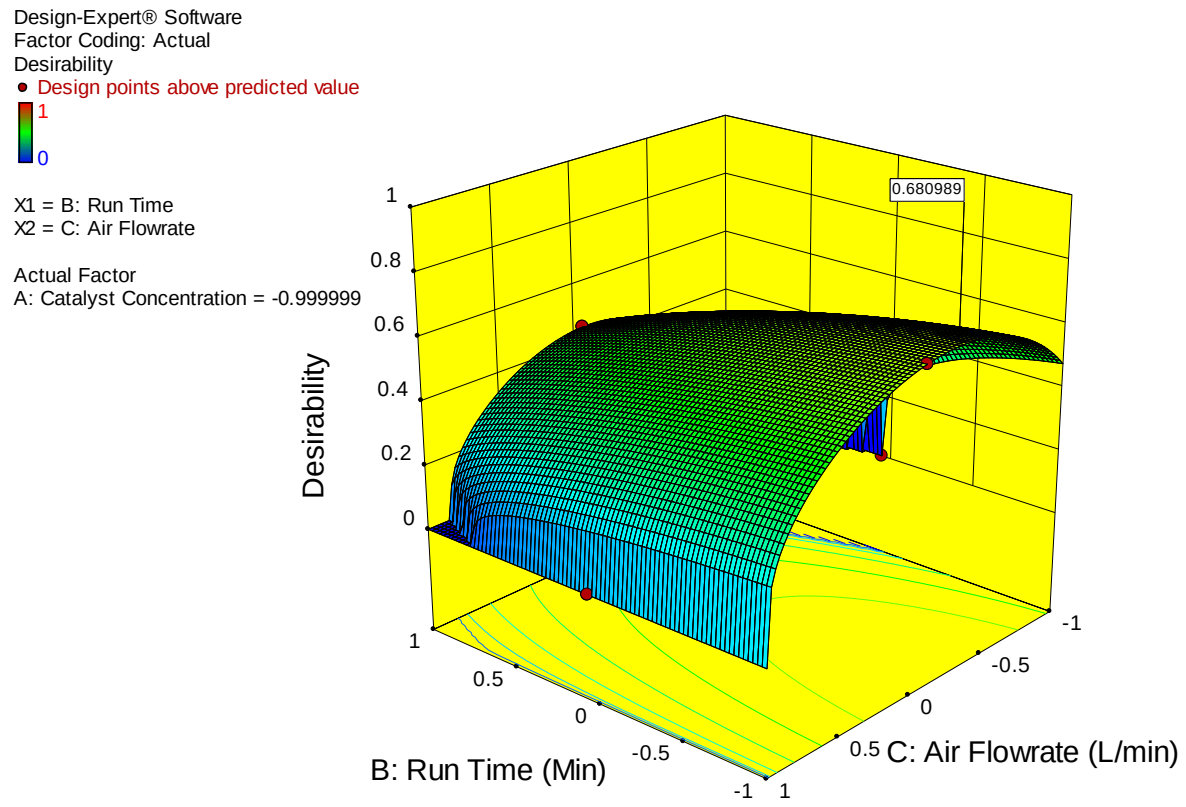

Figure 5.27: Response surface plot indicating optimum conditions for the BBD model.

Figure 5.28 below provides contour plots of the performance of oil and phenol degradation:

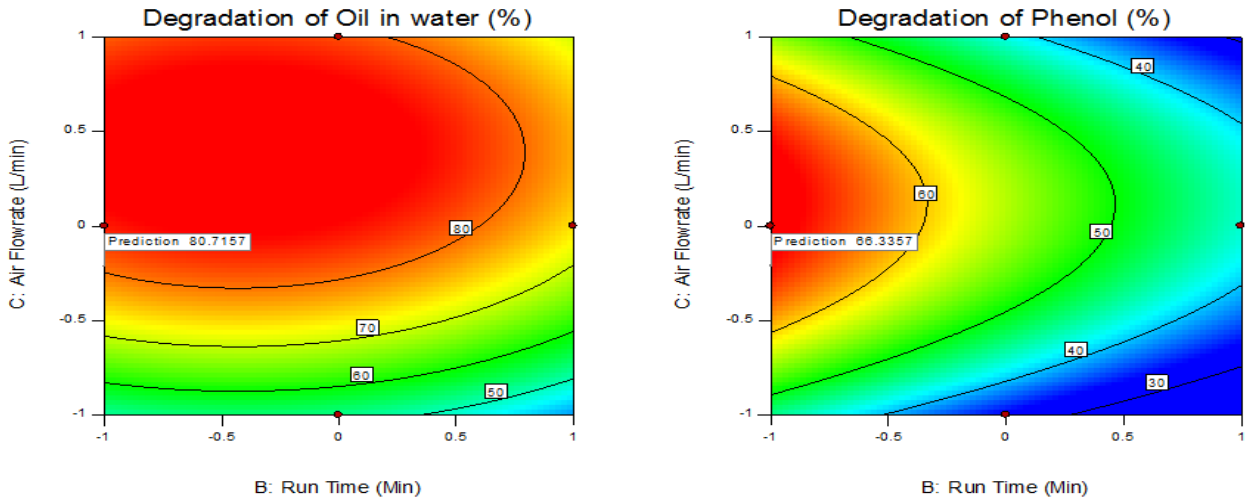

Figure 5.28: Contour plots for oil and phenol degradation when using the BBD model

Outputs from the BBD model indicate that the best desirability for the photocatalytic degradation of oil and phenol was 68.1%. This degradation occurred at a coded catalyst concentration of -1, run time of -1 and air flow rate of -0.214. This indicated that the optimum conditions for photocatalytic degradation of oil and phenol take place with a catalyst concentration of 2 g/L, a run time of 30 minutes and an air flow rate of 1.04 L/min. Refer to appendix G-4 for optimisation diagram.

Summary

The optimisation of the CCD and BBD models for the total degradation of both oil and phenol was noted to be 71.5% and 68% respectively. This optimisation aimed at minimizing catalyst concentration and air flow rate as well as keeping run time within range. This was selected as it allowed for the most economical operation of the process. When considering degradation of individual contaminants, the degradation of oil can be best presented by the BBD model and phenol degradation by the CCD model.

CHAPTER 6: CONCLUSION AND RECOMMENDATIONS

Water is an integral part of sustaining life, which is why it should be used in a sustainable manner. Industries are a big part of any counties economy as they contribute significantly to the country's GDP. Industries generally entail processes of converting raw materials into high value final products. These processes are generally heavy water users and this causes them to generate large volumes of industrial wastewater. The study conducted placed focus on the crude refining industry as it is a major wastewater generator. It is imperative that refineries treat their wastewater and meet the specifications put in place by regulatory authorities. Traditional wastewater treatment methods may be inefficient and it is important that new methods are explored to keep up with the more stringent wastewater specifications.

The degradation of organics by photocatalytic processes is a wastewater treatment technique which is not explored much by the crude refining industry. This method involves the use of a titanium dioxide catalyst in the presence of UV light and oxygen. These environmental conditions support the advanced oxidation reaction to take place, which converts harmful organic contaminants into CO_2 and H_2O.

The aim of this research was to determine the effect of the photocatalytic degradation process on the degrading of oil and phenol as well as to monitor if it had any effect on sulphates. Models for contaminant degradation were then developed. These models were then optimised to determine the optimum conditions for the degradation of both oil and phenol in the synthetic crude refinery effluent. Micro scaled $Ti0_2$ was used at catalyst loadings of 2 g/L, 5 g/L and 8 g/L. Aeration of the reaction vessel took place at 0.768 L/min, 1.11 L/min and 1.48 L/min and run times of 30 min, 60 min and 90 min were conducted.

Experimental run matrices were developed during the DOE process. It was noted that no sulphate degradation took place, so focus was placed on the degradation of oil and phenol. The experimental runs provided data used for the multilevel factorial design, Central composite design and Box-Behnken design models to be developed. After model verification and evaluation was conducted, it was noted that the oil degradation could be best represented by the BBD model. The best phenol degradation was represented by the CCD model.

The testing of a local crude refinery effluent was conducted using the CCD and BBD optimum conditions. When using the CCD optimum conditions degradation of 76.98% and 84.21% was observed for both oil and phenol respectively. The BBD optimum conditions yielded a degradation of 83.33% for oil and 78.95% for phenol.

The CCD and BBD models were then optimised to determine the best operating conditions for the degradation of both oil and phenol degradation as well as the best desirability for the degradation of the contaminants simultaneously.

Optimisation of the CCD model achieved a desired combined oil and phenol degradation of 71.5%. This occurred at a catalyst concentration of 2.07 g/L, a run time of 90 minutes and an air flow rate of 0.768 L/min. When the BBD model was optimised, a desired combined degradation of both oil and phenol of 68% was obtained. This occurred at a catalyst concentration of 2 g/L, a run time of 30 minutes and an air flow rate of 1.04 L/min.

For future work intended on the photocatalytic degradation of crude refinery effluent, it is recommended that sunlight be used as a source of energy for the photo excitation and to drive the reaction. Also it is believed that a nano sized catalyst particle would achieve much greater degradation efficiency and would be a good comparator to the micro scaled titania used in this research.

REFERENCES

ABDELWAHAB, O., AMIN, N. K. & EL-ASHTOUKHY, E. S. 2009. Electrochemical removal of phenol from oil refinery wastewater. *J Hazard Mater,* 163**,** 711-6.

ADEWUMI, J. R., ILEMOBADE, A. A. & VAN ZYL, J. E. 2010. Treated wastewater reuse in South Africa: Overview, potential and challenges. *Resources, Conservation and Recycling*.

AHMADUN, F. L.-R., PENDASHTEH, A., ABDULLAH, L. C., BIAK, D. R. A., MADAENI, S. S. & ABIDIN, Z. Z. 2009. Review of technologies for oil and gas produced water treatment. *Journal of Hazardous Materials*.

AHMED, S., RASUL, M. G., MARTEN, W. N. & BROWN, R. 2010a. Recent Developments in Photocatalytic Degradation of Pesticides and Phenols in Storm and Wastewater effluent. *ERE Conference.* Australia: CSIRO Publishing.

AHMED, S., RASUL, M. G., MARTEN, W. N., BROWN, R. & HASHIB, M. A. 2010b. Heterogeneous Photocatalytic Degradation of Phenols in Wastewater: A Review on Current Status and Developments. *Desalination*.

AKPAN, U. G. & HAMEED, B. H. 2009. Parameters affecting the photocatalytic degradation of dyes using TiO2-based photocatalysts: A review. *Journal of Hazardous Materials*.

ALROUSAN, D. M. A., DUNLOP, P. S. M., MCMURRAY, T. A. & BYRNE, J. A. 2009. Photocatalytic inactivation of E. coli in surface water using immobilised nanoparticle TiO2 films. *Water Research*.

ANTONY, J. 2003. *Design of Experiments for Engineers and Scientists*, Elsevier Science & Technology Books.

BAJAJ, P. 2016. *SLM Manufacturing of Molybdenum (CCD)* [Online]. Researchgate. Available: https://www.researchgate.net/publication/312293337_SLM_Manufacturing_of_Molybdenum 2017].

BOWER, K. M. 2017. *What is Design of Experiments* [Online]. Available: http://asq.org/learn-about-quality/data-collection-analysis-tools/overview/design-of-experiments.html 2017].

CANADIAN WATER QUALITY GUIDELINES FOR THE PROTECTION OF AQUATIC LIFE 1999. Phenols. *In:* ENVIRONMENT, C. C. O. M. O. T. (ed.).

CHEMTREAT. 2017. *Flocculants & Coagulants* [Online]. Available: http://www.chemtreat.com/solutions/coagulants-flocculants/ 2017].

CHEN, C., WEI, L., GUO, X., GUO, S. & YAN, G. 2014. Investigation of heavy oil refinery wastewater treatment by integrated ozone and activated carbon -supported manganese oxides. *Fuel Processing Technology*.

CHONG, M. N., JIN, B., CHOW, C. W. & SAINT, C. 2010. Recent developments in photocatalytic water treatment technology: a review. *Water Res,* 44**,** 2997-3027.

CHOQUETTE-LABBÉ, M., SHEWA, W. A., LALMAN, J. A. & SHANMUGAM, S. R. 2014. Photocatalytic Degradation of Phenol and Phenol Derivatives Using a Nano-TiO2 Catalyst: Integrating Quantitative and Qualitative Factors Using Response Surface Methodology. *Water*

CLARK, J. 2013. *The Arrhenius equation* [Online]. Available: http://www.chemguide.co.uk/physical/basicrates/arrhenius.html 2017].

COELHO, A., CASTRO, A. V., DEZOTTI, M. A. & JR., G. L. S. A. 2006. Treatment of petroleum refinery sourwater by advanced oxidation processes. *Journal of Hazardous Materials*.

CORRÊA, A. X. R., TIEPO, E. N., SOMENSI, C. A., SPERB, R. M. & RADETSKI, C. M. 2010. Use of Ozone-Photocatalytic Oxidation O3 /UV/TiO2 and Biological Remediation for Treatment of Produced Water from Petroleum Refineries. *JOURNAL OF ENVIRONMENTAL ENGINEERING*.

DAS, L., DUTTA, M. & BASU, J. K. 2013. Photocatalytic degradation of phenol from industrial effluent using titania-zirconia nanocomposite catalyst. *INTERNATIONAL JOURNAL OF ENVIRONMENTAL SCIENCES,* 4.

DEPARTMENT OF WATER AND ENVIRONMENTAL AFFAIRS. 2017. *Projects and Programs* [Online]. Available: https://www.environment.gov.za/projectsprogrammes 2017].

DIYA'UDDEEN, B. H., DAUD, W. M. A. W. & ABDUL AZIZ, A. R. 2011. Treatment technologies for petroleum refinery effluents: A review. *Process Safety and Environmental Protection,* 89**,** 95-105.

DLAMINI, C. P. 2016. *Evaluation of micro-scaled TiO_2 on degradation and recovery of $mTiO_2$ from treated drinking water*. Master of Engineering, Durban University of Technology.

EL-NAAS, M. H., ALHAIJA, M. A. & AL-ZUHAIR, S. 2014. Evaluation of a three-step process for the treatment of petroleum refinery wastewater. *Journal of Environmental Chemical Engineering*.

FREY, D. D. & SUDARSANAM, N. 2006. An Adaptive One-Factor-at-a-Time Method for Robust Parameter Design: Comparison with Crossed Arrays via Case Studies. MIT.

FUJISHIMA, A. & ZHANG, X. 2006. Titanium dioxide photocatalysis: present situation and future approaches. *Comptes Rendus Chimie,* 9**,** 750-760.

GALLINA, A. 2009. *Response Surface Methodology as a tool for analysis of uncertainty in structural dynamics.* Ph.D, AGH University of Science and Technology.

GAYA, U. I. & ABDULLAH, A. H. 2008. Heterogeneous photocatalytic degradation of organic contaminants over titanium dioxide: A review of fundamentals, progress and problems. *Journal of Photochemistry and Photobiology C: Photochemistry Reviews*.

GHASEMI, Z., YOUNESI, H. & ZINATIZADEH, A. A. 2016. Preparation, characterization and photocatalytic application of TiO2/ Fe-ZSM-5 nanocomposite for the treatment of petroleum

refinery wastewater: Optimization of process parameters by response surface methodology. *Chemosphere*.

GRZECHULSKA, J., HAMERSKI, M. & MORAWSKI, A. W. 2000. Photocatalytic decomposition of oil in water. *Water Research*, 34.

HABIBI, M. H. & VOSOOGHIAN, H. 2005. Photocatalytic degradation of some organic sulfides as environmental pollutants using titanium dioxide suspension. *Journal of Photochemistry and Photobiology A: Chemistry*.

HASAN, D. U. B., ABDUL AZIZ, A. R. & DAUD, W. M. A. W. 2012. Oxidative mineralisation of petroleum refinery effluent using Fenton-like process. *Chemical Engineering Research and Design*.

HASHIM, H. A. A., MOHAMED, A. R. & TEONG, L. K. 2001. Solar Photocatalytic Degradation Of Tartrazine Using Titanium Dioxide. *Jurnal Teknologi*.

HAYDER, G., RAMLI, M. Z., MALEK, M. A., KHAMIS, A. & HILMIN, N. M. 2014. Prediction model development for petroleum refinery wastewater treatment. *Journal of Water Process Engineering*, 4**,** 1-5.

HOEKSTRA, A. Y. & HUNG, P. Q. 2005. Globalisation of water resources: international virtual water flows in relation to crop trade. *Global Environmental Change*.

KAHINDA, J. M., TAIGBENU, A. E. & BOROTO, J. R. 2007. Domestic rainwater harvesting to improve water supply in rural South Africa. *Physics and Chemistry of the Earth*.

KHAN, W. Z., NAJEEB, I., TUIYEBAYEVA, M. & MAKHTAYEVA, Z. 2015. Refinery wastewater degradation with titaniumdioxide, zinc oxide, and hydrogen peroxide in a photocatalytic reactor. *Process Safety and Environmental Protection*.

KHURI, A. I. & MUKHOPADHYAY, S. 2010. Response surface methodology. *WIREs Computational Statistics*, 2.

KONSTANTINOU, I. K. & ALBANIS, T. A. 2004. TiO2-Assisted Photocatalytic Degradation of Azo Dyes in Aqueous Solution: Kinetic and Mechanistic Investigations: A Review. *Applied Catalysis B Environmental*.

LAOUFI, N. A., TASSALIT, D. & BENTAHAR, F. 2008. The degradation of phenol in water solution by TiO2 photocatalysis in a helical reactor. *Global NEST Journal*, 10.

LAZAR, M. A., VARGHESE, S. & NAIR, S. S. 2012. Photocatalytic Water Treatment by Titanium Dioxide: Recent Updates. *Catalysts*.

LEIVISKÄ, K. 2013. *Introduction to Experiment Design.* University of Oulu.

LIWSIRISAENG, P., KALAMBAHETI, C., PONGKAO KASHIMA, D., JIEMSIRILERS, S. & JINAWATH, S. 2011. Photocatalytic degradation of phenolic compounds by TIO2 powder. *18th International conference on composite materials*.

MICHIGAN ENVIRONMENTAL EDUCATION CURRICULUM. 2016. *Coagulation* [Online]. Available: http://techalive.mtu.edu/meec/module03/WastewaterRegulations.htm 2017].

MONTGOMERY, D. C. 2001. *Design and Analysis of Experiments*, John Wiley and Sons.

MONTGOMERY, D. C. 2009. *Introduction to Statistical Quality Control*, United States of America, John Wiley & Sons, Inc.

MONTGOMERY, D. C., PECK, E. A. & GEOFFREY VINING, G. 2012. *Introduction to Linear Regression Analysis*, Hoboken, New Jersey, JOHN WILEY & SONS, INC.

MONTGOMERY, D. C. & RUNGER, G. C. 2003. *Applied Statistics and Probability for Engineers*, United States of America, John Wiley & Sons, Inc.

MORE STEAM. 2015. *Design of Experiments (DOE)* [Online]. Available: https://www.moresteam.com/toolbox/design-of-experiments.cfm 2017].

MOSLEHYANI, A., F., I. A., OTHMAN, M. H. D. & MATSUURA, T. 2015. Design and performance study of hybrid photocatalytic reactor-PVDF/MWCNT nanocomposite membrane system for treatment of petroleum refinery wastewater. *Desalination*.

MYERS, R. H., MONTGOMERY, D. C. & ANDERSON-COOK, C. M. 2009. *Response Surface Methodology Process and Product Optimization Using Designed Experiments*, Hoboken, New Jersey, John Wiley & Sons, Inc.

NAEEM, K. & FENG, O. 2009. Parameters effect on heterogeneous photocatalysed degradation of phenol in aqueous dispersion of TiO2. *Journal of Environmental Sciences*.

NEPPOLIAN, B., CHOI, H. C., SAKTHIVEL, S., ARABINDOO, B. & MURUGESAN, V. 2002. Solar/UV-induced photocatalytic degradation of three commercial textile dyes. *Journal of Hazardous Materials*.

NICKHESLAT, A., AMIN, M., IZANLOO, H., FATEHIZADEH, A. & MOHAMMADMOUSAVI, S. 2013. Phenol Photocatalytic Degradation by Advanced Oxidation Process under Ultraviolet Radiation Using Titanium Dioxide. *Journal of Environmental and Public Health*.

NOORJAHAN, M., PRATAP REDDY, M., DURGA KUMARI, V., LAVÉDRINE, B., BOULE, P. & SUBRAHMANYAM, M. 2003. Photocatalytic degradation of H-acid over a novel TiO2 thin film fixed bed reactor and in aqueous suspensions. *Journal of Photochemistry and Photobiology A: Chemistry*.

OLLER, I., MALATO, S. & SANCHEZ-PEREZ, J. A. 2011. Combination of Advanced Oxidation Processes and biological treatments for wastewater decontamination—A review. *Science of the Total Environment*.

PAKRAVAN, P., AKHBARI, A., MORADI, H., AZANDARYANI, A. H., MANSOURI, A. M. & SAFARI, M. 2015. Process modeling and evaluation of petroleum refinery wastewater treatment through response surface methodology and artificial neural network in a photocatalytic reactor using poly ethyleneimine (PEI)/titania (TiO2) multilayer film on quartz tube. *Appl Petrochem Res*.

PALAYESH, A. 2015. *Advanced Oxidation Processes* [Online]. Available: http://absunpalayesh.com/en/2015/12/30/advanced-oxidation-processes-aop/ 2017].

PAMBI, R. L. 2015. *Experimental and statistical evaluation of the performance of chitosan as a coagulant in the treatment of sugar refinery effluents.* Master of Engineering, Durban University of Technology.

PARDESHI, S. K. & PATIL, A. B. 2008. A simple route for photocatalytic degradation of phenol in aqueous zinc oxide suspension using solar energy. *Solar Energy,* 82.

PAVE MAINTENANCE. 2017. *Titanium Dioxide (TiO2) Photocatalysis* [Online]. Available: http://pavemaintenance.wikispaces.com/tio2+photocatalys+-+shannon 2017].

POSTEL, S. L. 2000. Entering an era of water scarcity: The challenges ahead. *Ecological Applications,* 4.

PRABHA, I. & LATHASREE, S. 2014. Photodegradation of phenol by zinc oxide, titania and zinc oxide–titania composites: Nanoparticle synthesis, characterization and comparative photocatalytic efficiencies. *Materials Science in Semiconductor Processing,* 26**,** 603-613.

RAND WATER. 2017. *Water Wise* [Online]. Available: http://www.waterwise.co.za/site/water/environment/situation.html 2017].

SAIEN, J. & NEJATI, H. 2007. Enhanced photocatalytic degradation of pollutants in petroleum refinery wastewater under mild conditions. *Journal of Hazardous Materials*.

SAIEN, J. & SHAHREZAEI, F. 2012. Organic Pollutants Removal from Petroleum Refinery Wastewater with Nanotitania Photocatalyst and UV Light Emission. *International Journal of Photoenergy,* 2012**,** 1-5.

SAVENIJE, H. H. G. 2000. Water Scarcity Indicators; the Deception of the Numbers. *Physics and Chemistry of the Earth Part B Hydrology Oceans and Atmosphere* 25.

SCHWIKKARD, G. W. 2001. *An Investigation Of Advanced Oxidation Processes In Water Treatment.* Doctor or Philosophy, University of Natal.

SCIENTIFIC RESEARCH. 2012. *Biomechanical prediction of abdominal aortic aneurysm rupture risk: Sensitivity analysis* [Online]. Available: http://file.scirp.org/Html/8-9101482_24768.htm 2017].

SHAHREZAEI, F., MANSOURI, Y., ZINATIZADEH, A. A. L. & AKHBARI, A. 2012. Process modeling and kinetic evaluation of petroleum refinery wastewater treatment in a photocatalytic reactor using TiO2 nanoparticles. *Powder Technology*.

SIEMENS. 2017. *API oil–water separator/Dissolved Air flotation (DAF)* [Online]. Available: https://web.archive.org/web/20070902123515/http://www.water.siemens.com/en/Industries/Hydrocarbon_Processing/Solutions_Newsletter/ 2017].

SKIMOIL. 2017. *API Oil water Separators* [Online]. Available: http://www.skimoil.com/api-oil-water-separator.html.

SOLTANIAN, G. R. & HAVAEE BEHBAHANI, M. 2011. The Effect Of Metal Oxides On The Refinery Effluent Treatment. *Iran. J. Environ. Health. Sci. Eng,* 8.

STAT-EASE 2014. *Handbook for Experimenters,* Minneapolis.

STEPNOWSKI, P., SIEDLECKA, E. M., BEHREND, P. & JASTORFF, B. 2002. Enhanced photo-degradation of contaminants in petroleum refinery wastewater. *Water Research,* 36**,** 2167-2172.

SUNDERARAJAN, K. 2000. *Design of Experiment* [Online]. Available: https://www.isixsigma.com/tools-templates/design-of-experiments-doe/design-experiments-%E2%90%93-primer/ 2017].

TETTEH, E. K. & RATHILAL, S. 2018. Evaluation Of The Coagulation Floatation Process For Industrial Mineral Oil Wastewater Treatment Using Response Surface methodology (RSM). *International Journal of Environmental Impacts,* 1.

THE NORTH SALT SPRING WATERWORKS. 2017. *Dissolved Air Floatation (DAF)* [Online]. Available: http://www.northsaltspringwaterworks.ca/st-mary-treatment-plant/daf-technology/ 2017].

THE WATER INFORMATION PROGRAM. 2004. *Water facts* [Online]. Available: https://www.waterinfo.org/resources/water-facts 2017].

THERMO FISHER SCIENTIFIC. 2017. *Gallery™ Automated Photometric Analyzer* [Online]. Available: https://assets.thermofisher.com/TFS-Assets/CMD/product-images/Gallery-PC-98610001.jpg-650.jpg 2017].

TUTORVISTA.COM. 2017. *Coagulation* [Online]. Available: http://chemistry.tutorvista.com/physical-chemistry/flocculation.html 2017].

UMAR, M. & AZIZ, H. A. 2013. Photocatalytic Degradation of Organic Pollutants in Water. *Intech*.

VAIANO, V., SACCO, O., PISANO, D., SANNINO, D. & CIAMBELLI, P. 2015. From the design to the development of a continuous fixed bed photoreactor for photocatalytic degradation of organic pollutants in wastewater. *Chemical Engineering Science,* 137**,** 152-160.

WESSELS, K. J., PRINCE, S. D., MALHERBE, J., SMALL, J., FROST, P. E. & VANZYL, D. 2007. Can human-induced land degradation be distinguished from the effects of rainfall variability? A case study in South Africa. *Journal of Arid Environments*.

YANG, R., ZHU, J., LI, Y. & ZHANG, H. 2016. A Study on the Preparation of Regular Multiple Micro Electrolysis Filler and the Application in Pretreatment of Oil Refinery Wastewater. *International Journal of Environmental Research and Public Health,* 13.

APPENDICES

Appendix A: Process Diagrams

A-1. Experimental Setup of two reaction vessels

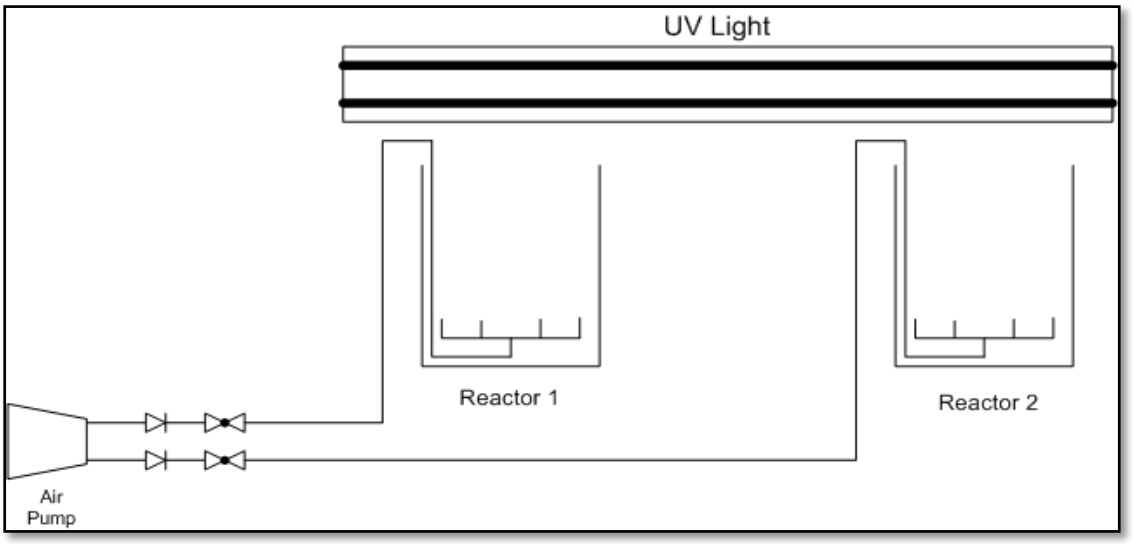

Figure A-1.1: Experimental setup for photocatalytic degradation.

A-2. Experimental run taking place

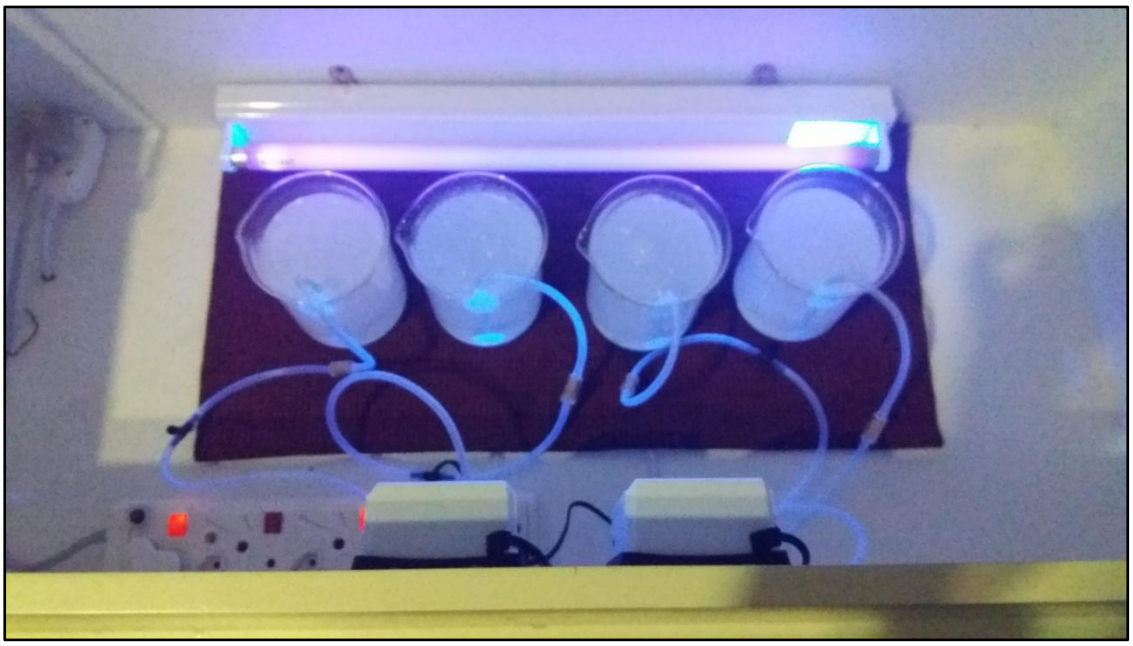

Figure A-2.1: Image of experimental run being conducted.

Appendix B: Synthetic feed

B-1. Development of synthetic feed-Projected composition prior to experiments

Analysis on Municipal water was conducted from 1 Feb 2017 to 22 March 2017. The results obtained were then averaged over the time period.

Synthetic feed (20Litre batch) = 100ml Oil (To achieve 50ppm)

= 20ml Phenol (To achieve 10ppm)

= 19 880ml Municipal water

Table B-1.1: Expected composition of synthetic feed

COMPONENT	COMPOSITION
Oil in water	50 ppm
Phenol	10 ppm
Phosphate	0.6
Calcium hardness	37
M-Alkalinity	77
TDS	233
pH	7.13
Iron (Fe)	0.06 ppm
Chlorides	99 ppm
Sulphates	22 ppm
Silica	6

The actual composition of the feed will be analysed once it is mixed.

Appendix C: Experimental Results

C-1: Multilevel factorial Design Outputs

Table C-1.1: Multilevel factorial design experimental outputs

		Factor 1	Factor 2	Factor 3	Response 1	Response 2	Response 3	
Std	Run	A:Catalyst Concentration	B:Run Time	C:Air Flow rate	Degradation of Oil in water	Degradation of Phenol	Degradation of Sulphates	
					%	%	%	pH
14	1	5g/L	60min	1.11L/min	85.71	40.00	0	9.55
6	2	8g/L	60min	0.768 L/min	61.79	20.00	0	8.77
1	3	2g/L	30min	0.768 L/min	73.75	33.33	0	9.05
8	4	5g/L	90min	0.768 L/min	32.23	33.33	0	8.81
13	5	2g/L	60min	1.11L/min	58.80	40.00	0	8.6
3	6	8g/L	30min	0.768 L/min	33.55	20.00	0	8.43
21	7	8g/L	30min	1.48 L/min	63.64	30.00	0	8.86
2	8	5g/L	30min	0.768 L/min	49.83	36.67	0	8.84
27	9	8g/L	90min	1.48 L/min	92.59	66.67	0	8.8
7	10	2g/L	90min	0.768 L/min	88.70	53.33	0	9.87
5	11	5g/L	60min	0.768 L/min	93.69	70.00	0	8.55
9	12	8g/L	90min	0.768 L/min	89.04	66.67	0	9.7
15	13	8g/L	60min	1.11L/min	93.69	53.33	0	8.74
23	14	5g/L	60min	1.48 L/min	62.79	30.00	0	9.09
16	15	2g/L	90min	1.11L/min	77.08	33.33	0	9.35
22	16	2g/L	60min	1.48 L/min	66.33	30.00	0	8.79
17	17	5g/L	90min	1.11L/min	87.21	46.67	0	8.82
25	18	2g/L	90min	1.48 L/min	79.73	33.33	0	9.05
12	19	8g/L	30min	1.11L/min	85.05	66.67	0	9.17
24	20	8g/L	60min	1.48 L/min	73.40	53.33	0	8.79
10	21	2g/L	30min	1.11L/min	83.39	40.00	0	9.02
11	22	5g/L	30min	1.11L/min	74.42	33.33	0	9.16
19	23	2g/L	30min	1.48 L/min	49.16	33.33	0	8.81
4	24	2g/L	60min	0.768 L/min	52.82	33.33	0	8.74
26	25	5g/L	90min	1.48 L/min	79.12	46.67	0	8.82

20	26	5g/L	30min	1.48 L/min	82.39	70.00	0	9.28
18	27	8g/L	90min	1.11L/min	68.44	33.33	0	9.33

C-2. Central Composite Design Outputs

Table C-2.1: Central composite design experimental outputs

		Factor 1	Factor 2	Factor 3	Response 1	Response 2	Response 3
Std	**Run**	**A:Catalyst Concentration**	**B:Run Time**	**C:Air Flow rate**	**Degradation of Oil in water**	**Degradation of Phenol**	**Degradation of Sulphates**
					%	%	%
9	1	2g/L	60 min	1.11 L/min	58.8	40	0
6	2	8g/L	30 min	1.48 L/min	63.64	30	0
15	3	5g/L	60 min	1.11 L/min	85.71	40	0
3	4	2g/L	90 min	0.768 L/min	88.7	53.33	0
5	5	2g/L	30 min	1.48 L/min	49.16	33.33	0
13	6	5g/L	60 min	0.768 L/min	93.69	70	0
8	7	8g/L	90 min	1.48 L/min	92.59	66.67	0
14	8	5g/L	60 min	1.48 L/min	62.79	30	0
10	9	8g/L	60 min	1.11 L/min	93.69	53.33	0
18	10	5g/L	60 min	1.11 L/min	85.71	40	0
4	11	8g/L	90 min	0.768 L/min	89.04	66.67	0
16	12	5g/L	60 min	1.11 L/min	85.71	40	0
12	13	5g/L	90 min	1.11 L/min	87.21	46.67	0
20	14	5g/L	60 min	1.11 L/min	85.71	40	0
7	15	2g/L	90 min	1.48 L/min	79.73	33.33	0
17	16	5g/L	60 min	1.11 L/min	85.71	40	0
11	17	5g/L	30 min	1.11 L/min	74.42	33.33	0
2	18	8g/L	30 min	0.768 L/min	33.55	20	0
1	19	2g/L	30 min	0.768 L/min	61.79	20	0
19	20	5g/L	60 min	1.11 L/min	85.71	40	0

C-3. Box-Behnken Design Outputs

Table C-3.1: Box-Behnken experimental outputs

		Factor 1	Factor 2	Factor 3	Response 1	Response 2	Response 3
Std	**Run**	**A:Catalyst Concentration**	**B:Run Time**	**C:Air Flow rate**	Degradation of Oil in water	Degradation of Phenol	Degradation of Sulphates
					%	%	%
8	1	8g/L	60 min	1.48 L/min	73.4	53.33	0
10	2	5g/L	90 min	0.768 L/min	32.23	33.33	0
15	3	5g/L	60 min	1.11 L/min	85.71	40	0
9	4	5g/L	30 min	0.768 L/min	49.83	36.67	0
2	5	8g/L	30 min	1.11 L/min	85.05	66.67	0
6	6	8g/L	60 min	0.768 L/min	61.79	20	0
5	7	2g/L	60 min	0.768 L/min	52.82	33.33	0
14	8	5g/L	60 min	1.11 L/min	85.71	40	0
11	9	5g/L	30 min	1.48 L/min	82.39	70	0
4	10	8g/L	90 min	1.11 L/min	68.44	33.33	0
13	11	5g/L	60 min	1.11 L/min	85.71	40	0
12	12	5g/L	90 min	1.48 L/min	79.12	46.67	0
16	13	5g/L	60 min	1.11 L/min	85.71	40	0
17	14	5g/L	60 min	1.11 L/min	85.71	40	0
3	15	2g/L	90 min	1.11 L/min	77.08	33.33	0
1	16	2g/L	30 min	1.11 L/min	83.39	40	0
7	17	2g/L	60 min	1.48 L/min	66.33	30	0

C-4. Evaluating performance using the average degradation

Table C-4.1: Average degradation results

	Cat concentration						**Run time**						**Air flow rate**					
	2g		5g		8g		30min		60min		90min		0.768L/min		1.11L/min		1.48L/min	
	% Oil	% Phenol	% Oil	% Phenol	% Oil	% Phenol	% Oil	% Phenol	% Oil	% Phenol	% Oil	% Phenol	% Oil	% Phenol	% Oil	% Phenol	% Oil	% Phenol
	73.75	33.33	85.71	40.00	61.79	20.00	73.75	33.33	85.71	40.00	32.23	33.33	61.79	20.00	85.71	40.00	63.64	30.00
	58.80	40.00	32.23	33.33	33.55	20.00	33.55	20.00	61.79	20.00	92.59	66.67	73.75	33.33	58.80	40.00	92.59	66.67
	88.70	53.33	49.83	36.67	63.64	30.00	63.64	30.00	58.80	40.00	88.70	53.33	32.23	33.33	93.69	53.33	62.79	30.00
	77.08	33.33	93.69	70.00	92.59	66.67	49.83	36.67	93.69	70.00	89.04	66.67	33.55	20.00	77.08	33.33	66.33	30.00
	66.33	30.00	62.79	30.00	89.04	66.67	85.05	66.67	93.69	53.33	77.08	33.33	49.83	36.67	87.21	46.67	79.73	33.33
	79.73	33.33	87.21	46.67	93.69	53.33	83.39	40.00	62.79	30.00	87.21	46.67	88.70	53.33	85.05	66.67	73.40	53.33
	83.39	40.00	74.42	33.33	85.05	66.67	74.42	33.33	66.33	30.00	79.73	33.33	93.69	70.00	83.39	40.00	49.16	33.33
	49.16	33.33	79.12	46.67	73.40	53.33	49.16	33.33	73.40	53.33	79.12	46.67	89.04	66.67	74.42	33.33	79.12	46.67
	52.82	33.33	82.39	70.00	68.44	33.33	82.39	70.00	52.82	33.33	68.44	33.33	52.82	33.33	68.44	33.33	82.39	70.00
Average	69.97	36.67	71.93	45.19	73.47	45.56	66.13	40.37	72.11	41.11	77.13	45.93	63.94	40.74	79.31	42.96	72.13	43.7

Appendix D: Graphical representation of the effects of variables on runs

D-1. Effects of catalyst concentration on Oil in water runs

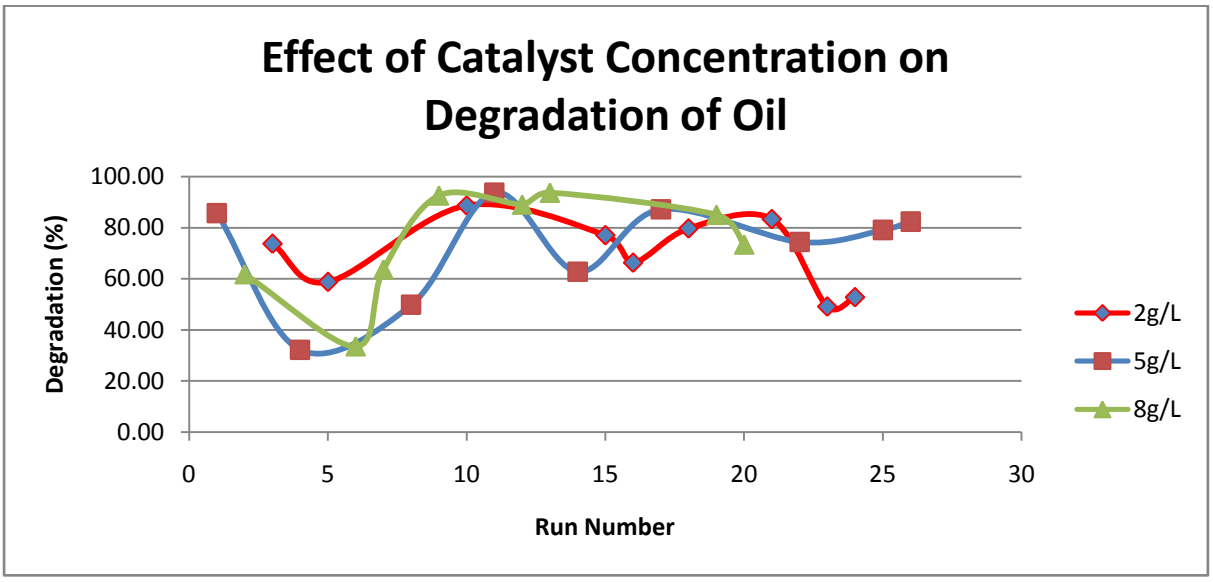

Figure D-1.1: Effect of catalyst concentration on the degradation of oil.

D-2. Effects of run time on Oil in water runs

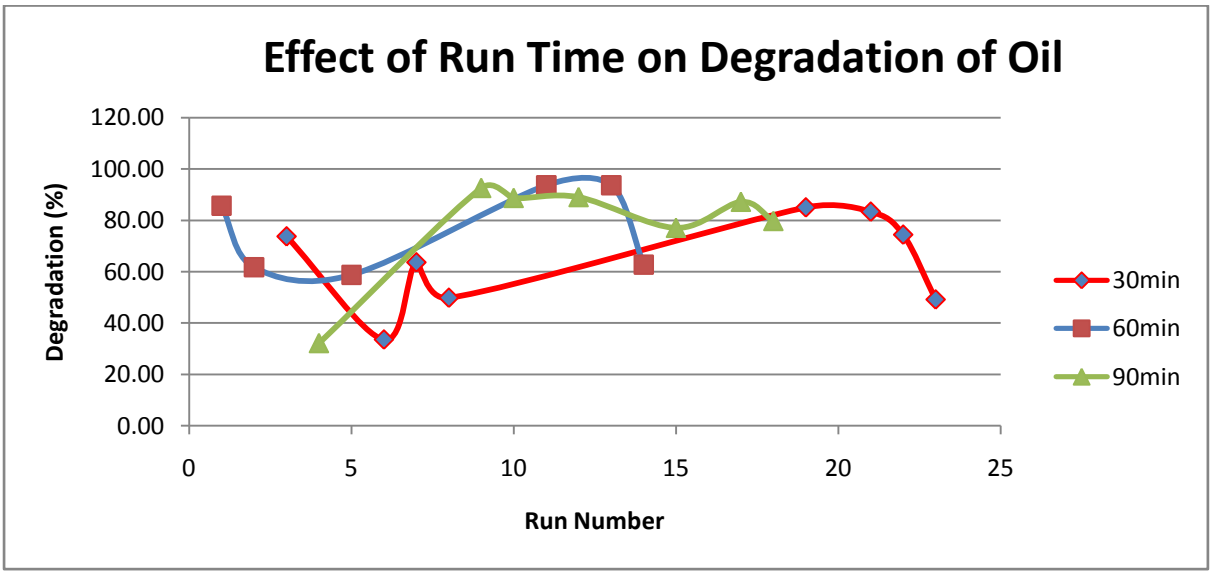

Figure D-2.1: Effects of run time on the degradation of oil.

D-3. Effects of air flow rate on Oil in water runs

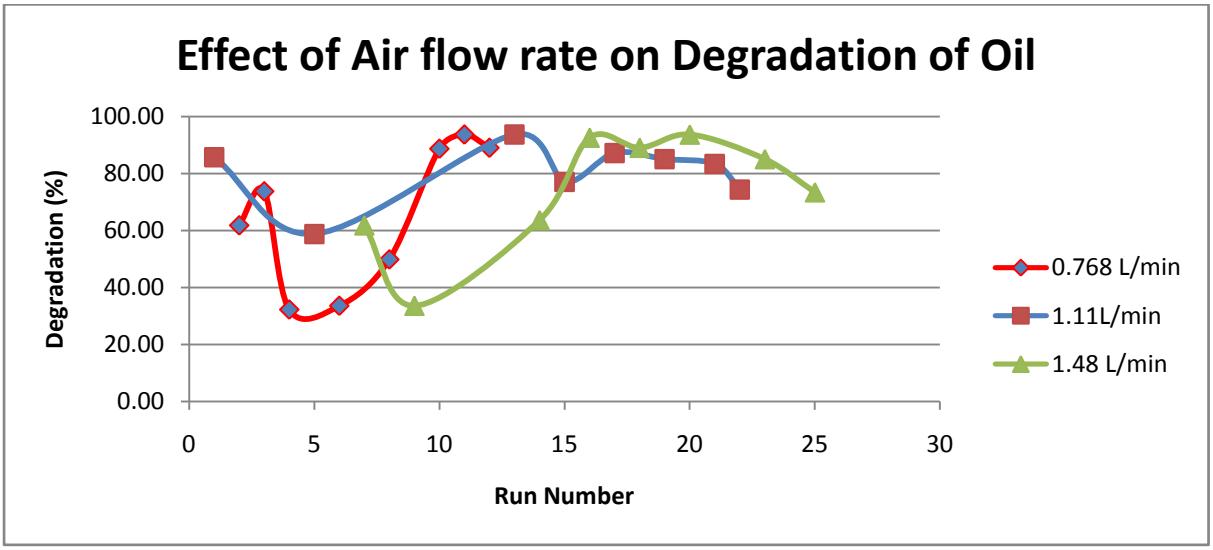

Figure D-3.1: Effects of air flow rate on the degradation of oil.

D-4. Effects of catalyst concentration on phenol runs

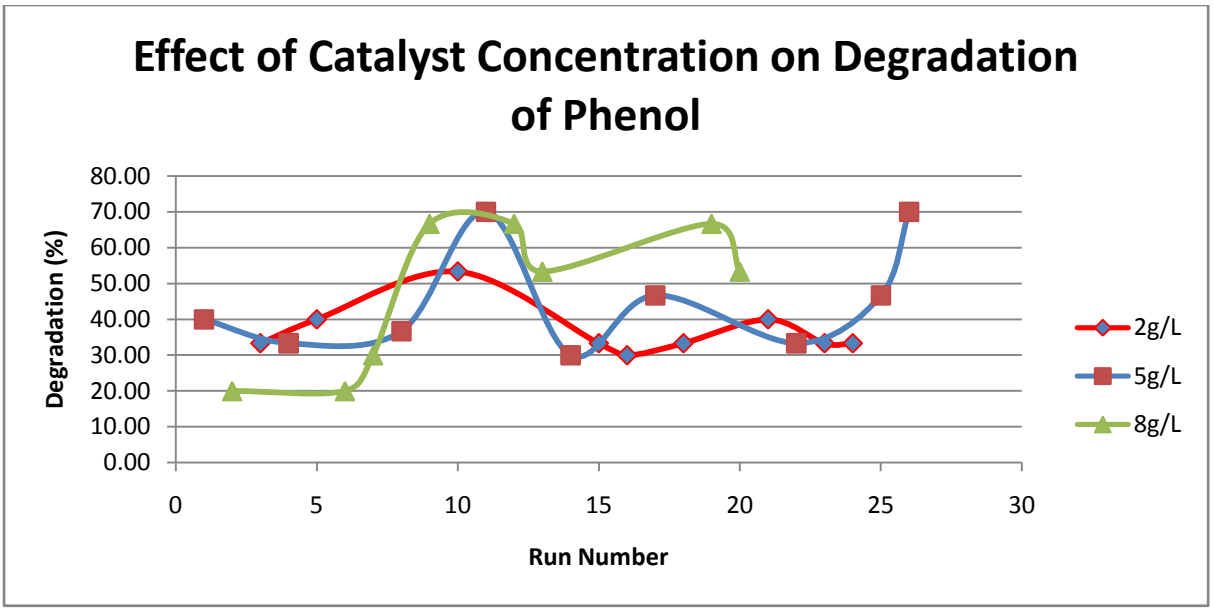

Figure D-4.1: Effects of catalyst concentration on the degradation of phenol.

D-5. Effects of run time on phenol runs

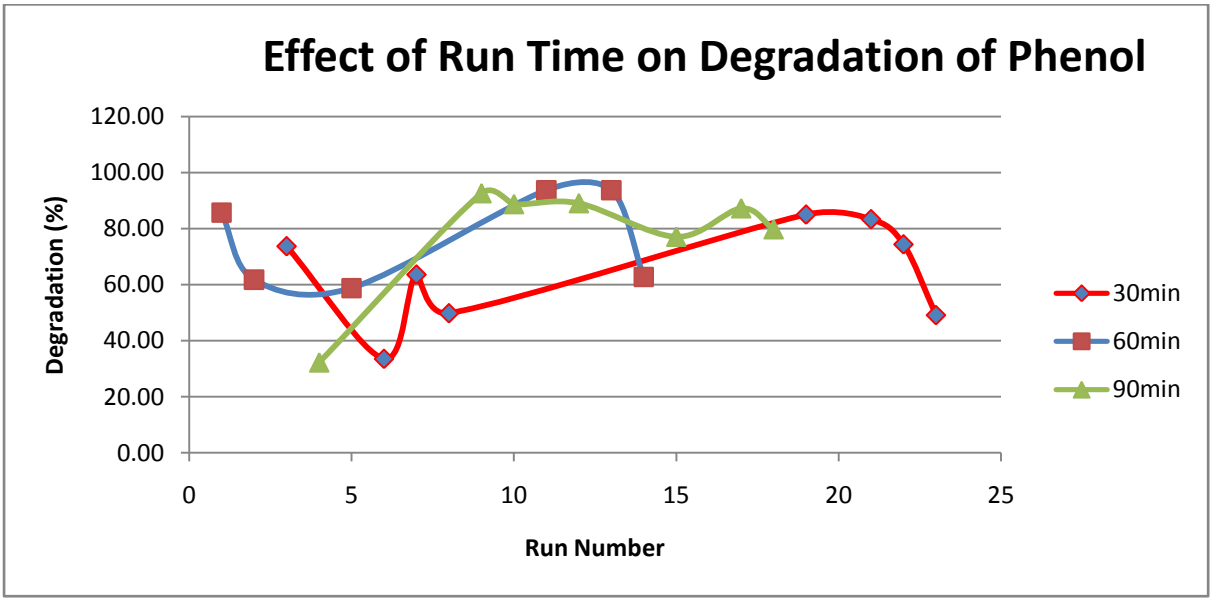

Figure D-5.1: Effects of run time on the degradation of phenol.

D-6. Effects of air flow rate on phenol runs

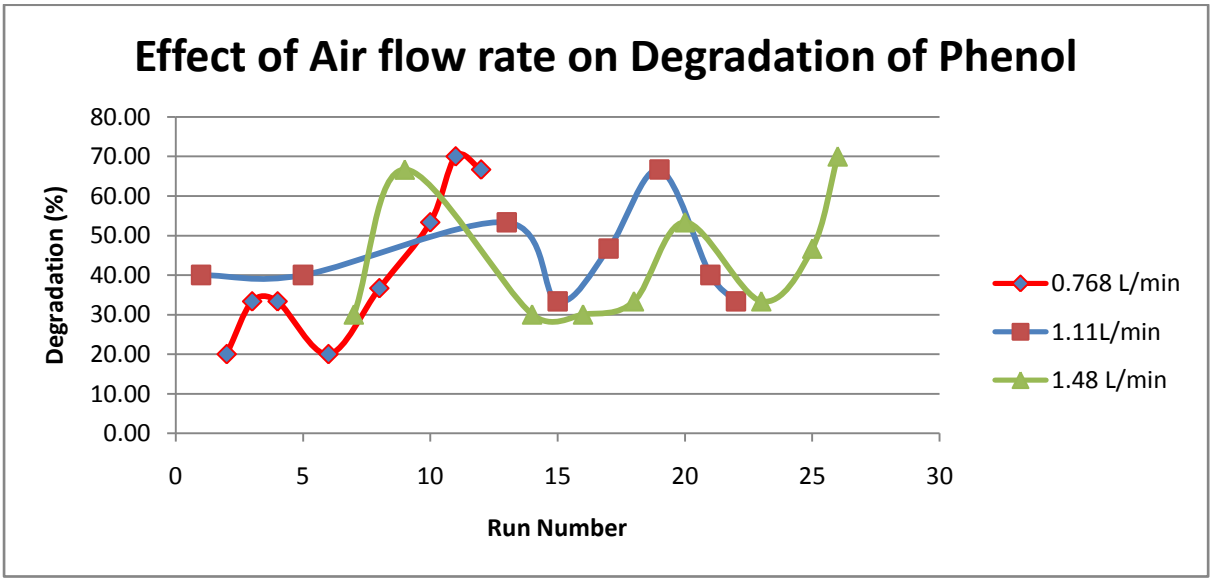

Figure D-6.1: Effects of air flow rate on the degradation of phenol.

Appendix E: pH monitoring of the outputs from the degradation process.

E-1. The effect of degradation on pH for experiment outputs

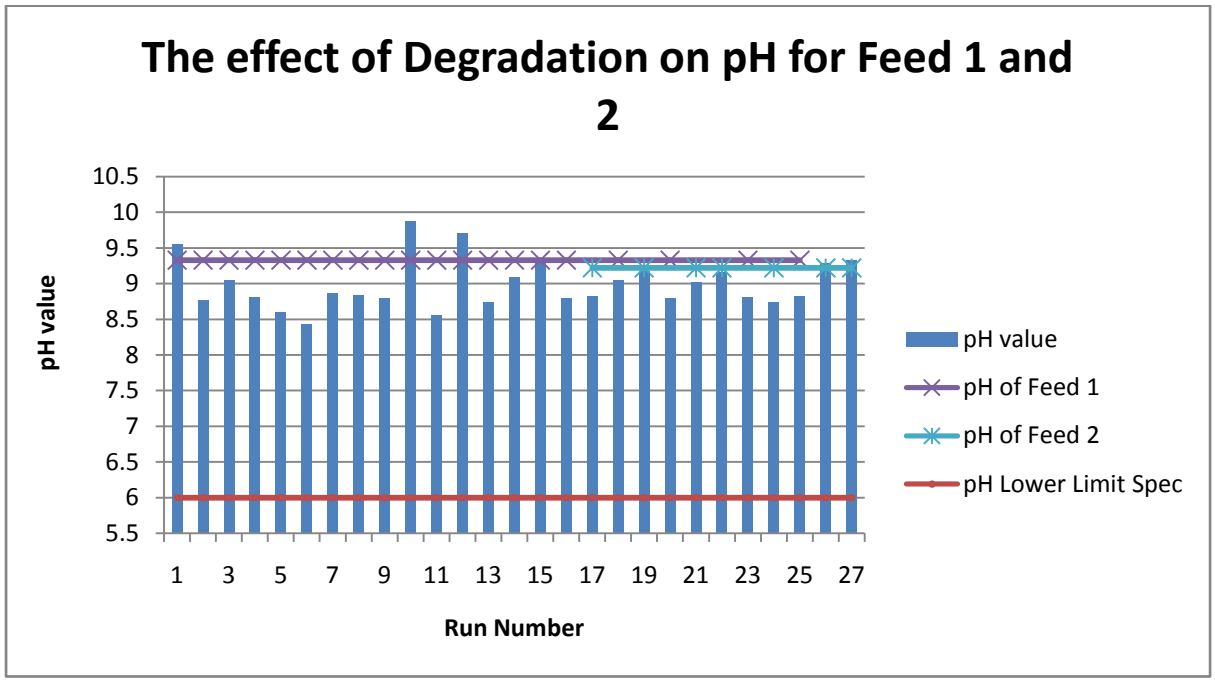

Figure E-1.1: The effect of degradation on pH for feed 1 and feed 2.

Appendix F: Model development and selection

F-1. Multilevel factorial Design model (Oil)

Table F-1.1: Multilevel factorial design for the degradation of oil

Response	**1**	**Degradation of Oil in water**			
ANOVA for selected factorial model					
Analysis of variance table [Classical sum of squares - Type II]					
	Sum of		Mean	F	p-value
Source	Squares	df	Square	Value	Prob > F
Model	6439.281	16	402.4551	2.901216	0.046128 significant
B-Run Time	545.4682	2	272.7341	1.966084	0.190505
C-Air Flow rate	1065.525	2	532.7627	3.840577	0.057869
AB	1383.797	4	345.9493	2.493877	0.109951

ABC	3444.491	8	430.5614	3.103829	0.048512
Residual	1387.194	10	138.7194		
Cor Total	7826.476	26			

Std. Dev.	11.77792	R-Squared	0.822756
Mean	71.79037	Adj R-Squared	0.539166
C.V. %	16.40599	Pred R-Squared	-0.29211
PRESS	10112.65	Adeq Precision	6.099426
-2 Log Likelihood	182.9811	BIC	239.0104
		AICc	284.9811

F-2. Multilevel factorial Design model (Phenol)

Table F-2.1: Multilevel factorial design for the degradation of phenol

Response	**2**	**Degradation of Phenol**			
ANOVA for selected factorial model					
Analysis of variance table [Classical sum of squares - Type II]					
	Sum of		Mean	F	p-value	
Source	Squares	df	Square	Value	Prob > F	
Model	5257.543	18	292.0857	3.889024	0.02788	significant
A-Catalyst Concentration	455.3943	2	227.6971	3.031711	0.104712	
AC	633.6428	4	158.4107	2.109186	0.171334	
BC	821.4033	4	205.3508	2.734178	0.105436	
ABC	3347.103	8	418.3879	5.570695	0.01275	
Residual	600.8412	8	75.10515			
Cor Total	5858.385	26				

Std. Dev.	8.666323	R-Squared	0.897439
Mean	42.46852	Adj R-Squared	0.666677

C.V. %	20.40646	Pred R-Squared	-0.16823
PRESS	6843.957	Adeq Precision	6.87857
-2 Log Likelihood	160.39	BIC	223.0109
		AICc	306.9614

F-3. Central Composite Design model (Oil)

Table F-3.1: Central composite design for the degradation of oil (Try 1)

Response	**1**	**Degradation of Oil in water**			
ANOVA for Response Surface Reduced Linear model					
Analysis of variance table [Partial sum of squares - Type III]					
	Sum of		Mean	F	p-value	
Source	Squares	df	Square	Value	Prob > F	
Model	1955.751	1	1955.751	10.65064	0.004315	significant
B-Run Time	1955.751	1	1955.751	10.65064	0.004315	
Residual	3305.297	18	183.6276			
Lack of Fit	3305.297	13	254.2536			
Pure Error	0	5	0			
Cor Total	5261.048	19				

Std. Dev.	13.55093	R-Squared	0.371742
Mean	77.153	Adj R-Squared	0.336839
C.V. %	17.56371	Pred R-Squared	0.199549
PRESS	4211.209	Adeq Precision	9.393231
-2 Log Likelihood	158.9085	BIC	164.9
		AICc	163.6144

F-4. Central Composite Design model (Phenol)

Table F-4.1: Central composite design for the degradation of phenol (Try 1)

Response	**2**	**Degradation of Phenol**				
ANOVA for Response Surface Linear model						
Analysis of variance table [Partial sum of squares - Type III]						
	Sum of		Mean	F	p-value	
Source	Squares	df	Square	Value	Prob > F	
Model	2032.99	3	677.6633	6.17558	0.005441	significant
A-Catalyst Concentration	316.7251	1	316.7251	2.886333	0.108691	
B-Run Time	1416.888	1	1416.888	12.91217	0.002433	
C-Air Flow rate	299.3766	1	299.3766	2.728234	0.118075	
Residual	1755.724	16	109.7327			
Lack of Fit	1755.724	11	159.6112			
Pure Error	0	5	0			
Cor Total	3788.713	19				

Std. Dev.	10.47534	R-Squared	0.536591
Mean	41.833	Adj R-Squared	0.449702
C.V. %	25.04085	Pred R-Squared	0.146948
PRESS	3231.97	Adeq Precision	8.403301
-2 Log Likelihood	146.2556	BIC	158.2386
		AICc	156.9223

F-5. Box-Behnken Design model (Oil)

Table F-5.1: Box-Behnken design for the degradation of oil (Try 1)

Response	**1**	**Degradation of Oil in water**			
ANOVA for Response Surface Linear model					
Analysis of variance table [Partial sum of squares - Type III]					
	Sum of		Mean	F	p-value	
Source	Squares	df	Square	Value	Prob > F	
Model	1902.39	3	634.1301	3.993626	0.032217	significant
A-Catalyst Concentration	0.357013	1	0.357013	0.002248	0.962901	
B-Run Time	239.6955	1	239.6955	1.509555	0.240985	
C-Air Flow rate	1662.338	1	1662.338	10.46908	0.006506	
Residual	2064.212	13	158.7855			
Lack of Fit	2064.212	9	229.3569			
Pure Error	0	4	0			
Cor Total	3966.602	16				

Std. Dev.	12.60101	R-Squared	0.479602
Mean	73.59824	Adj R-Squared	0.35951
C.V. %	17.12135	Pred R-Squared	0.088994
PRESS	3613.597	Adeq Precision	6.507684
-2 Log Likelihood	129.8318	BIC	141.1647
		AICc	141.1652

F-6. Box-Behnken Design model (Phenol)

Table F-6.1: Box-Behnken design for the degradation of phenol (Try 1)

Response	**2**	**Degradation of Phenol**			
ANOVA for Response Surface Reduced Quadratic model					
Analysis of variance table [Partial sum of squares - Type III]					
	Sum of		Mean	F	p-value	
Source	Squares	df	Square	Value	Prob > F	
Model	2770.716	4	692.6789	4.60181	0.017499	significant
A-Catalyst Concentration	0	1	0	0	1	
B-Run Time	1250.5	1	1250.5	8.307692	0.013771	
C-Air Flow rate	138.9445	1	138.9445	0.923077	0.355628	
C^2	1381.271	1	1381.271	9.176471	0.010481	
Residual	1806.278	12	150.5232			
Lack of Fit	917.0334	8	114.6292	0.515625	0.802737	not significant
Pure Error	889.2445	4	222.3111			
Cor Total	4576.994	16				

Std. Dev.	12.2687	R-Squared	0.605357
Mean	47.0582	Adj R-Squared	0.47381
C.V. %	26.0715	Pred R-Squared	0.273777
PRESS	3323.91	Adeq Precision	7.098573
-2 Log Likelihood	127.562	BIC	141.7288
		AICc	143.0172

Appendix G: Optimisation of the best suited models using RSM

G-1. Identifying the best fit models for degradation

Table G-1.1: Selection of the best fit models for oil and phenol degradation

Comparison of Model result to Actual result for the verification Run				
Model selected	**Model Result (%)**	**Actual degradation (%)**	**Difference (%)**	
Factorial Design				
Degradation of Oil in water	71.79	87.54	15.75	
Degradation of Phenol	39.83	46.67	6.84	
Box-Behnken Design				
Degradation of Oil in water	85.18	87.54	2.36	**Best Oil Model**
Degradation of Phenol	55.56	46.67	8.89	
Central Composite Design				
Degradation of Oil in water	79.96	87.54	7.58	
Degradation of Phenol	48.01	46.67	1.34	**Best Phenol model**

G-2. Optimisation of the CCD model

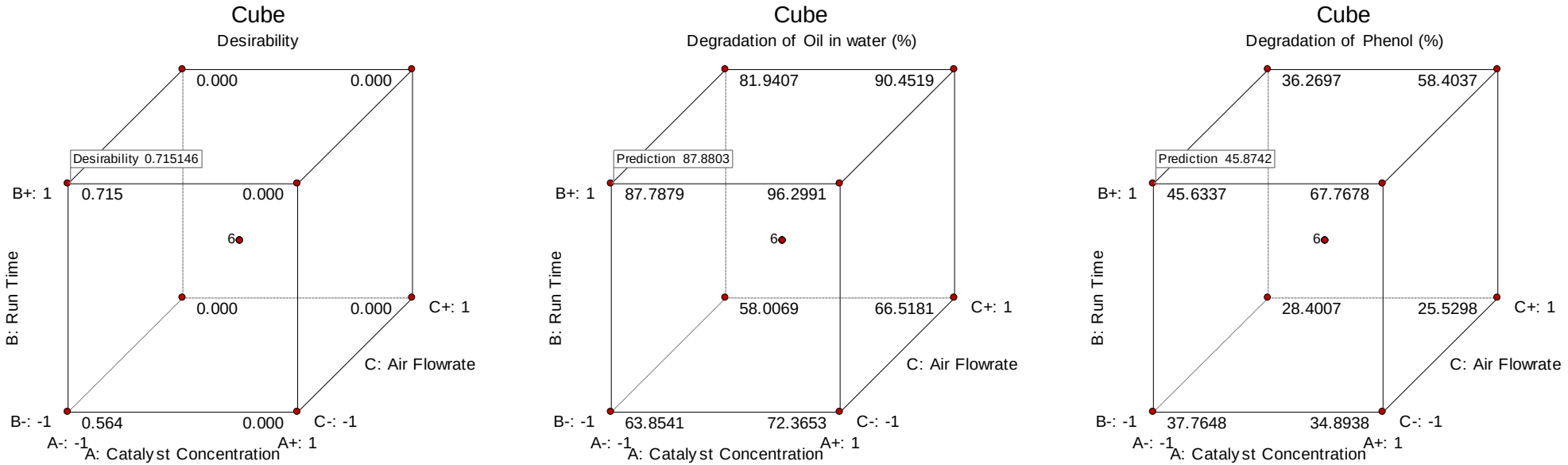

Figure G-2.1: Cube representation of the CCD model

G-3. Ramp diagram of the CCD optimisation

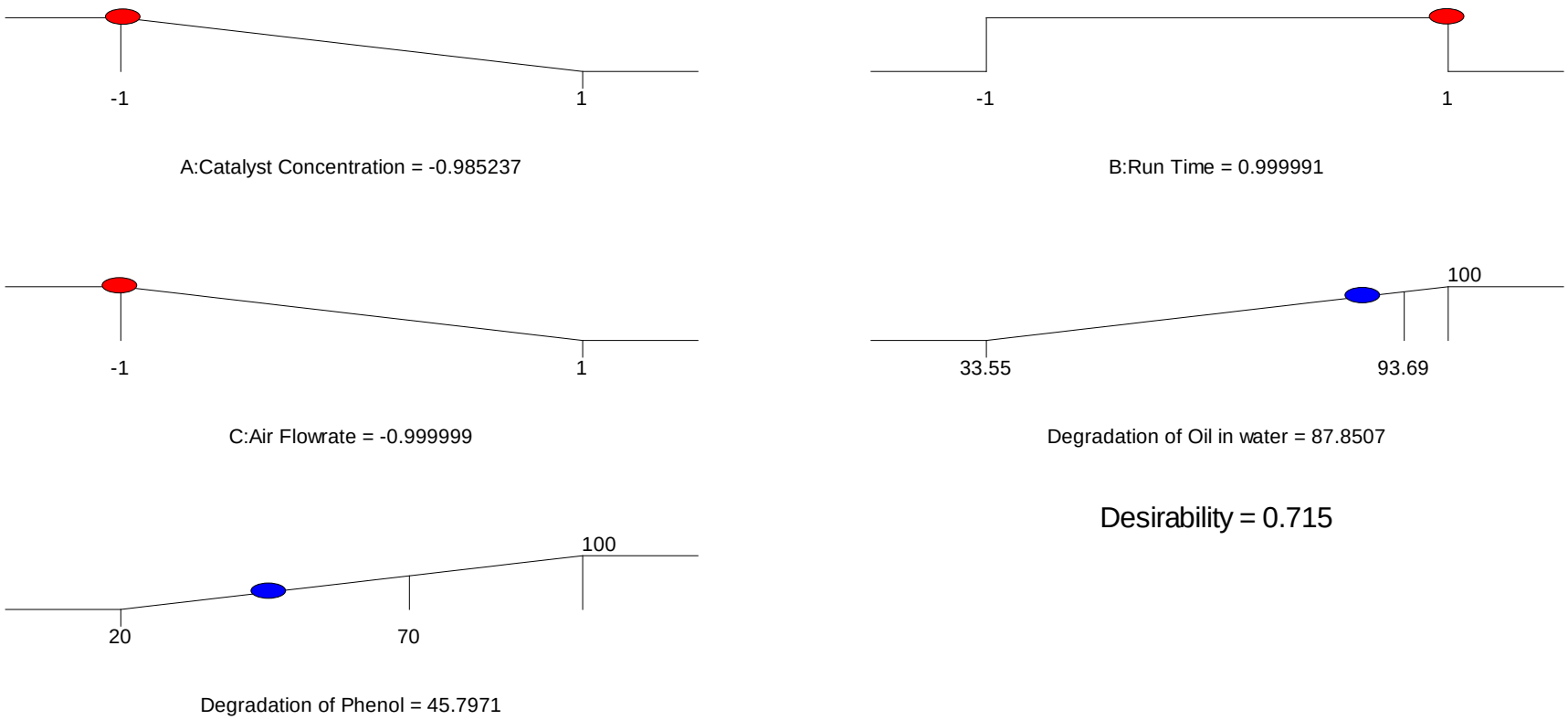

Figure G-3.1: Ramp Diagram for the optimisation of the CCD model

G-4. Ramp diagram of the BBD Model

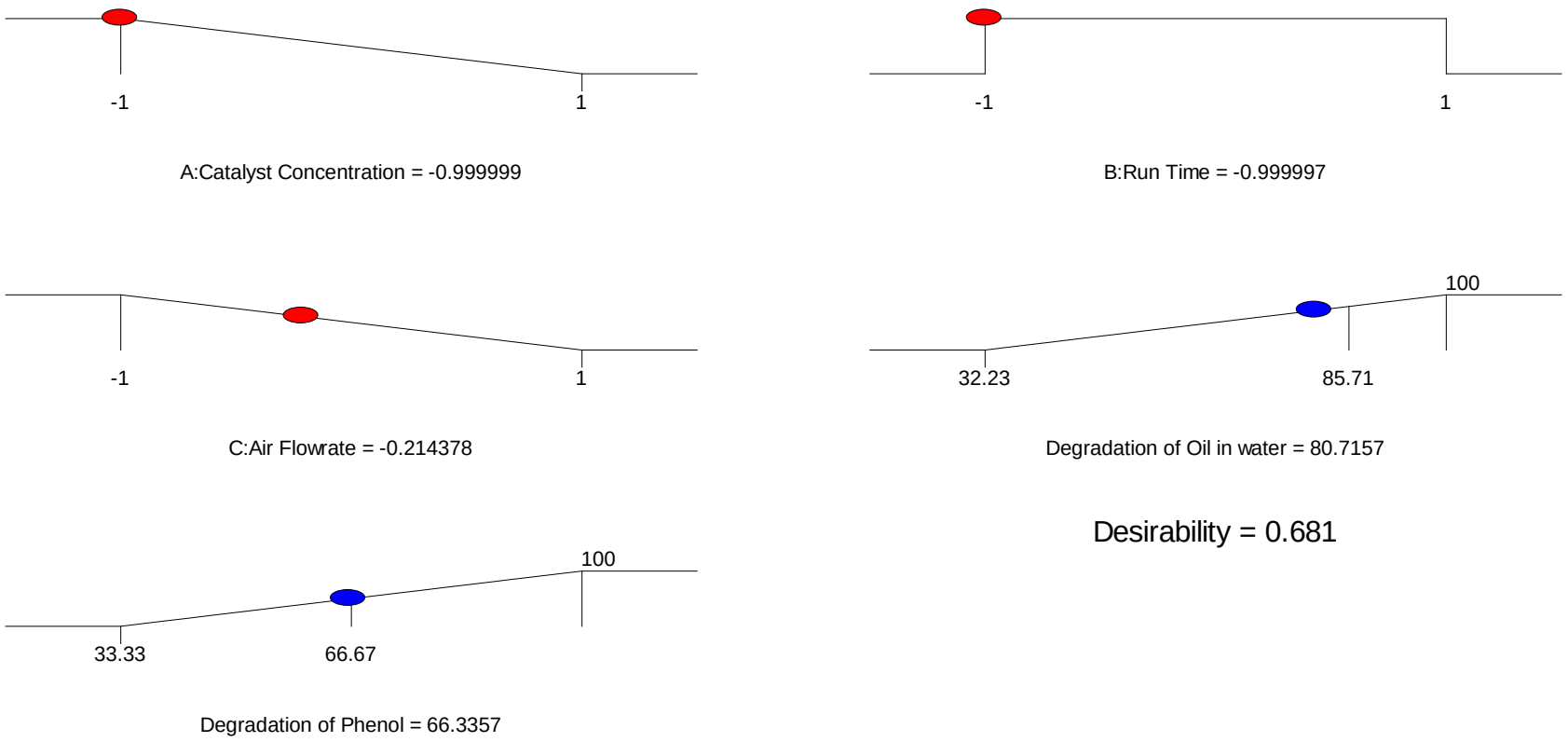

Figure G-4.1: Ramp Diagram for the optimisation of the BBD model

G-5. Graphical performance of models for oil degradation

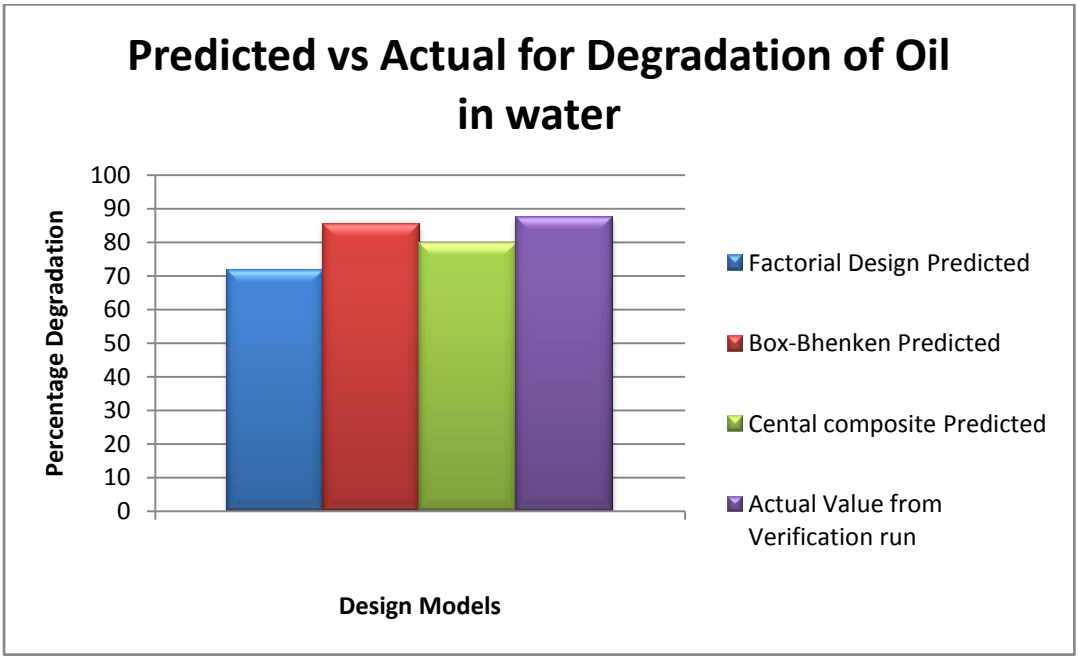

Figure G-5.1: Indicating the closest model value to actual value obtained from the BBD model.

G-6. Graphical performance of models for phenol degradation

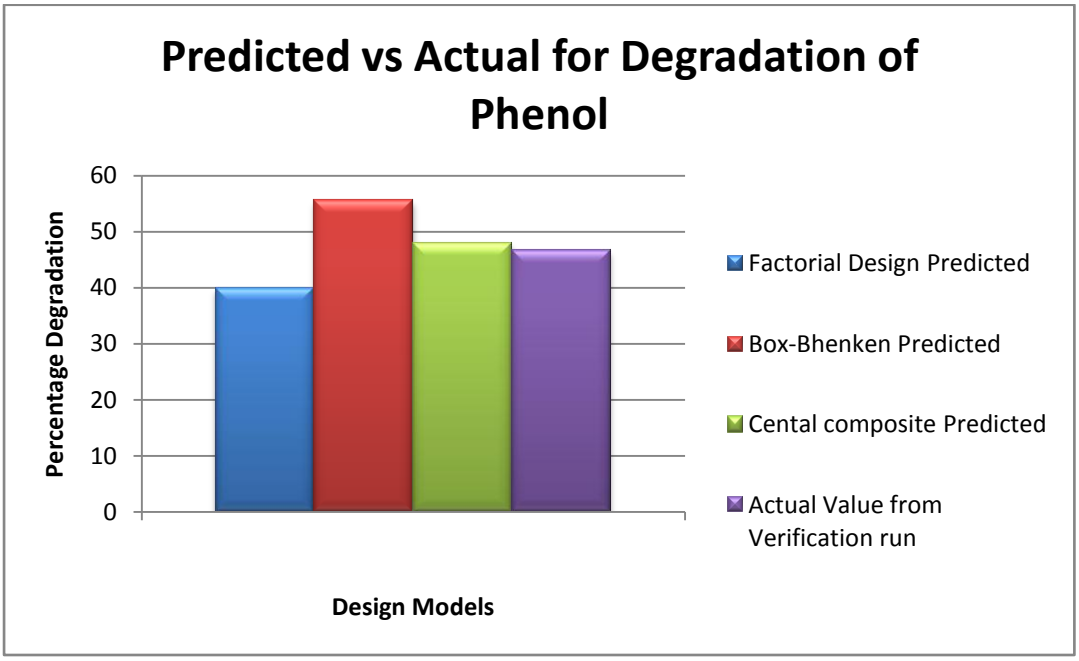

Figure G-6.1: Indicating the closest model value to actual value obtained from the CCD model.